ASM Handbook, Volume 11, *Failure Analysis and Prevention*
B. Miller, R. Shipley, R. Parrington, D. Dennies, editors
DOI 10.31399/asm.hb.v11.a0006829

Fretting Wear Failures

Siegfried Fouvry, Ecole Centrale de Lyon

FRETTING IS A WEAR PHENOMENON that occurs between two mating surfaces; initially, it is adhesive in nature, and vibration or small-amplitude oscillation is an essential causative factor. Fretting generates wear debris, which oxidizes, leading to a corrosion-like morphology. Fretting of ferrous materials in air produces a characteristic reddish-brown debris of ferric oxide, which, when mixed with oil or grease, produces debris that is often referred to as "blood," "cocoa," or "red mud." Hence, in components that are lubricated so that ordinary corrosion is not likely to occur, the presence of reddish-brown debris is indicative of fretting. Fretting also occurs in noble materials, such as gold, platinum, and cupric oxide in connectors. If fretting occurs in an inert or protective atmosphere, oxide debris cannot be formed, leading to a full adhesive wear response with little debris produced.

The general characteristics of fretting wear, with an emphasis on steel, are reviewed in this article. This review is followed by several examples of failures related to fretting wear. Common sites for fretting are in joints that are bolted, keyed, pinned, press fitted, or riveted; in oscillating bearings, splines, and press fits on shafts; and in universal joints and orthopedic implants. Generally, fretting occurs at contacting surfaces that are intended to be fixed in relation to each other but that actually undergo small oscillating motion usually induced by vibration. Other situations concern cyclic thermal dilatation and contact between balls and raceways in bearings and between mating surfaces in oscillating bearings and flexible couplings.

Fretting Wear

In general, fretting occurs between two tightly fitting surfaces that are subjected to a cyclic, relative motion of extremely small amplitude (Ref 1, 2). For oxidizing metals, one of the immediate consequences of the process in normal atmospheric conditions is the production of oxide wear debris; thus, the inaccurate term *fretting corrosion* was previously considered, although the actual term *fretting wear* is more consistently used now. The movement is usually the result of external vibration, but in many cases, it is the consequence of one of the members of the contact being subjected to a cyclic stress (that is, fatigue), which gives rise to another and usually more damaging aspect of fretting fatigue or contact fatigue.

Fatigue cracks are nucleated by the fretting contact stresses and propagate due to the bulk fatigue stress. The object of this article is to focus on fretting wear related to debris formation and ejection, so the specific problem of fretting fatigue is not discussed in detail. Most of the fretting wear concerns quasi-static normal load, but some situations can be complicated by the combined application of an oscillating normal load. This leads to a hammering effect, which is termed impact fatigue. In this case, the phase relationship between the two motions can be an important factor.

Other terms that have been used to designate fretting-type damage are *false Brinelling*, which is applied particularly to bearings in which the craters caused by the vibration of the ball against the race are circular and resemble Brinell impressions, and *fitting rust*, in which gages or shims are clamped together and experience vibration.

Fretting was first reported in 1911 by Eden, Rose, and Cunningham (Ref 3), who found that brown oxide debris was formed in the steel grips of their fatigue machine in contact with a steel specimen. It was not until 1927 that the first investigation of the process was conducted and two machines were designed to produce small-amplitude rotational movement between two annuli in the first case, and an annulus and a flat in the second case (Ref 4). The movement was controlled by a long lever system. Because the resultant debris on steel specimens was the red iron oxide α-Fe_2O_3, which had risen from a chemical reaction with oxygen in the air, Tomlinson (Ref 4) coined the phrase *fretting corrosion*. The investigation also established that the damage could be caused by movements with amplitudes as small as a few millionths of an inch (125 nm) and the important fact that relative movement, which was termed slip, had to occur.

The next important stage in the development of fretting studies was made in 1941, when fretting damage was produced on the gage length of steel fatigue specimens, and a subsequent reduction in fatigue strength of 13 to 17% was found due to pitting of the surface (Ref 5). This result was to be expected, but later investigations, particularly that presented in Ref 6, showed that the conjoint action of fretting and fatigue, which is the usual case in practice, was much more dangerous, producing strength-reduction factors of 2 to 5 and even greater. Since the 1950s, numerous studies demonstrated that fretting greatly accelerated the crack-initiation process. In normal fatigue, crack initiation may account for 90% of fatigue life, whereas in fretting fatigue, initiation could occur in 50% of the fatigue life (Ref 7).

Fretting Wear in Mechanical Components

Because vibration is one of the main causes of fretting movement, it follows that the most likely area for it to occur is in machinery. The contacts between hubs, shrink and press fits, and bearing housings on loaded rotating shafts or axles are particularly prone to fretting damage, but because the movement arises from alternating stresses in the shaft surface, the problem is more fatigue than wear. However, wear rather than fatigue can be a problem in bearing housings. Thin-shell bearings are used universally in diesel engines, and such bearings involve an interference fit between the bearing and the housing. Due to the structural deformation of the connecting rod, fretting damage occurs at the interface of the thin-shell bearings (Ref 8–11) (Fig. 1).

Flexible couplings and splines, particularly where they form a connection between two shafts and are designed to accommodate some slight misalignment, can suffer severe fretting wear problems. Examples of such cases are described in Ref 8.

Jointed structures are another source of fretting problems. It has been reported (Ref 12–14) that there is no such thing as a static joint

on an aircraft. An aircraft structure is largely an assemblage of aluminum and steel components riveted together or joined by fasteners. Even in a simple riveted joint, there are at least three possible sites where fretting can occur (Fig. 2):

- Between the riveted panels
- Between the underside of the rivet head and the panel
- Between the shank of the rivet and the rivet holes

Typical fretting wear damage is observed in turbines, both steam and gas, operating under conditions that subject these components to fretting damage in such positions as:

- The point at which the turbine disk is either shrink fitted onto the driving shaft or attached to the shaft by means of a bolted flange
- The place at which snubbers at the outer ends of the blades contact those on adjacent blades

However, the most critical location of fretting damage in the turbine engine is usually observed in the dovetail joint interface between the disk and the blades (Fig. 3). During the fly sequence (i.e., takeoff and landing) macro gross slip slidings are combined with aerodynamic micro partial slidings, which can generate combined fretting wear (i.e., wear volume induced by debris formation and debris ejection) but also fretting fatigue (i.e., crack nucleation and crack propagation) (Ref 10, 15–18). Fortunately, new surface treatments combining shot and laser peening with a thick self-lubricant plasma coating are now applied to prevent any critical damage process (Ref 17).

Steel ropes are used widely as mooring ropes, haulage ropes, mining ropes, and on cable cars. Overhead power lines are, in effect, ropes made up of aluminum wires wound on a steel support rope; more recently, they have been made up entirely of aluminum (the all-aluminum conductor). Any bending movement or alternating tension of the rope can result in local movement in the numerous interwire contacts, leading to fretting wear phenomena (Fig. 4) (Ref 19–23).

Most ropes include some form of internal lubrication to lessen the effects of such movement. Again, one of the main dangers is the fretting fatigue failure of an individual wire, which increases the load on the remaining wires. Furthermore, fretting wear may induce fretting notch effect, lead to removal of the lubricant from the fretted interface, and allow access of the corrosive ambient, which further promotes such fatigue crack damages. The accumulation of debris also leads to a reduction in flexibility at this point, and, in the case of a mining rope, can cause jolting when this part of the cable passes onto the winding drum.

In steam generators and heat exchangers, flow-induced vibration results in fretting between the tubes and the supports or baffles through which they pass. In the past, this phenomenon appears to have been a particular problem in the nuclear power industry (Ref 24–26) and chemical processing plants.

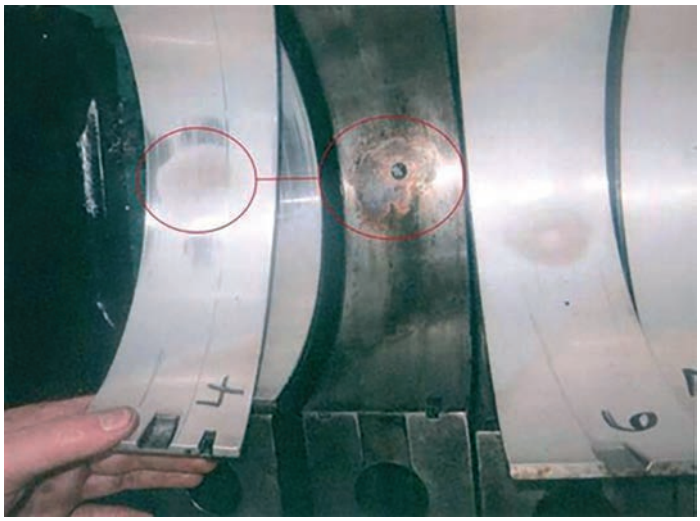

Fig. 1 Example of fretting and related visible imprint on the main bearing shell. Adapted from Ref 10. Reprinted with permission from MAN Energy Solutions

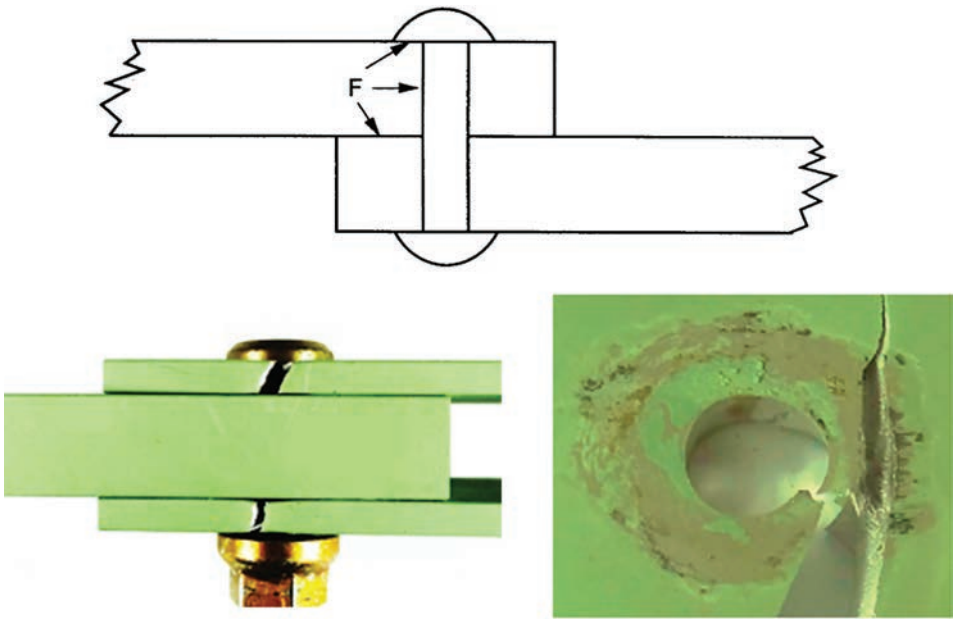

Fig. 2 Fatigue crack generated by fretting damage in a rivet hole and fastened assemblies. Bottom two images reprinted from Ref 14 with permission from Elsevier

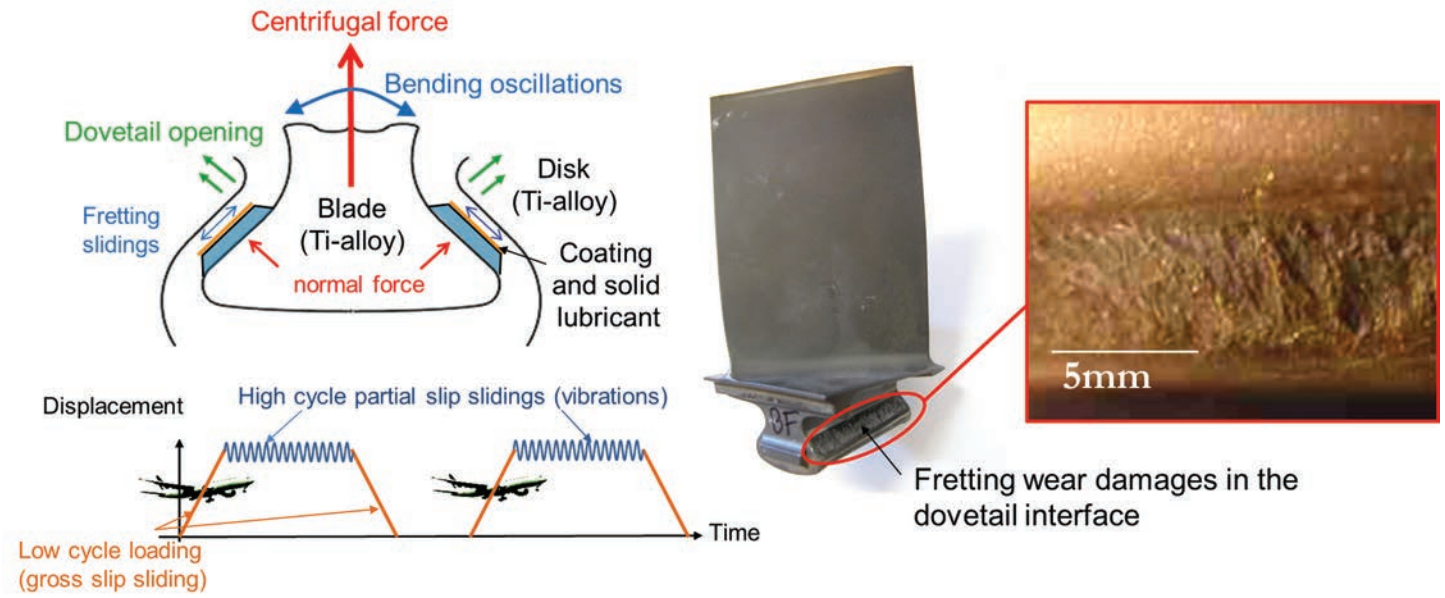

Fig. 3 Fretting wear damage process in turbine engine dovetail interface. Adapted from Ref 17. Reprinted with permission from Elsevier

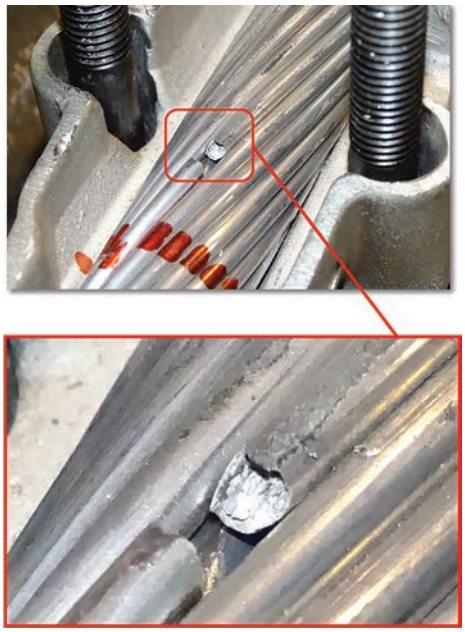

Fig. 4 Representation of fretting wear damage in overhead power lines, inducing failure of a wire (located below the clamping assembly)

A large contribution to fretting in these industries is from impact fretting, which is discussed in the section "Impact Fretting" in this article.

The accumulation of oxide debris is also the main problem in fretting of electrical contacts (Ref 27–32). Because the oxide debris is nonconducting, interference or distortion of electrical signals can take place in electrical connectors when subjected to fretting wear. Indeed, the huge developments in electronic control and data analysis imply the use of numerous sensors and therefore connectors right next to the engines (automotive, plane, train, etc.). Enduring high-frequency vibrations as well as cyclical thermal loadings, the pin-clip interface experiences fretting wear damage (Fig. 5). Noble materials such as gold plating are usually applied to prevent the formation of insulating oxide debris. However, when the coating is worn out and the interface reaches the nonnoble copper alloy substrate, insulating oxide debris is formed and the electrical conductivity is decayed. The durability of the electrical contact resistance depends on the nature of the coating (noble versus nonnoble) and can be formalized using decreasing power-law functions of the sliding amplitude (Ref 33).

The transportation of goods by road or rail obviously means that these items are subjected to vibrations. This fact gives rise to the classic case of fretting in the bearings of automobiles being transported by rail from Detroit to the west coast of the United States. Because the bearings were stationary, fretting occurred between the loaded balls and the race, giving rise to the false Brinelling phenomenon. This has also been a problem with the transport of stacks of aluminum sheets with highly polished finishes. High-purity aluminum "logs" transported by rail to the plant without careful protection were shown to display fretting scars with oxide debris. When these sheets were extruded, serious surface tears were observed, proving that surface damage induced by fretting (i.e., vibration during transport) can significantly affect any production process if packaging aspects are not carefully considered (Ref 34).

Fretting can also occur in certain orthopedic devices, particularly between the bone and the metallic femoral stem of a total hip joint prosthesis (Ref 35–39). This concept was extended in Fig. 6. Strain deformation related to walking and related vibrations induces fretting sliding between the bone and the metallic surfaces. Fretting in body fluids, which represents a corrosive medium, induces effective fretting-corrosion phenomena, resulting in the disruption of otherwise protective surface films and the continual release of heavy metal ions into the body fluids, with possible toxic reactions. To reduce this phenomenon, polymer cement can be added between the bone and the metallic femoral stem. However, significant fretting wear phenomena can still take place, inducing the loosening of the entire total hip joint prosthesis. Note that the development of modular-design hip joints involving numerous interfaces tends to exacerbate fretting wear problems in the prosthesis assembly, underlining the necessity to develop new palliatives to reduce such phenomena (Ref 40).

The possible situations in which fretting can occur are legion; therefore, it is possible in this review to give only some typical examples. In most of the cases described, suitable methods of overcoming the problem have been forthcoming as the result of detailed investigation. These studies are described in detail in the section "Prevention of Fretting Damage" in this article. This theory extends the possibility of fretting damage to materials other than metals. With the increased use of polymers, both simple and reinforced, in addition to ceramics, this

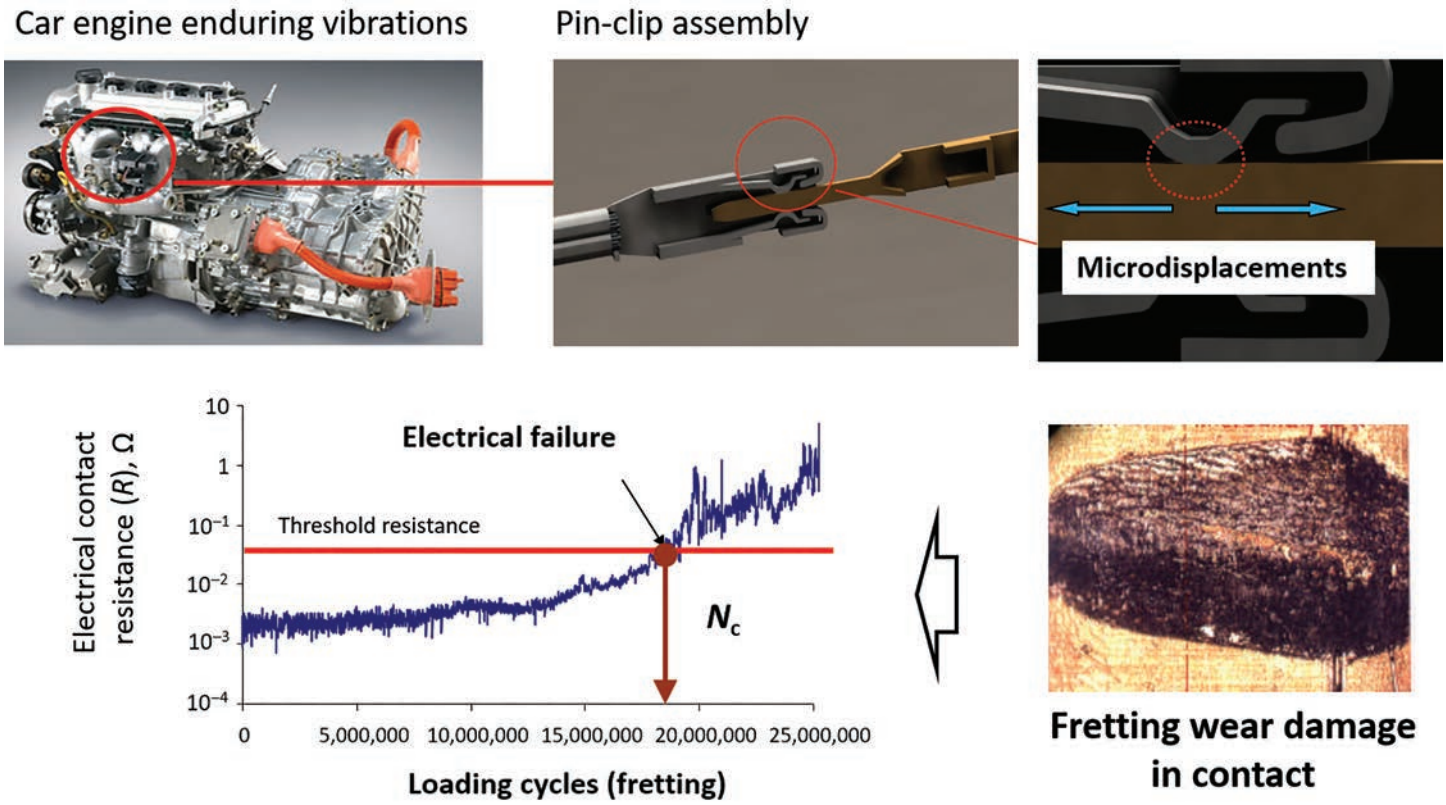

Fig. 5 Fretting wear damage in electrical connectors

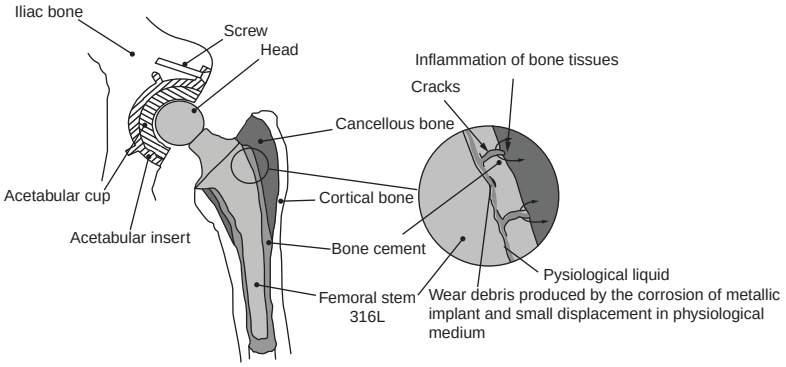

Fig. 6 Illustration of fretting wear damage between a bone cement and a metallic femoral stem. Adapted from Ref 36

is an area in which further examples of a somewhat different nature are likely to be encountered. Some research already has been devoted to the topic and is described in the next section, "Parameters Affecting Fretting," in this article.

Parameters Affecting Fretting

Many experimental investigations have concentrated on the effect of specific physical variables (such as amplitude of slip, normal load, frequency of vibration, and the circumstances of the fretting situation, such as type of contact, mode of vibration, and the condition of the surfaces) to indicate how the problem can be overcome in the future design of contacting components. Before discussing to a greater depth how loading conditions can influence fretting damage evolution, it is important to better describe the various test configurations usually applied to investigate this aspect.

Fretting Test Experiments

Figure 7 illustrates the principle of a basic fretting wear test (i.e., plain fretting test without external bulk stress as usually applied in fretting fatigue experiments) (Ref 41, 42). This test configuration consists of applying a normal force, P, and a cyclic displacement, δ_m (amplitude δ_m^*), using, for example, a hydraulic electromagnetic actuator. The latter alternated displacement results in a tangential force, Q (amplitude Q^*). The measured displacement, δ_m, is obtained from an external extensometer (linear variable differential transformer, laser, etc.), while the loading and tangential forces (P and Q) are recorded from load cells.

It is interesting to note that the measured displacement amplitude, δ_m^*, is not equal to the contact displacement, δ^*. Indeed, under small fretting oscillations, a significant part of the measured displacement is in fact accommodated by the test assembly deformation, δ_A. The latter depends on the applied tangential force and the compliance of the test assembly (C_A):

$$\delta_m^* = \delta^* + \delta_A = \delta^* + C_A \times Q^* \quad \text{(Eq 1)}$$

The process to determine C_A is time-consuming and complicated and requires the stiffness estimation of the test apparatus (i.e., $C_A = 1/K_A$). However, by plotting the ($\delta_m - Q$) fretting loop (Fig. 7), the tangential force amplitude, Q^*, is determined, allowing the contact stress investigation to predict, for example, the cracking phenomena. In addition, the effective sliding amplitude, δ_S, can be derived from the fretting

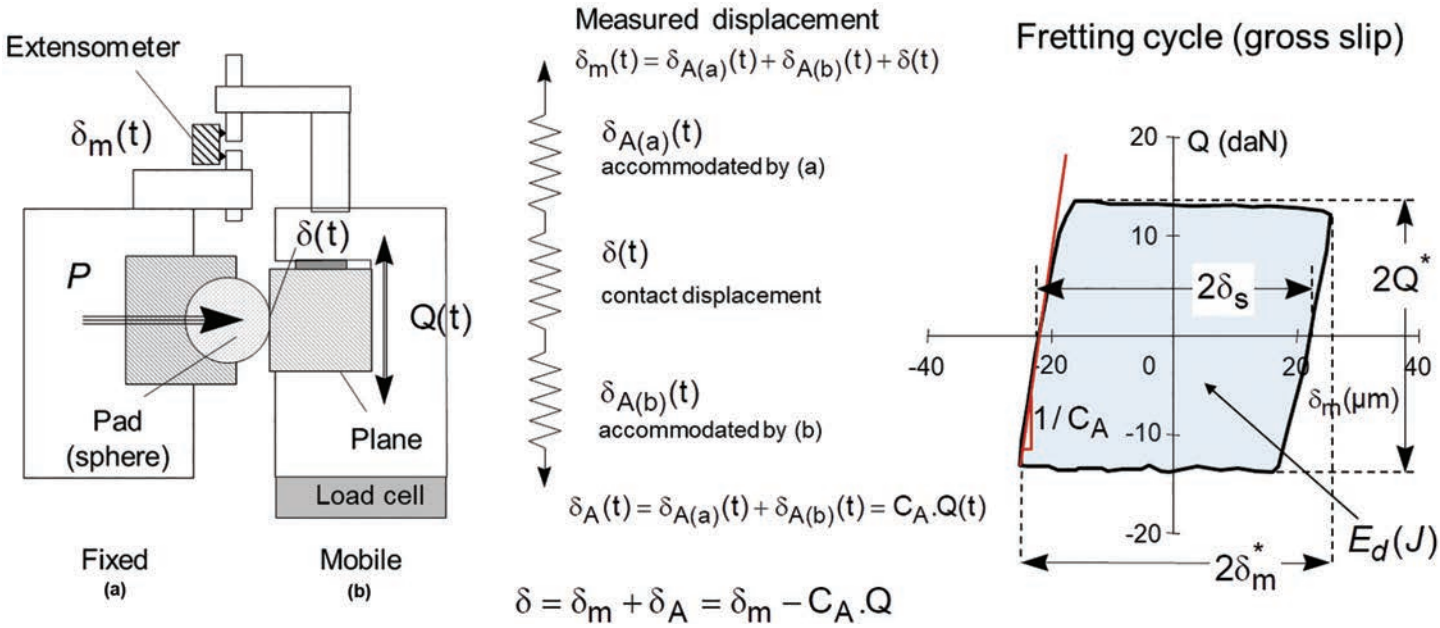

Fig. 7 Schematic of a basic fretting wear test and related fretting cycle. Adapted from Ref 41. Reprinted with permission from Elsevier

cycle by measuring the displacement amplitude when $Q = 0$, such that:

$$\delta_S = \delta_m\,(Q = 0) = \delta(Q = 0) \quad \text{(Eq 2)}$$

Finally, by integrating the fretting loop, the friction energy, E_d(J) (i.e., friction work), inputted in the interface can be estimated. Both E_d(J) and δ_S variables can be considered to quantify the wear rate.

Fretting Sliding Condition

Most of the research work and industrial feedback emphasize that fretting damage chiefly depends on the displacement amplitudes and related sliding condition imposed on the interface (Fig. 8) (Ref 41–44).

Partial Slip Condition

If the displacement amplitude, δ, remains smaller than a threshold value, referred to as the sliding transition (δ_t), a partial slip sliding condition takes place. This sliding condition implies a composite contact structure with an inner undamaged stick domain surrounded by a sliding annulus (Fig. 8) (Ref 45, 46). The tangential force amplitude, Q^*, increases with the applied displacement amplitude until reaching the threshold transition value, $Q^* = \mu \times P$ (with μ being the coefficient of friction). The interface is subjected to cyclic contact stressing, inducing crack nucleation (and crack propagation if an external fatigue loading is applied). The fretting loop is very closed, which means nearly no friction dissipation, so that wear volume induced by debris formation and ejection is nearly negligible.

Gross Slip Condition

After reaching the sliding transition, a full sliding condition takes place. In this case, the tangential force amplitude is constant (i.e., $Q^* = \mu \times P$), whereas the ($\delta - Q$) fretting hysteresis displays a large dissipative open quadratic loop shape. Stabilized gross slip conditions not only favor surface wear by debris formation and debris ejection but also decrease the cracking risk by removing the incipient cracks nucleated on the top surface and reducing the pressure profile.

Note that the gross slip amplitude can also be estimated from the measured displacement amplitude by knowing the transition amplitude, according to:

$$\delta_S = \delta^* - \delta_t = \delta_m^* - \delta_{m,t} \quad \text{(Eq 3)}$$

Reciprocating Condition

When the sliding amplitude, δ_S, becomes larger than the contact radius, a, the whole interface will be exposed to the ambient air, and the reciprocating sliding condition will prevail. If the transition from partial to gross slip is clearly established by contact mechanics and formalized by the Mindlin theory for Hertzian interfaces (i.e., sphere-on-flat and cylinder-on-flat contacts) (Ref 45), the transition from gross slip to reciprocating sliding is less evident and can only be related to the transition from a partial to a full exposition of the fretted interface to the ambient air. The sliding condition can be quantified by considering various sliding criteria, such as the friction energy criterion, A (Ref 47):

$$A = \frac{E_d}{4 \times Q^* \times \delta_S} \quad \text{(Eq 4)}$$

Based on the Mindlin theory, it was demonstrated that there is a constant, $A_t = 0.2$, for sphere-on-flat contact below which the contact operates under partial slip (i.e., $A < A_t$) and above which the contact runs under gross slip (i.e., $A > A_t$).

Note that the slip ratio discussed in Ref 48 also displays a constant value at the gross slip/partial slip transition in sphere-on-flat contact, so that (Ref 41) gross slip occurs when $B = \delta_S/\delta^* > B_t = 0.26$.

For gross slip condition ($A > A_t$), analysis of the fretting data provides the nominal coefficient of friction, defined as:

$$\mu = \frac{Q^*}{P} \quad \text{(Eq 5)}$$

Additionally, it gives the energy friction coefficient, which represents the averaged friction value over the gross slip fretting cycle, given by:

$$\mu_e = \frac{E_d}{4 \times P \times \delta_S} \quad \text{(Eq 6)}$$

Fretting Regime Concept

Most of the industrial interfaces undergo varying loading conditions (Fig. 9). In addition to the evolution of the coefficient of friction during contact, the contact can also shift from partial to gross slip conditions (Ref 44, 50, 51). Therefore, the fretting regime concept was

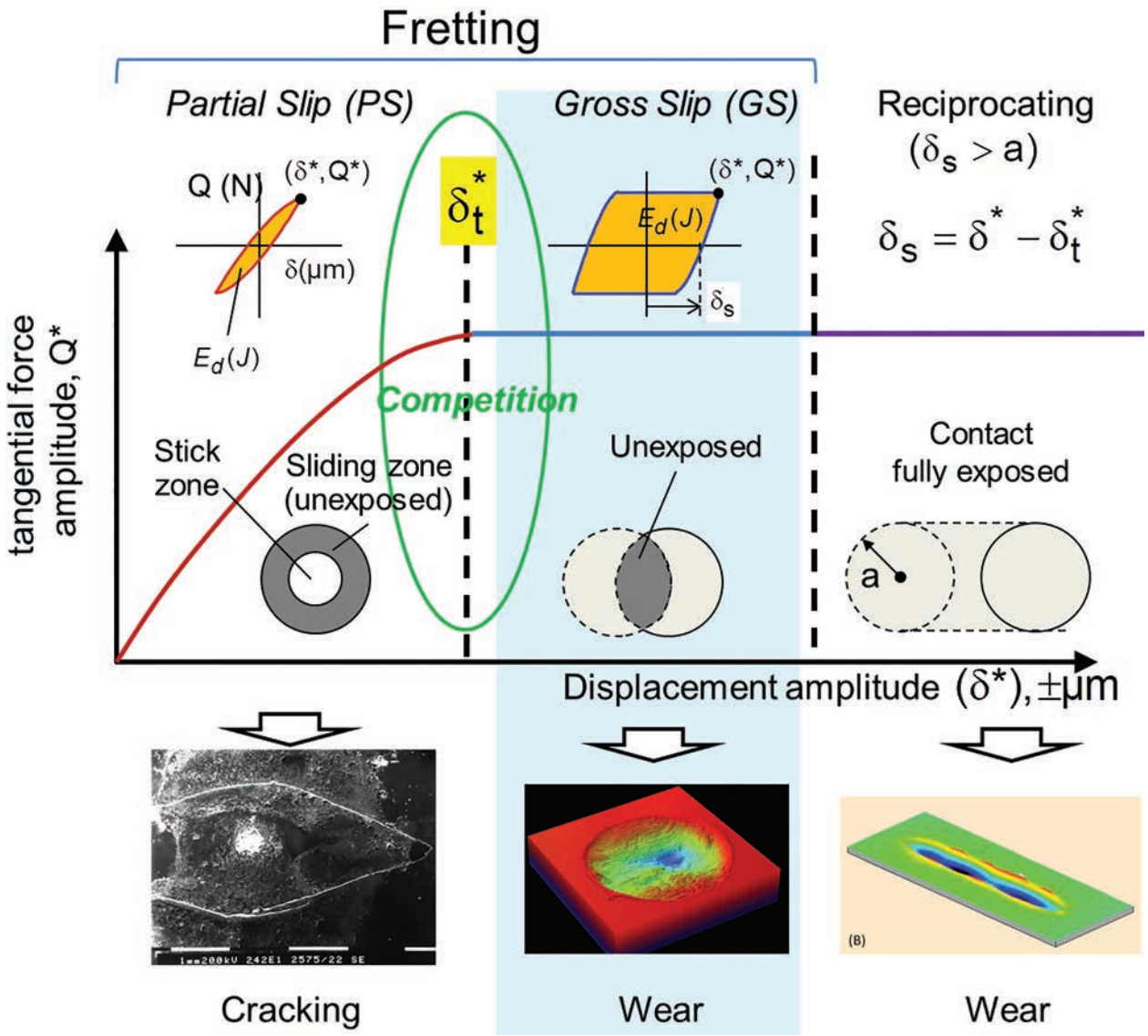

Fig. 8 Schematic illustration of partial slip fretting, gross slip fretting, and reciprocation sliding conditions as a function of the displacement amplitude (e.g., sphere-on-flat contact). Adapted from Ref 43. Reproduced with permission from P.J. Kennedy, M.B. Peterson, and L. Stallings, An Evaluation of Fretting at Small Slip Amplitudes, *Materials Evaluation under Fretting Conditions*, STP 780, American Society for Testing and Materials, 1982, p 30–48, copyright ASTM International, 100 Barr Harbor Drive, West Conshohocken, PA 19428

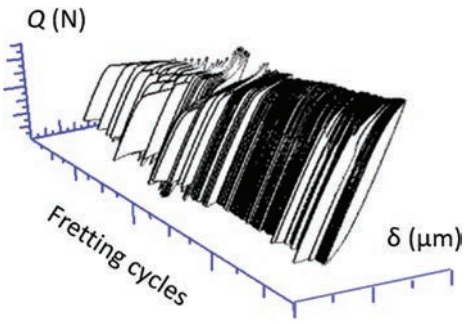

Fig. 9 Diagram showing the mixed fretting regime fretting log (i.e., plotting of the fretting cycle as a function of a log scale of the fretting cycles). Adapted from Ref 49. Reprinted with permission from Elsevier

introduced to better describe the stress history imposed on the interface. Stable gross slip conditions are related to a gross slip regime (GSR) promoting surface wear. Constant partial slip condition is denoted by a partial slip regime (PSR), which favors cracking phenomena. Finally, the mixed fretting regime (MFR), usually observed for intermediate displacement amplitudes close to the sliding transition zone, promotes a competition between wear and cracking phenomena.

The fretting regime can also be quantified by estimating the proportion of gross slip cycle during the whole test duration and defining the percent gross slip (%GS) parameter as (Ref 49):

$$\%GS = \frac{N(A > A_t)}{N} \quad \text{(Eq 7)}$$

Stating that:

PSR: %GS = 0%
MFR: 0% < %GS < 100%
GSR: %GS = 100%

Hence, by using this approach, the competition between fretting wear and fretting cracking as a function of the applied displacement can be better rationalized.

Figure 10(a) compares the evolution of the crack length and wear volume as a function of the applied displacement amplitude, δ_m^*, and the related %GS fretting regime parameter (Ref 49). As previously underlined, the crack extension starts in PSR, reaches a maximum value in MFR when %GS = 70%, then decreases until no crack nucleation takes place under GSR when $\delta_m^* = \pm 50$ μm. The wear volume is negligible under PSR, very small under

MSR, and increases quasi-linearly when the GSR regime is reached (%GSR = 100%).

From this analysis, the necessity to take into account the sliding condition and, above all, to differentiate the (measured) displacement amplitude from the effective sliding amplitude to properly quantify the fretting wear rate becomes obvious. Indeed, if the displacement amplitude is considered instead of the sliding amplitude to estimate the friction work, very strange and nonrepresentative specific wear rates can be observed. This is clearly illustrated in Fig. 10(b), where the researchers did not take into account this aspect, inducing nonrepresentative specific wear rate estimations. Indeed, under partial and mixed slip regimes ($\delta_m^* < 100$ µm), the sliding amplitude is significantly smaller than the displacement amplitude; consequently, the friction work computed from the displacement amplitude is overestimated. This implies an underestimation of the wear rate. Above the gross slip transition ($\delta_m^* > 100$ µm), the relative proportion of displacement accommodated by the test system is reduced, so the measured displacement converges to the effective sliding value. Hence, the friction work is better estimated and is more representative. More stable and reliable specific wear rates are identified. Therefore, to properly quantity the fretting wear, it is crucial to properly consider the effective sliding amplitude or, better yet, the friction energy deduced from the fretting cycles. The (measured) displacement amplitude in fretting must only be considered as a semiquantitative variable.

Nevertheless, recent developments allowing direct measurement of the displacement at the contact position, using high-performance laser systems, open new possibilities to better formalize the sliding condition by a direct assessment of the displacement amplitude variable (Ref 52).

Alternative strategies, such as measuring the acoustic emission generated during fretting sliding, also could be considered to quantify the sliding condition and the sliding instabilities between partial and gross slip (Ref 53). One advantage of this approach is that it does not require recording the fretting cycle, which is sometimes not possible in an industrial setting.

Fretting Map Approach

The former analysis can be extended by varying the normal force, leading to the fretting map approach (i.e., sliding regimes and the related damage reported as a function of the applied displacement amplitude, δ_m^*, and the applied normal force, P, for a given contact configuration and a given number of fretting cycles). The running condition fretting map displays the different PSR, MFR, and GSR regimes (Ref 50).

The boundaries are usually characterized by power-law evolutions, although various authors consider linear approximations. Investigating the Mindlin formalism given for the elastic Hertzian sphere-on-flat contact for a homogeneous contact (i.e., similar elastic properties of the two counterfaces) leads to (Ref 41):

$$\delta_t^* = \frac{\mu}{R^{1/3}} \times \left(\frac{P}{E}\right)^{2/3} \times H_M \qquad \text{(Eq 8)}$$

with

$$H_M = \frac{3^{2/3} \times (2-\nu)}{2^{5/3} \times (1+\nu) \times (1-\nu^2)^{1/3}} \qquad \text{(Eq 9)}$$

where R is the sphere radius, E is the elastic modulus, and ν is the Poisson coefficient of the material. The corresponding Hertzian contact radius (a_H), the maximum Hertzian pressure ($p_{0,H}$) at the center of the contact, and the corresponding mean Hertzian pressure ($p_{m,H}$) are given by (Ref 45, 46):

$$a_H = \left(\frac{3 \times P \times R}{2} \times \frac{(1-\nu^2)}{E}\right)^{1/3} \qquad \text{(Eq 10)}$$

$$p_{0,H} = \frac{3P}{2\,\pi\, a_H^2} = \left(\frac{3 \times P}{2 \times \pi^3 \times R^2} \times \frac{E^2}{(1-\nu^2)^2}\right)^{1/3} = \frac{3}{2} \times p_{m,H} \qquad \text{(Eq 11)}$$

The pressure profile is characterized by an elliptical distribution:

$$p(r) = p_{0,H} \times \left(1 - \frac{r^2}{a_H^2}\right)^{1/2} \qquad \text{(Eq 12)}$$

where r is the radial distance from the contact center.

Assuming Amontons' laws of friction and a full gross slip condition, the shear profile is given by:

$$q(r) = \pm\,\mu\, p(r) \qquad \text{(Eq 13)}$$

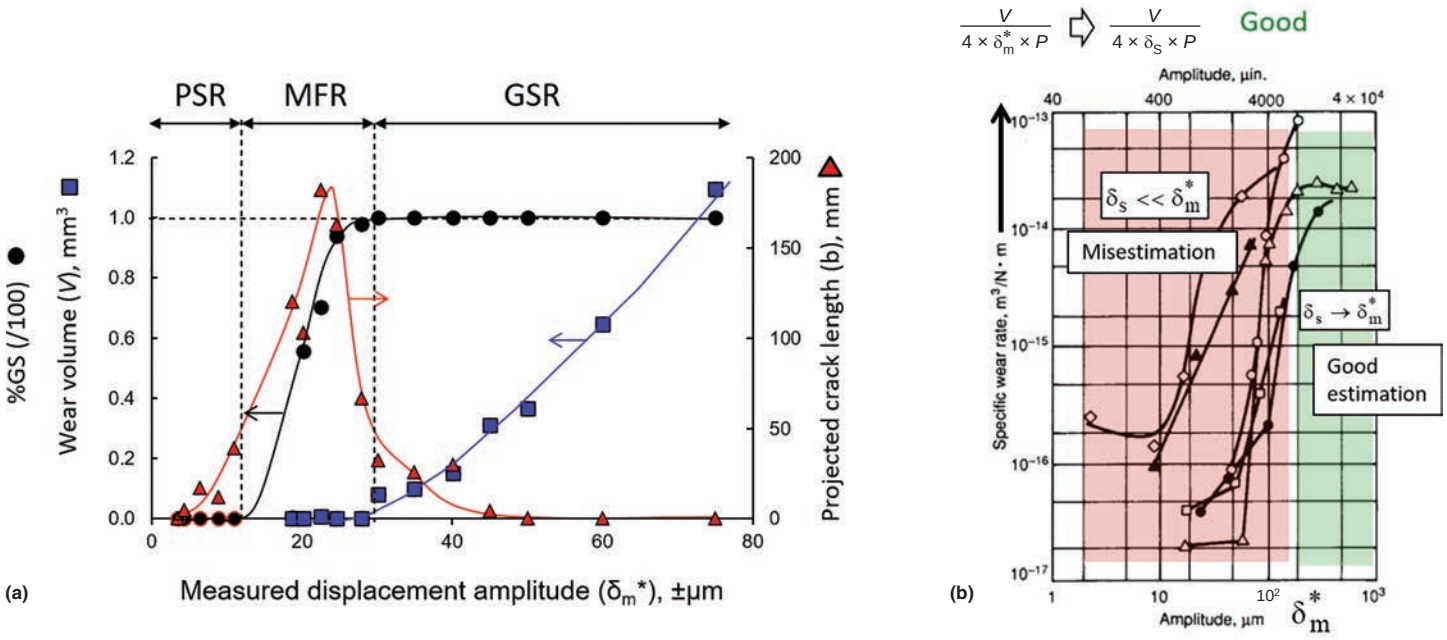

Fig. 10 (a) Fretting wear damage chart as a function of the applied displacement amplitude for a cylinder-on-flat contact. Quantification of the wear volume and crack length extension as a function of the fretting regime parameter, %GS. PSR, partial slip regime; MFR, mixed fretting regime; GSR, gross slip regime. Adapted from Ref 49. (b) Chart depicting how ignoring the difference between the displacement and the sliding amplitude can lead to a false deduction of the variation of the specific wear rate

This implies that the maximum shear, which is observed at the center of the contact, is equal to:

$$q\max,_{\mathrm{H}} = \mu \times p_{0,\mathrm{H}} \quad \text{(Eq 14)}$$

Under partial slip condition, the analysis must consider the presence of an inner zone inside the contact (Fig. 11). The radius of the stick annulus (c) and, more precisely, the ratio between the stick radius and the contact radius ($k = c/a_H$) is expressed by (Ref 46, 47):

$$k = \frac{c}{a_H} = \left(1 - \frac{\delta*}{\delta_t^*}\right)^{\frac{1}{2}} = \left(1 - \frac{Q*}{Q_t^*}\right)^{\frac{1}{3}} \quad \text{(Eq 15)}$$

where Q_t^* is the tangential force at the sliding transition, so that $Q_t^* = \mu \times P$.

Finally, the maximum shear under partial slip is not detected at the center of the contact but the stick boundary, such that:

$$q(r=c) = \mu p_{0,H}(1-k^2)^{\frac{1}{2}} \mu p_{0,H}\left(\frac{\delta*}{\delta_t^*}\right)^{\frac{1}{2}}{}_{\max} \quad \text{(Eq 16)}$$

Figure 11 illustrates the pressure and shear profiles, depending on the sliding condition.

After this theory, the theoretical transition is directly proportional to the coefficient of friction, proportional to the normal force to the power 2/3, and inversely proportional to the sphere radius to the power 1/3 (Ref 41).

The measured displacement amplitude is therefore given by:

$$\delta_{m,t}^* = \delta_t^* + C_A \times Q_t = \mu \times P \times \left[\frac{P^{\frac{-1}{3}} \times H_M}{R^{\frac{1}{3}} \times E^{\frac{2}{3}}} + C_A\right] \quad \text{(Eq 17)}$$

The latter can be effectively approximated by a linear relationship between $\delta_{m,t}^*$ versus P when C_A is large compared to the contact compliance. Then, from the running condition fretting map, the material response fretting maps can be established (Fig. 12). Four domains are observed. For very small displacement amplitudes inducing very small tangential force amplitude, no damage occurs (I). Above a threshold displacement related to threshold cyclic tangential force, crack nucleation can be observed (II). When the mixed fretting regime is achieved, cracking is still predominant, but surface wear begins (III) to induce a competition between the damage processes. Then, when a gross slip regime is established, fretting damage is essentially governed by wear induced by debris formation and debris ejection (IV). The fretting map approach is a very useful strategy to compare materials as well as surface treatments and palliatives against fretting wear phenomena, but it still remains a semiquantitative approach (Ref 50).

Quantification of Wear Induced by Fretting

Fretting cracking is detrimental only when a bulk fatigue stress is applied. Otherwise, the cracks will systematically stop. Furthermore, wear is negligible under PSR and MFR regimes. Therefore, this article focuses only on fretting wear problems and fretting wear phenomena under a gross slip regime.

Wear is a complex problem, and many strategies have been developed to quantify this phenomenon in order to predict the wear volume extension (Ref 54). The usual strategy to quantify the wear rate in tribology consists of comparing the wear volume (V) as a function of the Archard loading (W) (Ref 55). The Archard loading parameter is defined as the product of the normal force and the total sliding distance. For the gross slip fretting regime or sliding, it is expressed by:

$$\sum W = \sum_{i=1}^{N} 4 \times \delta_S\,(i) \times P(i) \quad \text{(Eq 18)}$$

For constant loading conditions, it is simplified to:

$$\sum W = 4 \times \delta_S \times P \times N \quad \text{(Eq 19)}$$

Then, by plotting the evolution of the wear volume, V, versus $\sum W$, linear correlations are approximated to determine the so-called wear coefficient, K ($mm^3/N \cdot m$), or specific wear rate (Fig. 13a):

$$V = K \times \sum W \quad \text{(Eq 20)}$$

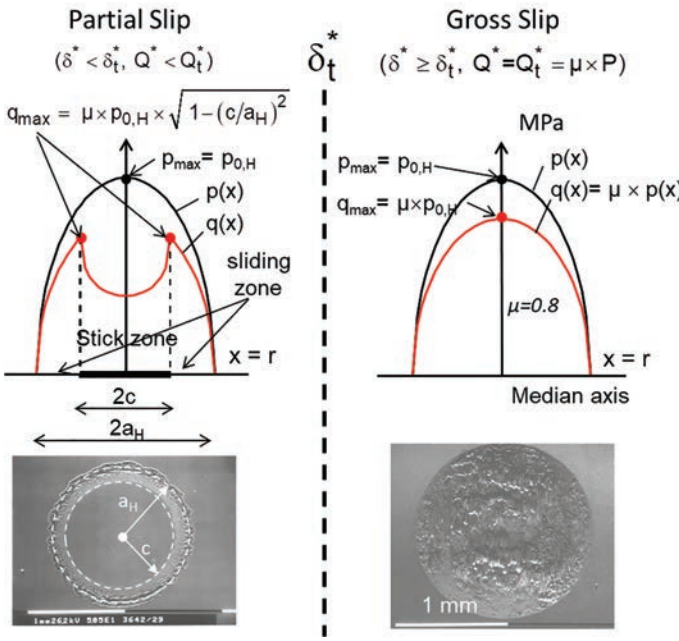

Fig. 11 Illustration of the pressure (p) and the shear (q) profiles along the median axis of the sliding direction for a Hertzian sphere-on-flat contact. Adapted from Ref 45, 46

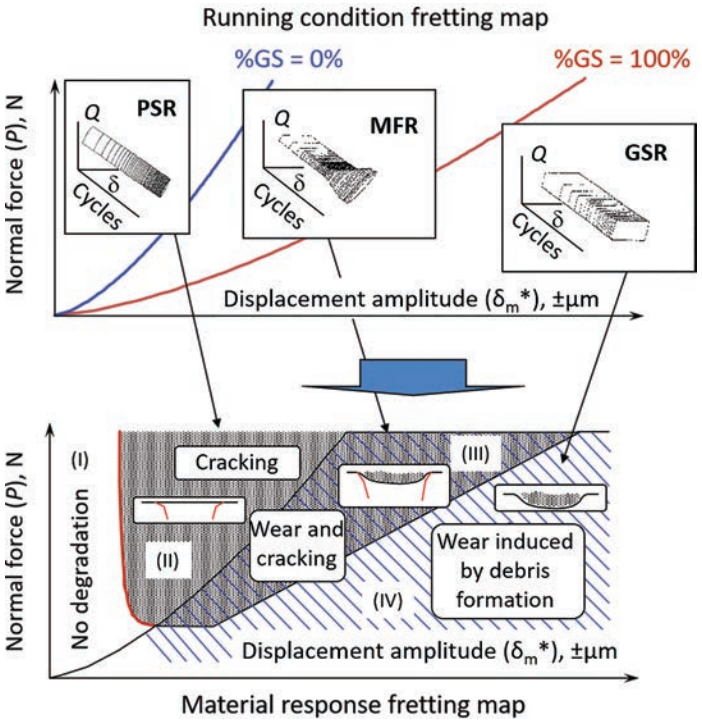

Fig. 12 Illustration of the fretting map approach. PSR, partial slip regime; MFR, mixed fretting regime; GSR, gross slip regime. Adapted from Ref 42

One limitation of the Archard approach is that it does not consider the coefficient of friction in its formulation. Hence, under varying friction response, a significant fluctuation can be observed.

An alternative strategy to quantify the wear is based on the accumulated friction energy, that is, the accumulated friction work (Fig. 13b) (Ref 41, 56–58):

$$\sum E_d = \sum_{i=1}^{N} E_d(i) \quad \text{(Eq 21)}$$

This approach is consistent with the fretting analysis, and it only requires one to sum up the fretting loop area over the whole test duration. If the coefficient of friction is constant, then both the Archard and the friction energy approaches are equivalent, so that:

$$\sum E_d = \mu_e \times \sum W = 4 \times \mu_e \times \delta_S \times P \times N \quad \text{(Eq 22)}$$

The wear volume is then quantified using an α energy wear coefficient:

$$V = \alpha \times \sum E_d \quad \text{(Eq 23)}$$

Figure 14 illustrates how, for a given wear mechanism (abrasive wear of ceramic

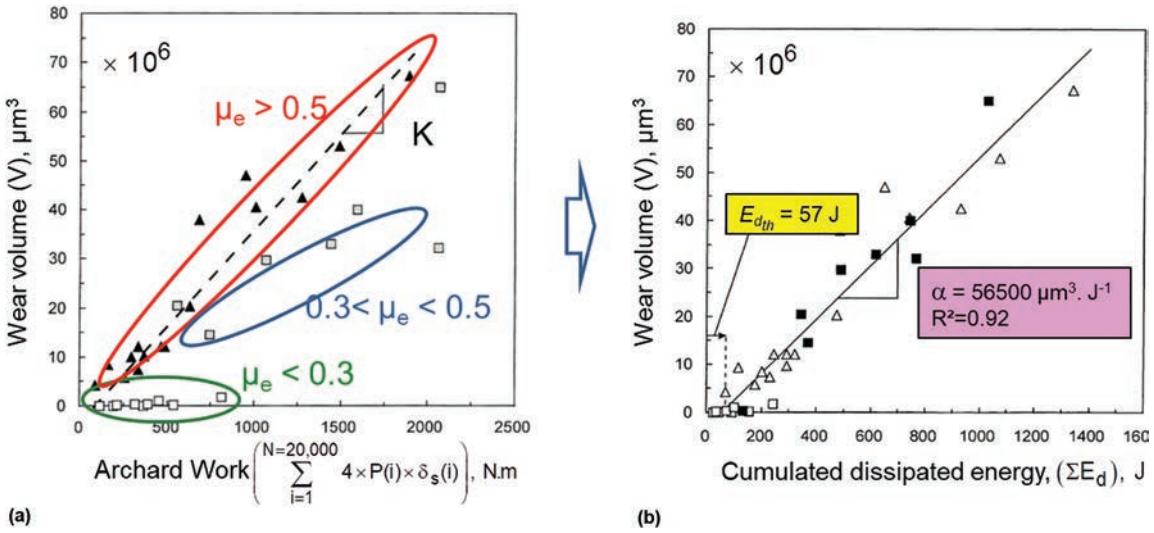

Fig. 13 Comparison between (a) Archard approach and (b) friction energy wear approach to quantify the wear evolution of a sintered steel displaying a significant fluctuation of the friction coefficient, depending on the loading condition. Adapted from Ref 42

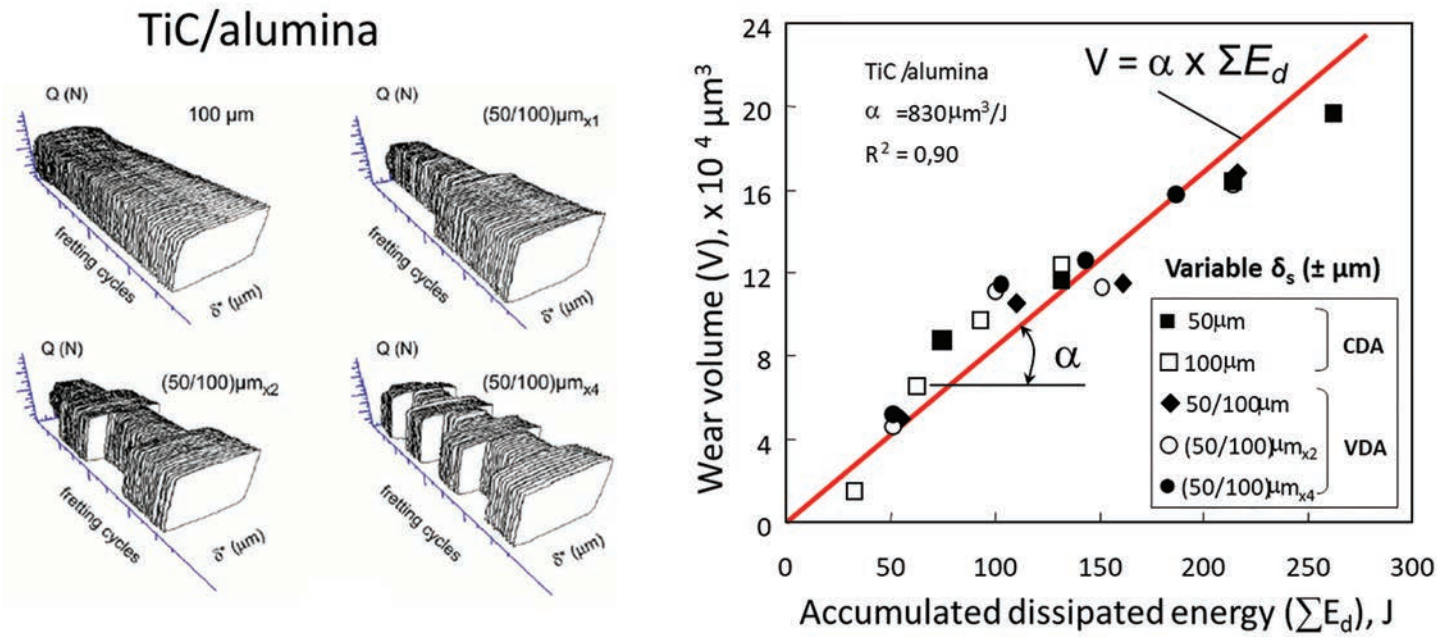

Fig. 14 Illustration and chart of the quantification of wear rate under gross slip using the accumulated friction energy parameter for constant (CDA) but also variable (VDA) gross slip displacement amplitudes; (TiC/alumina) sphere-on-flat contact. Adapted from Ref 59. Reprinted with permission from Elsevier

material) and a restricted spectrum of loading conditions, the energy approach is able to predict the wear volume approximation even for complex varying gross slip sliding conditions.

However, for a metallic interface, plastic transformation is activated within the interface before wear debris is even generated. This promotes a plastic recrystallization process, inducing formation of the so-called tribological transformed structure (TTS), which is very hard and brittle (Ref 60, 61). This initial transformation consumes a threshold energy, $E_{d_{th}}$. The wear law then must be corrected by introducing an energy offset in the formulation (Ref 42) (Fig. 13b):

$$V = \alpha \times \left(\sum E_d - E_{d_{th}}\right) \quad \text{(Eq 24)}$$

with $E_{d_{th}}$ the threshold incubation energy related to the transformation of the metal interface to TTS (Fig. 15).

As expected, hard ceramic materials such as TiC and TiN coatings display very low energy wear coefficient α (i.e., the highest wear resistances) but also very low threshold incubation energy ($E_{d_{th}}$) because no plasticity can be activated (Fig. 16).

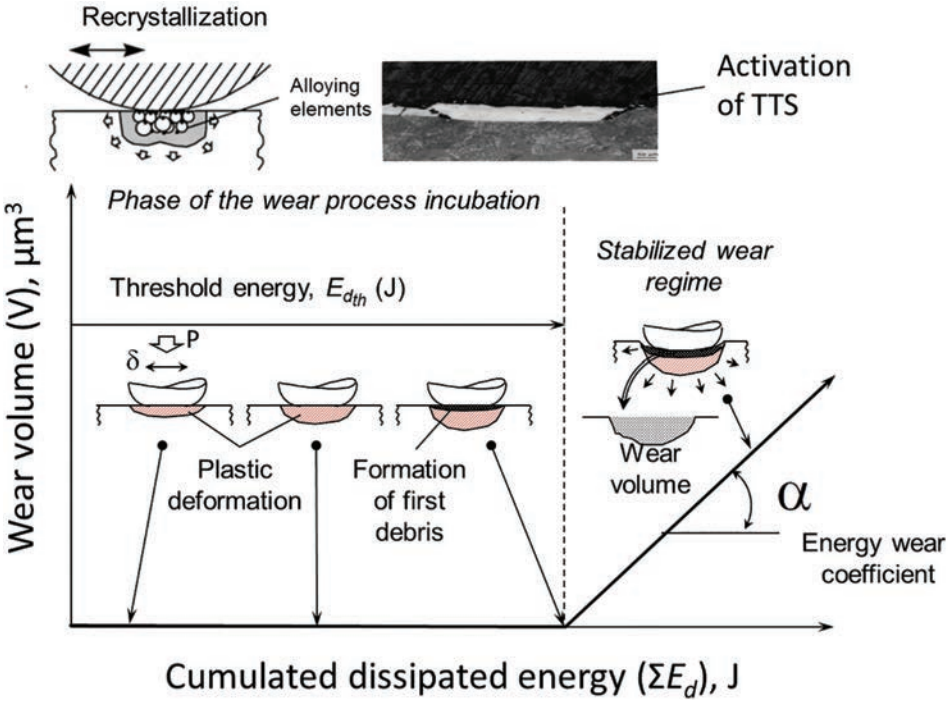

Fig. 15 Illustration of the fretting wear process related to metal interfaces (incubation period related to the formation of tribological transformed structure, or TTS). Adapted from Ref 42. Reprinted with permission from Elsevier

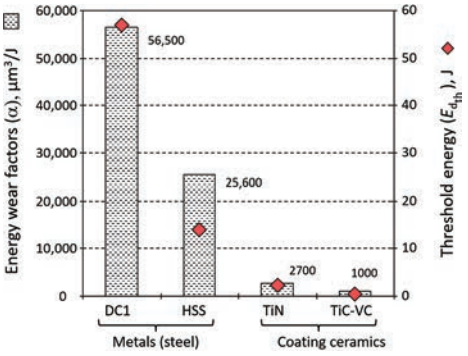

Fig. 16 Comparison between metals and ceramic coatings fretted against an alumina ball for similar lading conditions. HSS, high-strength steel. Adapted from Ref 42

Third-Body Theory

The Archard and friction energy wear approaches are consistent as long as a similar wear process is activated. However, in many situations the wear volume approximation cannot be described assuming a single wear coefficient. Indeed, like any other tribological phenomenon, fretting wear is a very complex process that not only depends on the contact materials but also on the whole contact system. A key aspect concerns the debris layer (also called third body or debris bed). Entrapped within the interface, debris greatly influences both friction and wear processes (Fig. 17). This is particularly evident for fretting sliding, because small sliding amplitudes tend to maintain the wear debris within the interface. Many investigations have been performed to better quantify this aspect, introducing the third-body theory (Ref 63). According to this theory, the wear rate evolution is not controlled by the friction work introduced in the interface but is related to the balance between the debris formation flow (Φ_f) generated from the degradation of the first body (bulk materials) and the debris ejection flow (Φ_e). Because wear debris can be recirculated within the interface, it needs a certain period of time to travel within the contact before being ejected. This approach implies an initial transition period during which the debris layer is formed. When it stabilizes, the wear rate evolves toward a stable steady-state response where it is equal to the debris ejection flow and thus to the debris formation flow:

$$\Phi_V = \Phi_f = \Phi_e \quad \text{(Eq 25)}$$

Figure 17 illustrates the principle of the third-body theory, in which both debris formation and debris ejection flows are plotted versus the debris layer thickness. The thicker the debris layer (H), the larger the debris ejection flow during each sliding sequence. Alternatively, the thicker the debris layer, the higher

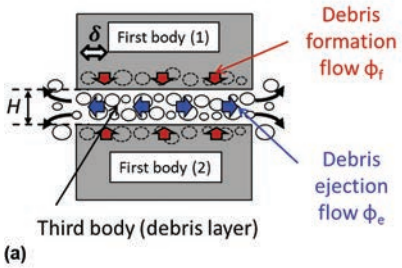

Fig. 17 (a) Schematic of the third-body theory. (b) Graph of debris flow concept as a function of debris layer thickness. Adapted from Ref 62

the friction energy consumed by the debris bed, the less damaged the first bodies, and finally the lower the debris formation flow. The equilibrium is reached when the debris ejection flow equals the debris formation flow, satisfying the former relationship (Eq 25). This theory also suggests that the steady-state wear regime corresponds to a constant debris layer thickness (H_{ss}). Obviously, by modifying the contact condition, another equilibrium point will be established, inducing another steady-state debris thickness. Later, this article details the potential interest in this approach to better interpret wear rate fluctuations as a function of applied fretting loadings, contact size, and contact geometry but also the rheological properties of the debris layer (Ref 64–67).

Contact Oxygenation Concept

The third-body theory is strategic to better interpret the effect of the debris layer in fretting wear. However, as detailed previously, the stability of the wear rate also depends on the stabilized wear mechanism. Fretting wear usually promotes either abrasive wear or adhesive wear phenomena. Abrasive wear implies a plowing process of the softer material by harder asperities, favoring the formation of oxide powder debris. It could be a two-body abrasive wear process in which the harder counterpart is the first body that directly interacts with the softer counterpart. However, it could be a three-body process in which the abrasive wear is controlled by the harder oxide particles constituting the third-body layer. Abrasive wear favors debris ejection, producing a huge quantity of oxidized particles. It generally leads to rather high wear rates, although no seizure phenomena are observed. In contrast, adhesive wear phenomena inducing severe metal-metal transfers usually trigger rather low fretting wear rates, because small sliding amplitudes limit the ejection of cohesive metal debris. However, catastrophic seizures inducing interface blocking are commonly observed. In many fretting interfaces, both abrasive and adhesive wear phenomena are observed simultaneously. The partition between abrasive and adhesive processes was recently formalized using the so-called contact oxygenation concept (Fig. 18) (Ref 68, 69), or the air distilling (Ref 17) or oxygen exclusion process (Ref 70).

According to this concept, the adhesive wear process is activated when the available di-oxygen partial pressure in the interface falls below a threshold value, p_{O_2th}. The di-oxygen partial pressure profile is at maximum at the contact borders (open air) but decreases toward the inner part of the contact due to the consumption of di-oxygen molecules reacting with fresh metal to form oxide debris or an oxide layer. The interface di-oxygen partial pressure profile can therefore be established as a balance between the di-oxygen diffusion rate from the external borders and the reaction rate with the metal surface exposed by the friction work. The reaction rate can itself be related to the friction power density or equivalent "$p \times v$" factor (i.e., pressure × sliding speed). Using this approach, one can explain the extension of the inner adhesive wear domain when increasing the contact pressure and sliding frequency (i.e., increasing the $p \times v$ factor) but also the contact size. Indeed, even if similar contact loadings are imposed, a larger contact reduces the access of di-oxygen molecules toward its central part, which explains the transition from pure abrasive wear in small contacts toward composite adhesive-abrasive interfaces in larger contacts. Note that adhesive wear extension was recently simulated by modeling the diffusion of the di-oxygen molecules within the interface and the reaction

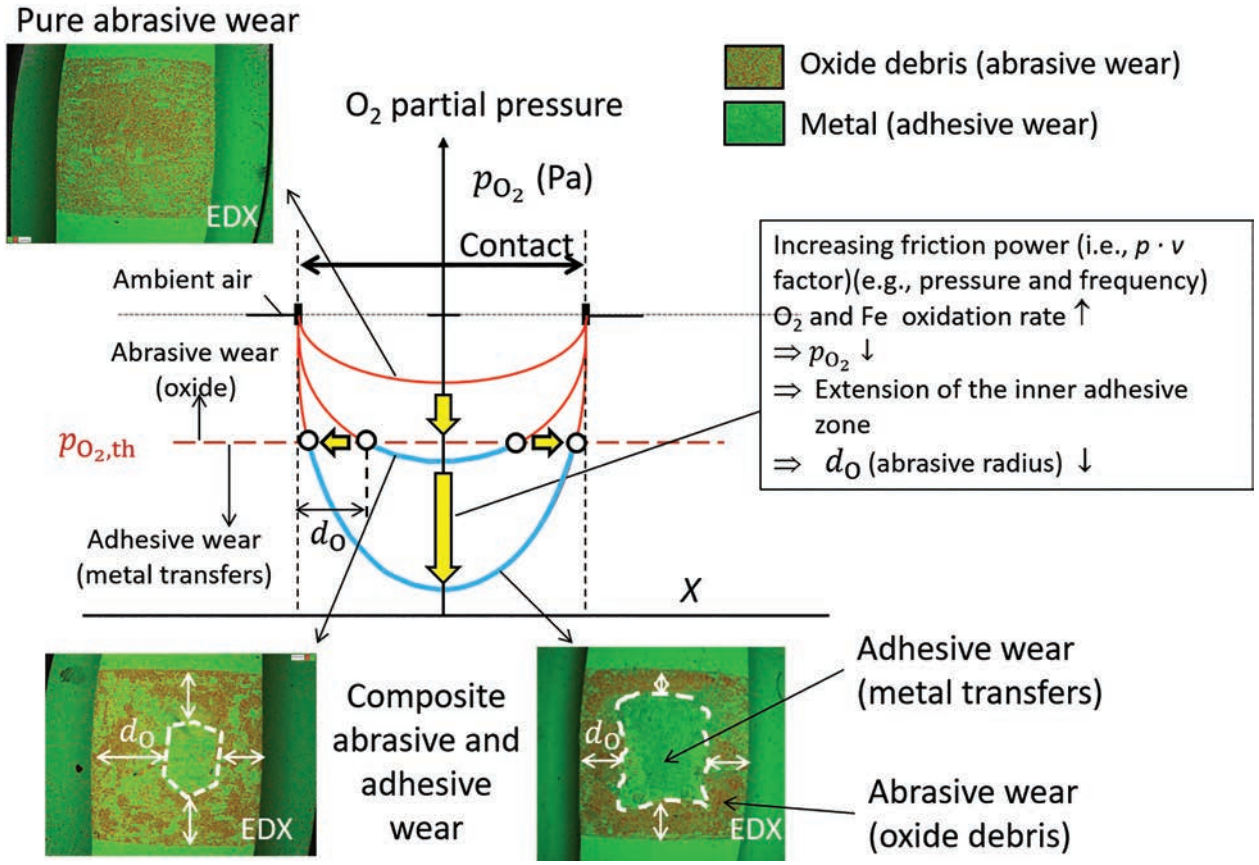

Fig. 18 Illustration of the contact oxygenation concept to formalize the transition from pure abrasive to composite abrasive-adhesive fretting scar interface (experimental validation using flat-on-flat interface). EDX, energy-dispersive x-ray. Adapted from Ref 68, 69. Reprinted with permission from Elsevier

rate through the oxidation process of the surface metal exposed by the friction process (Ref 71).

Obviously, the transition from pure abrasive to composite adhesive-abrasive wear mechanisms modifies the global fretting wear response as well as the corresponding wear rate. Hence, in addition to the third-body theory, the contact oxygenation concept must be considered to better interpret wear rate fluctuation under complex fretting sliding conditions. In the following section, various aspects of loading conditions regarding fretting wear are examined.

Sliding Amplitude

As detailed previously, the wear rate is highly dependent on the displacement amplitude and the transition from partial to gross slip regimes. However, when gross slip is activated, both Archard and friction energy suggest a proportional increase in wear volume with applied displacement, which, in turn, proposes a constant wear rate independent of the sliding amplitude (Fig. 19). Nonetheless, numerous investigations highlighted an increase in energy wear rate with sliding amplitude, particularly for materials prone to adhesive wear (Ref 72). This tendency was explained by the third-body theory, assuming that the larger the sliding amplitude, the easier the debris ejection flow, and consequently, the better the energy wear rate efficiency. To formalize this synergistic effect, the power-law function can be considered, in which the exponent expresses the sliding amplitude influence regarding wear rate evolution (Ref 72).

Normal Load

If the sliding amplitude is kept constant, there is a running-in period in which metal-to-metal contact predominates (Fig. 20) (Ref 74). This running-in period was shown to increase with the applied normal load (Ref 75). However, when the third-body layer is stabilized, a steady-state wear regime is established, and a linear increase of the wear volume can be observed. This linear behavior is the basement of the Archard and related friction energy wear approaches.

The second basement of the Archard wear formulation is related to the interaction between rough surfaces. The Bowden and Tabor theory is still applicable: When two surfaces are placed in contact and loaded, plastic deformation of contacting high spots (asperities) occurs (Ref 76). The real area of contact, A, is therefore directly proportional to the applied load, P:

$$A = \frac{P}{p_0} \qquad \text{(Eq 26)}$$

where p_0 is the yield pressure, which is approximately equal to $3Y$, and Y is the yield stress in tension. Note that the real contact area is very small compared to the apparent contact area. Because fretting occurs only at contacting areas, it follows that the amount of wear should be directly proportional to the applied load. This justifies the Archard and related friction energy wear formalism (i.e., $\sum W \propto P$), suggesting that the wear rate should be constant and nearly independent of the mean "apparent" contact pressure (i.e., normal load divided by apparent contact area). The investigation of a flat-on-flat low-alloyed steel interface, allowing constant apparent contact area condition, confirmed that as long as the mean contact pressure remains lower than the threshold value (i.e., $p_{m,th} \approx 100$ MPa, or 15 ksi, for the studied steel interface), the wear rate remains low and constant, defining the so-called mild wear regime (Fig. 21a) (Ref 77). Above the threshold pressure, a sharp increase in wear rate is observed, defining the so-called severe wear regime. The transition from mild to severe fretting wear rate can be interpreted using the Johnson diagram (Fig. 21b), where the elastic, elastic shakedown, and plastic shakedown or ratcheting metal responses are reported as a function of the friction coefficient and applied contact pressure. With this approach, as long as the metal stabilizes under elastic response, the accumulated plastic deformation dissipation is zero or negligible. Alternatively, if it does not stabilize, the plastic deformation continuously increases, promoting high wear rates.

Frequency

The effect of frequency has been extensively investigated (Ref 76–79). This research found increased wear rate with decreasing sliding frequency. The rise was related to the formation and disruption of oxide films. The longer the period, the thicker the oxide layer removed after each sliding sequence and, finally, the higher the wear rate. The question was considered more recently and was investigated as a

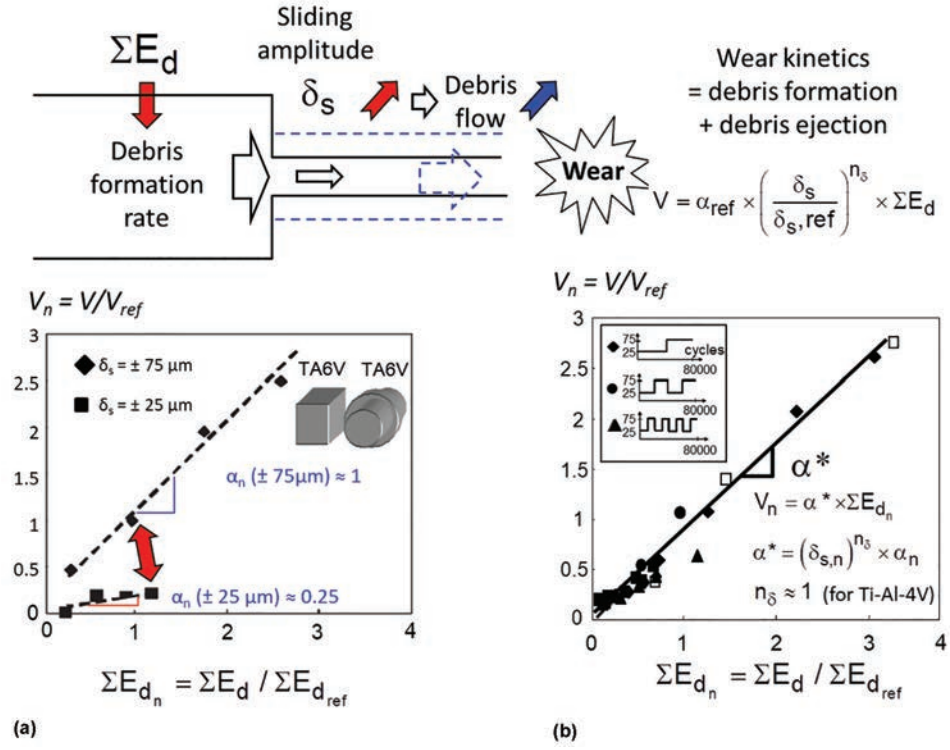

Fig. 19 Evolution of fretting wear rate increase with applied sliding amplitude for an adhesive wear Ti-6Al-4V interface. (a) Basic friction energy approach. (b) Extended friction energy approach (results normalized versus a reference test condition: $\alpha_n = \alpha/\alpha_{ref}$; $\delta_{S,n} = \delta_S/\delta_{S,ref}$). Diagram at top adapted from Ref 72. Graph in (b) adapted from Ref 73 and reprinted with permission from Elsevier

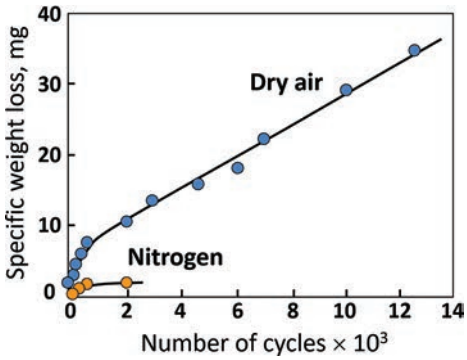

Fig. 20 Fretting wear weight loss versus fretting cycles for mild steel under gross slip 90 µm displacement amplitude in both dry air and nitrogen atmosphere. Adapted from Ref 74

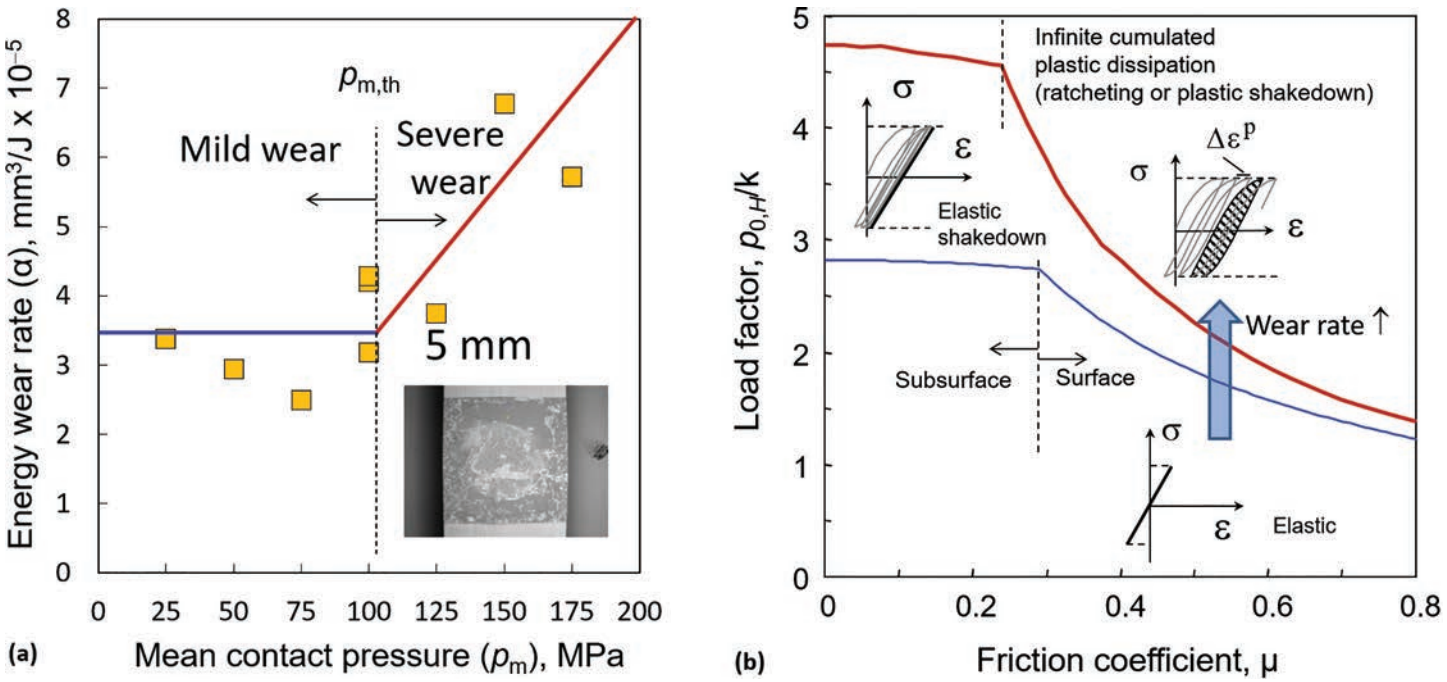

Fig. 21 (a) Evolution of wear rate of a flat-on-flat low-alloyed steel contact as a function of the mean contact pressure for gross slip fretting sliding. Adapted from Ref 77. (b) Johnson diagram displaying the various elastic and elastoplastic responses of metals as a function of the mean contact pressure and the friction coefficient (sphere-on-flat contact). Adapted from Ref 46

means of speeding up fretting wear tests, assuming that high frequencies had no significant effect. The range of frequencies investigated was from 10 to 10^4 Hz (Ref 78), using steel specimens in a crossed-cylinder contact. The conclusion was that, in the partial slip situation, although there was little effect on measurable wear, the increase in the interfacial strain rate at high frequencies led to increased fatigue damage and increased corrosion due to the rise in temperature. However, under the gross slip situation, the wear rate can be multiplied by two when the sliding frequency is reduced from 10 to 1 Hz (Ref 68, 77) (Fig. 22). These conclusions suggest that caution must be taken regarding acceleration tests (i.e., increasing the fretting frequency), because it can underestimate the fretting wear rate. In addition, as detailed previously through the contact oxygenation concept, an increase in sliding frequency by increasing the friction power favors adhesive wear extension, which, again, can explain the lower wear rate observed under high-frequency conditions.

Not all movements that can lead to fretting damage take place at frequencies higher than 5 to 10 Hz. Relative movement can be due to differential thermal expansion, which, if arising from diurnal changes in temperature, can have a frequency of only a few cycles a day. The pressurizing of airplane cabins is in a similar frequency range. The movement of mooring cables due to water flow is of considerably higher frequency but is assumed to be 0.1 Hz. In such circumstances, the environmental and corrosion effects have much greater importance. This suggests that many investigations are still required to deepen the fretting wear response under low and very low sliding frequency (i.e., below 1 Hz).

Type of Contact

As discussed previously regarding the third-body theory, the ease with which debris can escape from the contact region is an important factor in the fretting process itself. It also gives rise to further problems by contamination of other surfaces (in a machine, for example). The original design of an apparatus with torsional fretting of annulus-on-flat (Ref 4) (Fig. 23a) has many advantages, including the fact that no part of the contacting surfaces becomes exposed, and for debris to escape, it must move at right angles to the direction of motion. Another slight advantage is that the amplitude of slip has a small variation from the inner to the outer edge and can therefore be used to investigate the effect of amplitude in one test. With flat-on-flat contact surfaces, however, the initiation and development of areas of wear damage are sporadic no matter how carefully the surfaces are prepared and the alignment controlled (Fig. 23b). Contact pressure is usually expressed as the nominal value calculated from the apparent area of contact and the applied load. Measurement of the real area of contact would require contact-resistance measurements at the outset of the test, or it could be calculated with knowledge of the yield pressure. Contacts consisting of

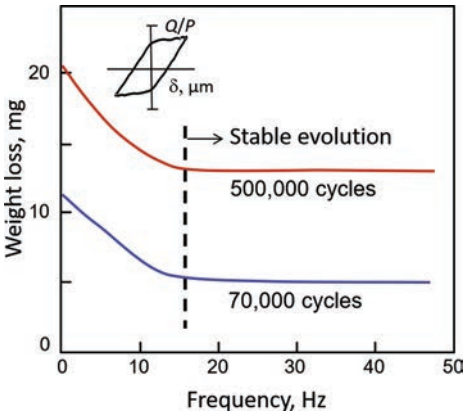

Fig. 22 Plot of wear versus frequency of fretting vibration. Adapted from Ref 24

Hertzian-type geometrical surfaces such as sphere-on-flat, cylinder-on-flat, and crossed cylinders (Fig. 23c) allow some initial calculations based on elastic theory of the area of contact and stress distribution therein. However, these quantities are rapidly changed as the wear process proceeds.

Also, such contacts increase the possibility for debris to escape. It was shown that the escape of debris in the crossed-cylinder arrangement is greatly influenced by the direction of motion (Ref 80). The arrangement shown in Fig. 24(a), with sliding direction perpendicular to the static bottom cylinder axis, allows for fast debris ejection. The debris

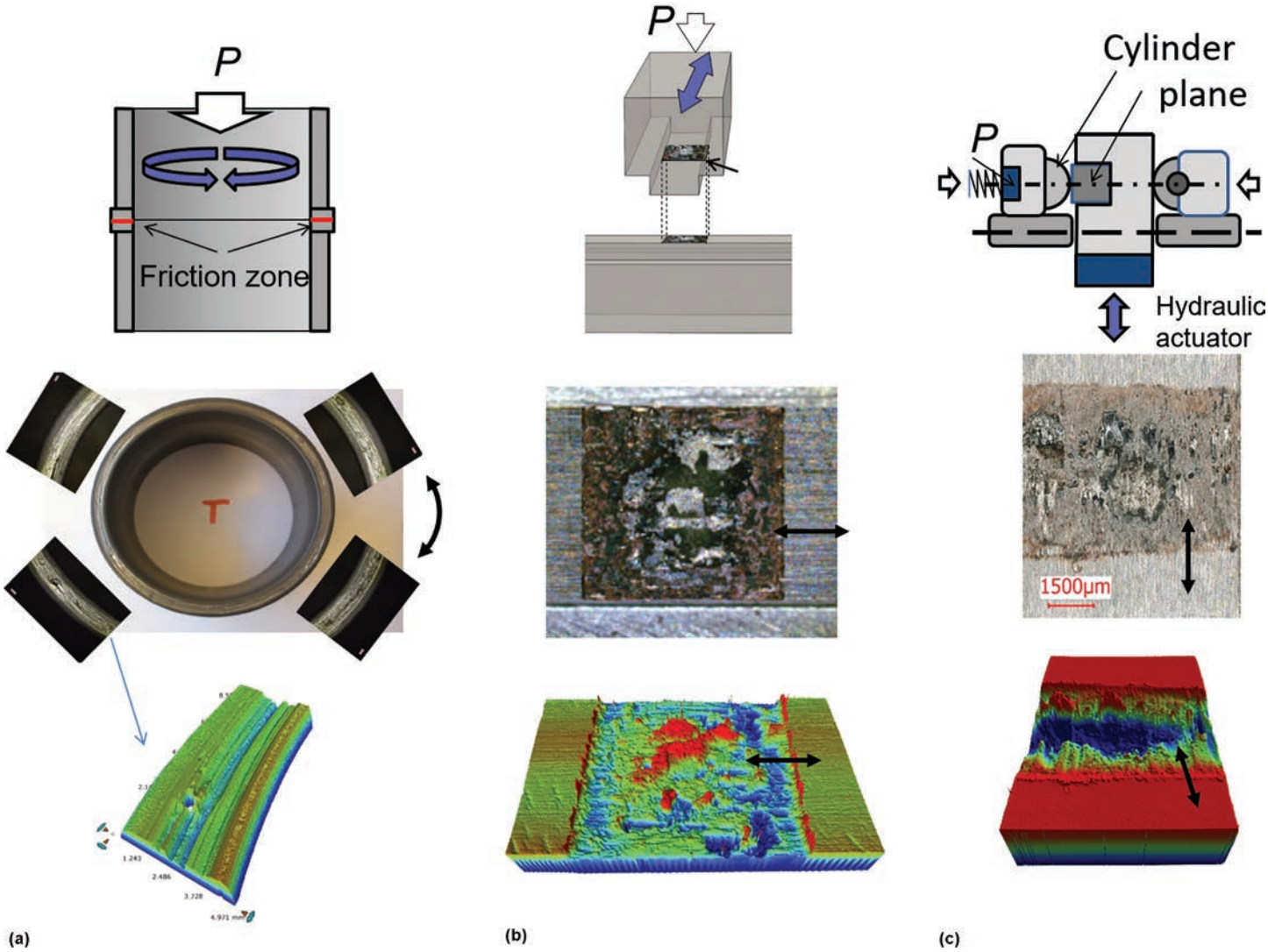

Fig. 23 Various contact configurations. (a) Torsional fretting of annulus. (b) Flat-on-flat contact. (c) Cylinder-on-flat contact

layer thickness is small, leading to more frequent metal-to-metal interaction and a higher wear rate than the arrangement shown in Fig. 24(b), in which the sliding direction is collinear to the bottom cylinder axis. However, in experimental investigations, the ease and cost of preparing specimens is a significant factor, and the crossed-cylinder arrangement is one of the most convenient. It also mirrors somewhat the situation of contact between wires in steel ropes.

More recently, investigations have focused on evaluating how contact size can influence the fretting wear rate. Keeping constant the contact pressure and the sliding amplitude, an asymptotic decreasing of the wear rate as a function of the contact size (i.e., half-contact width) was detected (Fig. 25) (Ref 73). This tendency was ascertained by showing that the fretting wear rate stabilizes above a threshold contact size. This tendency can be explained by considering both the third-body and contact oxygenation approaches. By increasing the contact size, the delay to eject the debris is longer, the debris ejection flow is reduced, and consequently the wear rate is decreased. Alternatively, by increasing the contact size, the inner adhesive area is extended, and the global wear rate is consequently reduced, because adhesive wear under fretting sliding tends to generate a lower wear rate than abrasive wear processes (Ref 68). One important conclusion is that small laboratory contact conditions tend to overestimate the fretting wear rate observed in large industrial assemblies, providing conservative predictions of fretting wear damage.

Type of Vibration

In most experimental investigations, vibration is a simple harmonic motion of constant amplitude. This may be so in practical cases of rotating shafts, but it is very different in situations where frequencies may vary and pass through areas of resonance. In addition, aircraft structures are entirely under the influence of random loading, with no fixed frequency or amplitude. The same can be said of ropes and cables in moorings, overhead ropeways, and elevator ropes.

There have been few investigations into this aspect of fretting wear. To investigate, specific fretting test machines must be developed, allowing frequency variations, phase differences between tangential and normal vibration, and the control of resonance (Ref 81). To account for these effects, three areas were identified:

- Subresonant loading conditions in which the damage was said to resemble typical fretting damage
- Resonant conditions in which the surface damage was significantly less due to the lower dissipation of energy due to friction

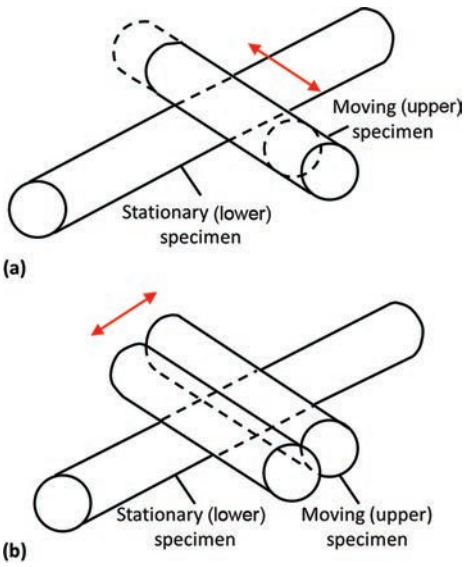

Fig. 24 Two test directions for determining fretting in a crossed-cylinder arrangement. (a) Parallel to the axis of the lower specimen. (b) At right angles to the axis of the lower specimen

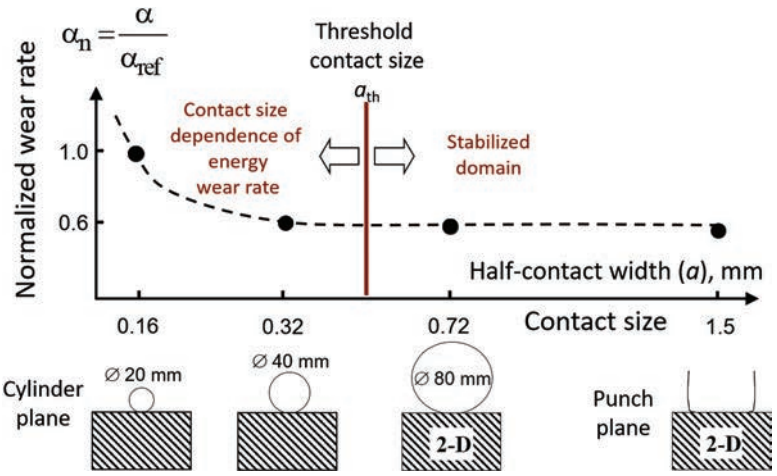

Fig. 25 Normalized evolution of the energy wear rate of a Ti-6Al-4V interface as a function of contact size (keeping constant all of the other fretting wear loading parameters). Adapted from Ref 73. Reprinted with permission from Elsevier

- Superresonant operation, which showed tearing of the surface that was associated with a phase shift of 90° between the tangential and normal vibrations

The fluctuation of the normal load during the fretting sliding condition was more recently investigated to reproduce the fretting wear process at the dovetail blade disk interface (Ref 17), where, during the macro sliding sequence, the normal force varies in phase from a minimum to a maximum contact pressure (Ref 68) (Fig. 26). This change in the wear process leads to significant fluctuation of the wear rate.

Due to the fluctuation of the normal load, the fretting cycle is not quadratic but displays a typical triangular fretting loop shape. Note that fluctuation of the normal load can modify the contact oxygenation, leading to the transition from composite abrasive-adhesive to pure abrasive wear response. When the normal load is kept constant, the contact is closed and a composite abrasive-adhesive wear process is observed. When the normal force fluctuates (i.e., $R_P = P_{min}/P_{max} < 1$), the interface is better oxygenated and the wear process evolves toward a pure abrasive phenomenon. This evolution can significantly modify the wear rate of the studied interface, which implies that variation of the normal force must be considered to reproduce the industrial situation, thus achieving reliable fretting wear predictions.

This concept was extended in Ref 82 and 83 using a very innovative test machine, which allowed the investigation of random normal force and sliding loadings. Using this experiment, it was shown that the energy wear rate under Gaussian random excitation, such as that detected in an industrial assembly, is significantly higher than that observed for a conventional sinusoidal signal. This result is very important, suggesting that the conventional sinusoidal-signal fretting wear investigations tend to underestimate the real wear rate operating in industrial contact assemblies in which Gaussian random excitation is usually encountered.

Impact Fretting

The former analysis of varying normal force superimposed on tangential movement is considered for situations in which the two surfaces remained in constant contact. The circumstances in which the two surfaces can become separated during some part of each cycle are somewhat different because of the contribution of impact. This fretting-impact configuration is a problem frequently encountered in heat exchangers, where pipes or fuel rod containers are restrained by supports or baffles but experience vibration as a result of fluid flow.

Two types of wear can be distinguished in the practical case encountered in nuclear reactors. The first type involves whirling of the tube, resulting in intermittent unidirectional sliding, and is obviously not fretting. The small-amplitude movement that results in fretting-type damage is the result of flow-induced vibrations. The important parameters are impact force, clearance between tube and support, support plate thickness, and frequency. The wear rate for stainless steel increases by an order of magnitude for a tenfold increase in impact force, and a similar increase for a fourfold increase in the clearance. Increasing the support plate thickness from 10 to 20 mm (0.4 to 0.8 in.) reduces the wear rate from 0.7 to 0.2 μm (30 to 8 μin.) per 10^6 cycles. At frequencies below 40 Hz, there is no effect of frequency, but at higher frequencies, the wear rate is reduced due to the reduction in contact time per cycle (Ref 83). These results were obtained at room temperature, whereas in operation, these devices would be at a higher temperature; thus the wear rates could be profoundly influenced both by temperature and environment.

Much research (Ref 84) indicates that the combination of impact and fretting is more severe than fretting alone, whereas much of the work on tube and tube support vibration suggests that impact contributes little to the wear rate and that continuous contact is more damaging (Ref 84, 85). An important variable in considering this type of motion is the phase relation between the normal and tangential vibrations. Differences are to be expected between impact at maximum tangential velocity and zero velocity (Ref 86). Also, the time period per cycle that contact is made is of great significance. In Ref 83, contact times per cycle are quoted as a function of frequency. Rigs have been constructed to study the effects of these phase relationships, particularly under severe environmental conditions (Ref 83). The effect of angle of incidence was more precisely investigated in Ref 87, showing that the maximum total energy loss was observed at approximately 30°, whereas the highest wear rate was observed at approximately 20°.

Surface Finish

Early observations of practical examples of fretting damage suggested that the more highly polished the contacting surfaces are, especially if flat, the worse the damage will be. On polished aluminum, where the debris is largely Al_2O_3 (corundum) with a high hardness, it could spread the damage, whereas on a rough surface the debris can escape into the hollows between the actual contact areas. There is also the possibility that on a rough surface, if the exciting force is of small amplitude, some of the relative movement will be taken up by elastic deformation of the asperities.

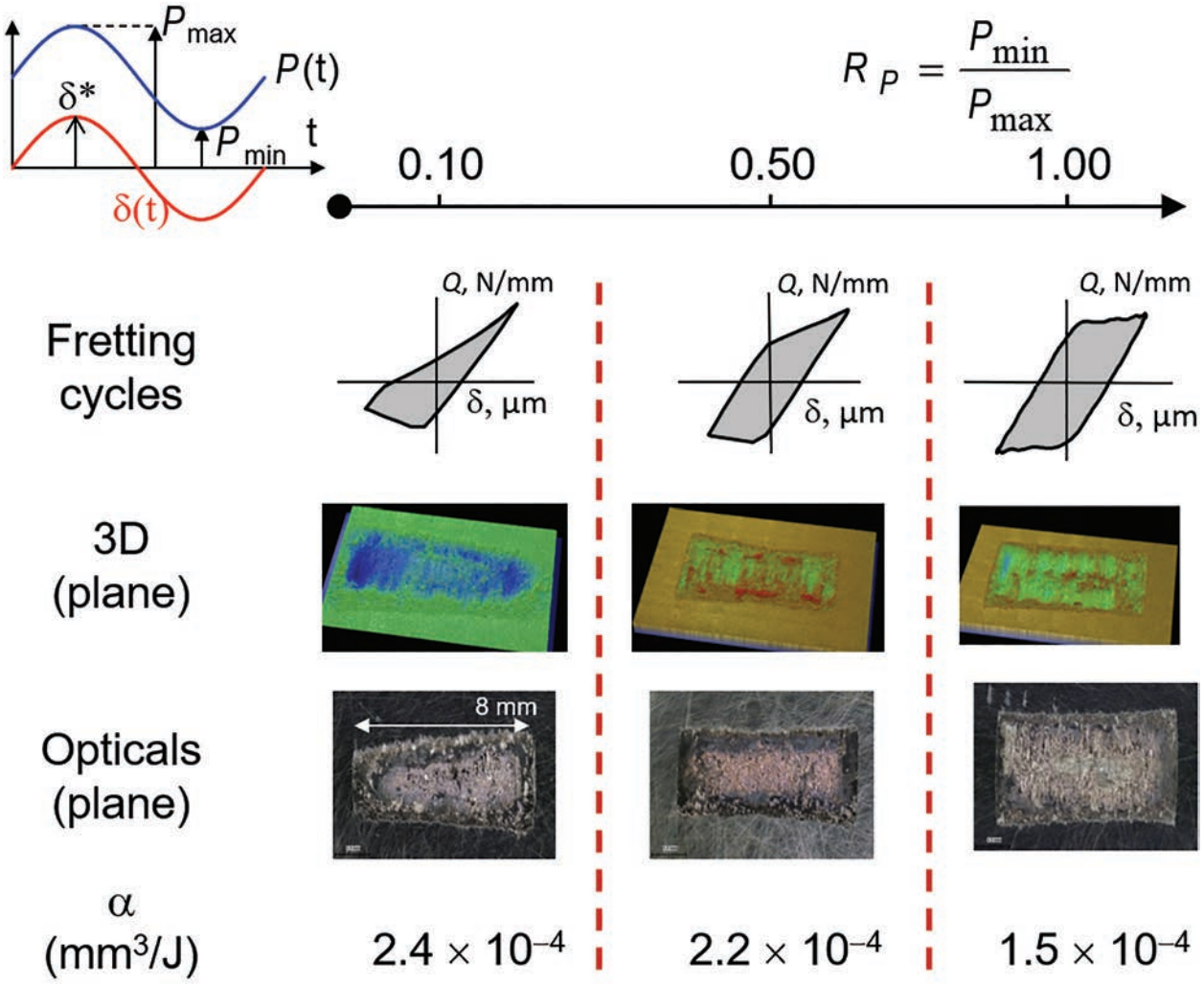

Fig. 26 Diagram revealing how fluctuation of the normal force during a fretting cycle can modify the fretting cycle and the related wear regime. Adapted from Ref 68. Reprinted with permission from Elsevier

One study shows that a rougher surface suffers less damage (Ref 88). A recent investigation underlined that a smooth interface tends to significantly increase the coefficient of friction but in turn decreases the energy wear rate, favoring adhesive wear processes (Ref 89). This tendency can again be explained, assuming the contact oxygenation concept. Smooth interfaces limit di-oxygen molecule access within the interface, consequently favoring the adhesive wear process. Metal transfers and adhesive wear phenomena thus prevail, inducing a high coefficient of friction and a small wear rate, although seizure phenomena are activated.

Shot peening is a widely applied surface treatment that produces roughening, work hardening, and residual compressive stress in the surface. Waterhouse showed that shot peening a steel surface reduced the coefficient of friction in fretting (Ref 90), but this could also be due to work hardening and possibly also to compressive stress. To investigate this phenomenon further, and to try to separate the three effects of shot peening, a series of tests were carried out on treated cylindrical steel specimens. The residual stress and work hardening could be removed by annealing, the residual stress could be reduced by controlled tensile straining, and the surface roughness could be removed by careful surface polishing (Ref 91). The shot-peened surface of 0.4% C steel leads to a lower fretting wear rate; however, polishing raised the level of wear to that of the unpeened steel. Hence, from this study it was concluded that compressive residual stress plays a small effect regarding wear rate, but the initial surface roughness induced by shot peening, by improving contact oxygenation and limiting metal seizure, is beneficial.

Residual Stresses

Because one of the possible mechanisms of fretting wear is surface fatigue, it is to be expected that a residual-stress field will have some effect on the wear process. To investigate this aspect, a decoupled approach—in which the crack analysis under partial slip was monitored as a function of the tangential force amplitude, and wear under a gross slip condition was investigated as a function of the friction work or sliding amplitude—must be used (Fig. 27) (Ref 92). It suggests that compressive shot peening residual stresses limit the crack propagation under partial slip but have no effect regarding wear volume under a gross slip condition (confirming former results, Ref 90, 91). Fretting wear under gross slip is better reduced by applying WC-Co coatings, which also increases crack resistance under the partial slip condition.

Alternatively, fretting sliding by promoting plastic deformation on a surface tends to erase the former compressive stress previously introduced by the shot peening treatment (Ref 93). Hence, if the shot peening compressive stresses fade under normal fatigue, they disappear much more rapidly under fretting fatigue

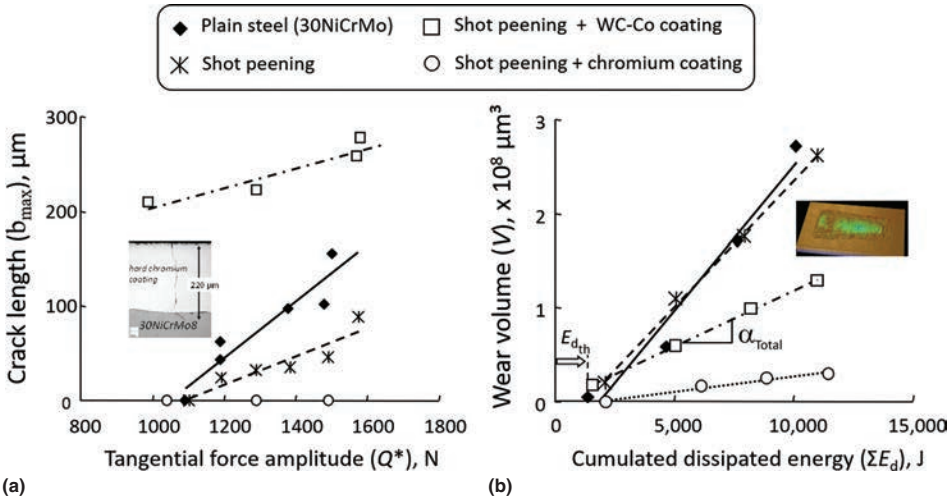

Fig. 27 (a) Investigation of crack length extension under a partial slip condition as a function of the tangential force amplitude. Compressive residual stresses limit the crack propagation. (b) Investigation of wear volume extension under a gross slip condition as a function of the friction energy. Compressive residual stresses do not influence the wear resistance. Adapted from Ref 92

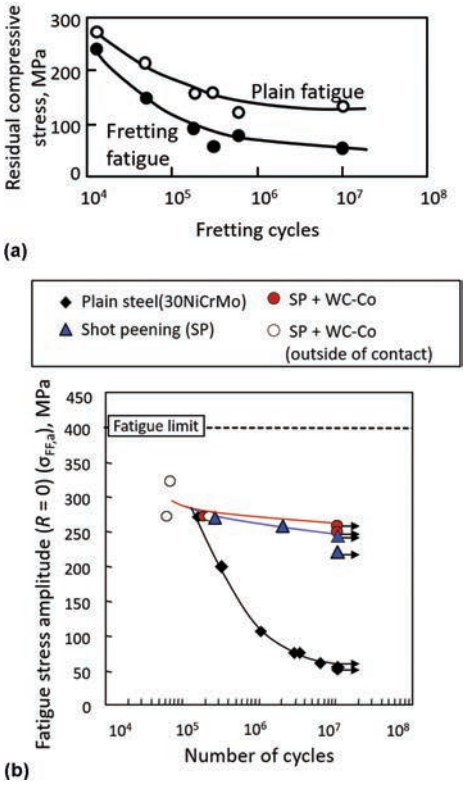

Fig. 28 (a) Fading of surface compressive stress induced with a number of fretting cycles by shot peening. Adapted from Ref 93. (b) Evolution of fretting fatigue endurance (cracking failure) as a function of fatigue stress for constant partial slip fretting loading (P = Cst, Q^* = Cst). Comparison between surface treatments (shot peening, or SP) and coatings. Source: Ref 95

(Fig. 28a). However, despite this limitation, most of the investigations confirm that shot peening treatments and the remaining residual compressive stress highly improve fretting fatigue endurance, particularly under a partial slip condition in which limited-contact plastic deformations temper the residual-stress-erasing process (Ref 94, 95) (Fig. 28b).

Materials

If fretting wear is a possible occurrence due to the design of a machine or structure, it may be possible to reduce the effect by choosing materials that are more resistant to such damage. This section deals with bulk materials not coated or surface treated; coated and surface-treated materials are dealt with in the section "Prevention of Fretting Damage" in this article. In addition, information on the behavior of new materials, such as composites and ceramics, also must be considered because of their increasing use in engineering applications.

Steels have been most extensively studied, largely because of their ability to change mechanical properties over a wide range by heat treatment without changing their chemical composition. In experiments with a steel ball on a steel flat, in which the hardness was varied from 220 to 850 HV, there was little difference in the wear loss (Ref 96). However, additional investigations suggest a lower wear rate by increasing the hardness (Ref 97). In crossed-cylinder experiments with three alloys of the same crystal structure, increasing hardness is shown to lead to a decrease of the transition amplitude from partial to gross slip. This could be explained by the fact that softer material allows a plastic accommodation within the interface, which in turn shifts the sliding transition. In addition, as detailed previously regarding tribological-transformed structures, in materials such as copper, austenitic stainless steel, carbon steel, titanium alloys, and all materials of low stacking-fault energy, work hardening occurred, leading to a hard, white, etch-resistant layer (Fig. 29).

This material is extremely hard and tends to develop cracks. It often is referred to as martensite, and some authors have regarded this as evidence that high local temperatures can be developed in fretting. The question of temperature rise is controversial due to the very small sliding amplitudes; the friction dissipation is in fact very small. Heat-source simulations suggest a rather small increase of contact temperature (less than 100 °C, or 180 °F), particularly for conductive metals. Hence, the hypothesis of high local temperatures inducing this martensite structure does not seem consistent.

More recent developments suggest that the formation of these very hard layers is in fact generated by an overaccumulated plastic deformation, constrained by the very high compressive hydrostatic stress state imposed by the quasi-static normal load, which induces a recrystallization process. A nanostructure is formed, leading to the so-called white layer, and this nanograin structure leads to very high hardness, according to the Hall-Petch theory.

Metals and alloys that rely on a protective oxide film for corrosion resistance can suffer considerable fretting damage in environments (for example, ambient air) that would not be considered particularly corrosive. These include the more reactive metals such as aluminum, titanium, zirconium, and chromium when used as elements to alloy stainless steels. When dissimilar metal pairs are fretted against each other, their mutual solubility is a factor in the severity of the damage. Nickel, chromium, and iron are damaged severely when fretted against iron or chromium because of high mutual solubility; however, the damage is mild when these metals are fretted against copper or silver, because there is no solubility (Ref 98).

In the fretting of polymers against steel, the possibility exists that one material will be transferred to the opposite surface. Damage arises in this case from platelike iron oxide particles adhering to the polymer; thus, the process becomes the fretting of two oxide-coated surfaces. Damage can occur to the polymer by the formation of cylindrical wear particles formed by the rolling up of thin detached surface layers, which are extruded in a direction at right angles to the motion (Ref 99).

In an investigation of fretting wear of fiber-reinforced polymers (composites) in contact with an aluminum alloy, weight loss was used to measure the damage (Ref 100). At amplitudes < 900 µm (<0.036 in.), the wear was low and showed a slight increase with increasing amplitude. Above 900 µm (0.036 in.), the wear accelerated. The wear rate showed a stepwise increase with frequency, the critical frequency being 35 Hz at room temperature, but decreased to 20 Hz at 80 to 100 °C (175 to 212 °F) due to a local rise in temperature. Unlike metals, which show a linear increase

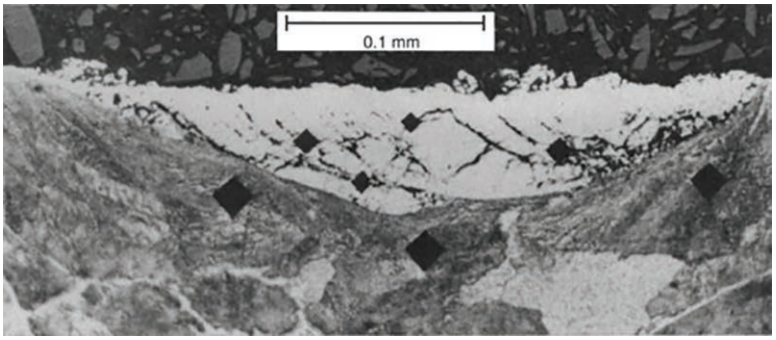

Fig. 29 Cross-sectional view of a white layer of martensite produced by fretting of a carbon steel connecting rod. Axial stress: 0 to 380 MPa (0 to 55 ksi); contact stress: 40 MPa (6 ksi); fretting cycles: 10^5. Sample was nital etched and viewed with scanning electron microscopy.

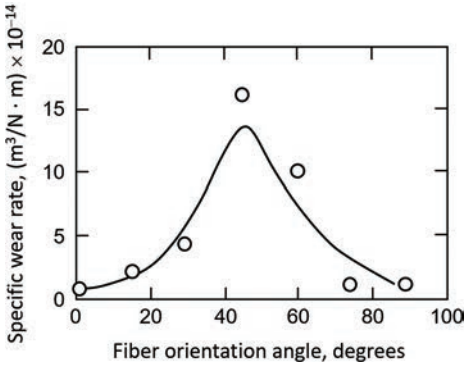

Fig. 30 Plot of fretting wear versus fiber orientation angle in a composite

in wear with increasing normal load, these materials show little effect of load up to a critical value at a pressure of 20 MPa (3 ksi), above which a rapid increase occurs. Fiber orientation with respect to sliding direction is another variable with these materials. Here, the specific wear rate was negligible at angles of 0 and 90° between fiber axis and sliding direction but showed a pronounced peak at 45°, as did the coefficient of friction (Fig. 30).

In experiments involving the fretting of sintered alumina against a wide variety of metallic materials in a crossed-cylinder configuration, no detectable wear was found on the alumina, although metal transfer to its surface occurred (Ref 101). A similar result was found in fretting a steel ball against alumina, silicon nitride, and zirconia in dry air (Ref 102); however, silicon carbide produced equal wear on the ceramic and steel. An increase in relative humidity generally resulted in a decrease in wear rate except in the case of silicon nitride, which exhibited behavior similar to that of silicon carbide. It appears that when oxides such as alumina and zirconia are fretted, there is little damage. Fretting alumina against alumina produced no measurable wear, although some polishing of the surface was apparent (Ref 80, 103) (Fig. 31).

Wear Debris

Debris oozing from a joint or connection in machinery is often the first indication that fretting damage is occurring. In recent years, the role of debris in wear processes has been given considerable attention, because it can build up between the sliding surfaces and increase the number of interfaces from one to two (Ref 63). This is particularly the case in fretting, where escape of the debris is greatly restricted compared with unidirectional sliding. This section focuses on the form, composition, and role of the debris.

It is well established that the debris on mild steel and other steels in air is essentially α-Fe_2O_3, which, when finely divided, is reddish brown in color and nonmagnetic. Its hexagonal crystal structure is identical to that of α-Al_2O_3. Under high compressive loads, it can become compacted, and its color is then black and iridescent. In this respect, it is identical to the mineral hematite, which in massive form is blackish but is red when powdered. On aluminum, the debris is black and consists of aluminum particles surrounded by Al_2O_3. The aluminum content is 23%, and the powder is pyrophoric (Ref 104). In other metals, such as copper and titanium, the debris is the expected oxide. In some cases, depending on the method of its production, the debris can contain some unoxidized metal. The oxide debris particles are usually very small, less than 1 μm in size (Fig. 32). However, depending on the contact loading and ambient condition, this fine powder debris structure can agglomerate, leading to thin platelets a few micrometers thick and 50 to 100 μm (0.002 to 0.004 in.) in diameter.

The role of debris regarding wear has been demonstrated by performing tests in which the fretting surfaces were periodically separated and the debris removed (Ref 105), resulting in an increase in the wear rate. This was then formalized through a third-body theory, which suggests that by protecting the bulk first body and consuming part of the friction work, the debris layer tends to reduce the wear rate. Therefore, by removing the debris, the global wear rate is increased. Conversely, the introduction of α-Fe_2O_3 powder oxides between the surfaces reduced the wear rate; the resultant surfaces were hardly damaged and showed signs of slight polishing. In long-term experiments, the terminal stage of fretting was identified as the formation of extensive beds of compacted oxide with a much-reduced wear rate (Ref 106). As detailed in the third-body wear theory, with small slip amplitudes of less than 10 μm (400 μin.), wear ceases because the oxide beds support the load and separate the surfaces.

The conclusion is that the accumulation of debris between the surfaces in compacted layers is more likely to reduce further wear, and that abrasion by the oxide debris is not a significant contribution to the problem.

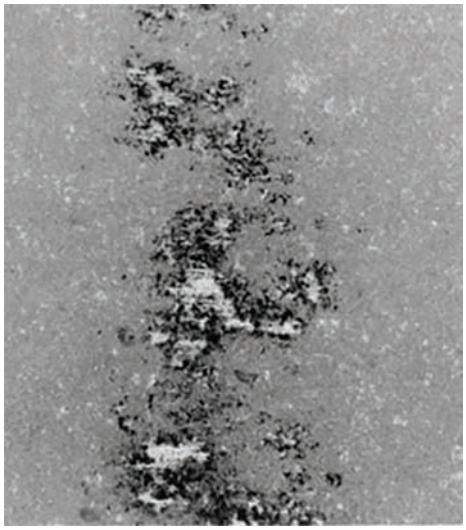

Fig. 31 Fretting mark generated by fretting an alumina cylinder against an alumina flat

Environmental Effects

Obviously, most investigations and reported cases of fretting wear occur in a normal atmosphere in which oxygen and water vapor are the main corrosive agents, although there is evidence that nitrogen may be involved in alloys containing nitride-forming elements.

Vacuum

An investigation of the effect of reduced air pressure on the fretting of a carbon steel cylinder on a flat showed that in a vacuum of 1 mPa (1.5×10^{-7} psi), the coefficient of friction was high at 3.0, and, although little measurable wear took place, considerable surface damage occurred due to the adhesive transfer of metal, which ceased at pressures above 0.1 Pa (1.5×10^{-5} psi) (Ref 107). As the pressure was increased further, the coefficient of friction fell to a value of ~1.0 at 10 Pa (1.5×10^{-3} psi), whereas the wear remained low up to this pressure. Above 10 Pa (1.5×10^{-3} psi), the coefficient of friction remained constant, but the

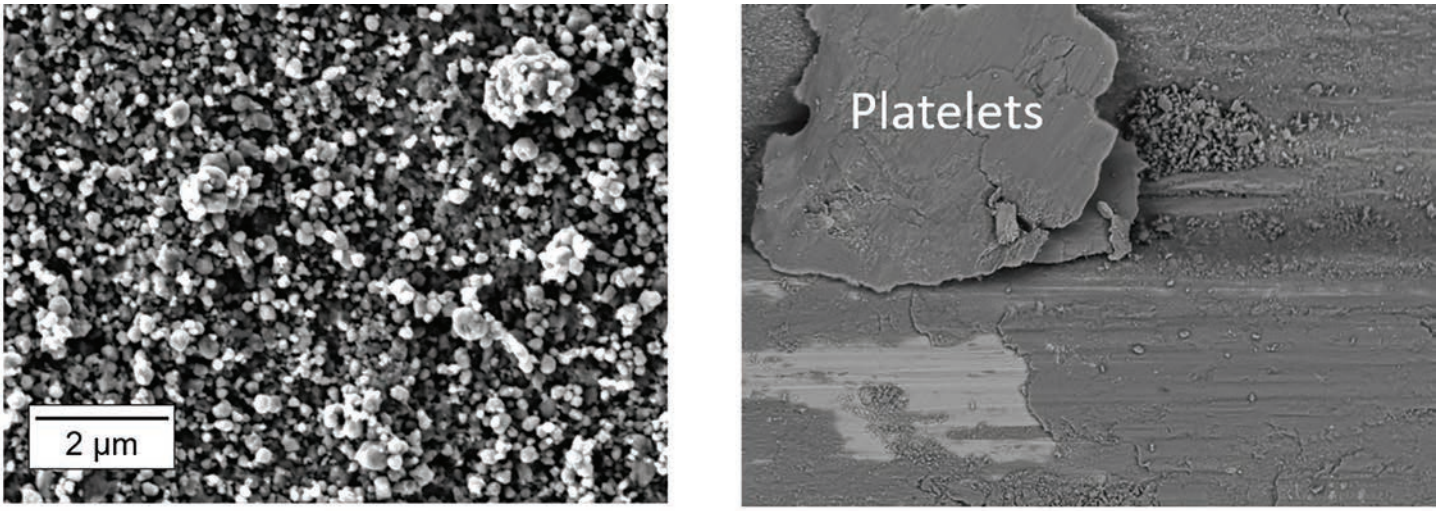

Fig. 32 Illustration of debris layer of steel/steel interface. (a) Powder debris bed in a steel/steel interface. Adapted from Ref 71. (b) Debris platelets generated from the compaction and agglomeration of thin oxide debris

wear rate increased rapidly (Fig. 33). Below this critical pressure, any debris formed was black and identified as Fe_3O_4; above the critical pressure, the debris was red and identified as α-Fe_2O_3. Similar results were obtained with an austenitic stainless steel, except in this case, the plastic deformation at low pressures resulted in martensite formation and the growth of surface fatigue cracks (Ref 108).

The increase in wear rate can be interpreted by combining both the contact oxygenation and third-body theories. As long as wear debris cannot be oxidized, the debris layer, consisting of metallic particles, is very cohesive, so the particles cannot be ejected from the interface. The friction coefficient is very high due to direct metal/metal seizure, but the debris flow ejection is negligible; thus, the wear rate is very low. When the partial pressure of oxygen becomes sufficient to form the first oxide debris ($p_{O_2} > 0.1$ Pa, or 1.5×10^{-5}), the debris layer becomes more compliant, and the coefficient of friction decreases. In addition, the debris bed becomes less cohesive, so the debris ejection flow increases, thus inducing an increase in the global wear rate.

This vacuum fretting investigation indirectly supports the contact oxygenation theory, whereby, for specific conditions, the adhesive wear phenomena observed inside the fretted interface can be related to a quasi-vacuum condition (i.e., $p_{O_2} < 0.1$ Pa, or 1.5×10^{-5}) even if the contact is fretted under ambient air. Viewed in this light, to interpret the fretting scar morphology, it must be recognized that most of the fretting interface is never directly exposed to ambient air, because the sliding amplitudes are very small compared to the contact size. On the other hand, a gradient description of the oxygen concentration within the interface must be considered, implying quasi-vacuum conditions in the inner part and quasi-ambient air conditions at the borders.

This environmental effect not only impacts wear induced by debris formation but also greatly affects the cracking process, due to the huge variation of the coefficient of friction. Hence, the effects of slip amplitude and normal load on the initiation and growth of such cracks were investigated at a pressure of 4 mPa (6×10^{-7} psi). As depicted by the fretting map approach, the tests showed that the number of cracks decreased rapidly at an amplitude $\geq$ 50 μm (0.002 in.), but the length of the longest crack increased markedly above this amplitude (Ref 108).

These results have considerable significance in relation to the fatigue aspects of fretting, particularly in connection with space research. In further work on an Fe-Cr-Ni-W amorphous alloy (1300 HV hardness), fretting against stainless steel gave similar results, although the coefficient of friction remained low over the whole pressure range, which was attributed to cylindrically shaped debris acting as rollers (Ref 109).

The effect of high pressure has not been investigated extensively. The studies that have been conducted on the effects of high pressure have been associated with the nuclear power industry, specifically relating to problems in the advanced gas-cooled reactor (AGR). In this case, the reactor is cooled by carbon dioxide at a pressure of 4 MPa (40 atm), with temperatures in the region of 600 °C (1110 °F) (see the section "Low and High Temperature" in this article).

Humidity

After oxygen, water vapor is the most significant environmental factor in fretting wear. In a study of a wide variety of pure metals

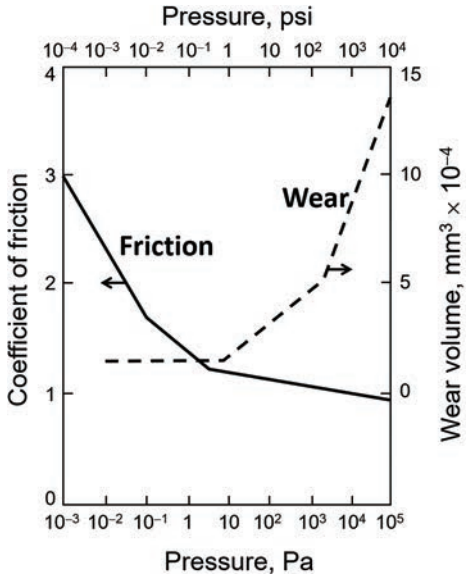

Fig. 33 Effect of atmospheric pressure on the friction and wear of a carbon steel cylinder. Adapted from Ref 107

tested in a hemisphere-on-flat configuration and at a slip amplitude of 80 μm (0.0030 in.), most metals, such as silver, copper, titanium, and iron, showed a peak coefficient of friction value between 10 and 15% relative humidity (RH), with a corresponding peak in wear volume (Ref 110). With chromium, the peaks appeared at 5% RH, but with aluminum and nickel, the peaks occurred at very low humidity. At normal atmospheric humidity (~50% RH), all of the metals except nickel showed a gradual decrease in fretting wear. This also corresponds well with earlier observations on steel specimens (Ref 74). However, because

aluminum alloys are particularly sensitive to the effects of water vapor in fatigue situations due to the reactivity of an exposed aluminum surface and the liberation of hydrogen, higher wear rates can be observed.

Indeed, it is well acknowledged that humidity can act as a lubricant, reducing the friction work dissipated in the interface. In addition, it favors the formation of a hydrated oxide debris layer structure, which is more cohesive than the dry powder debris bed and consequently less easily ejected from the interface. High-humidity conditions limit the debris ejection flow process and globally reduce the fretting wear rate (Ref 111–113). However, it must be viewed relative to the time, sliding frequency, and material properties. When very low frequencies are imposed, corrosion phenomena can dominate, increasing in consequence the fretting wear rate. Obviously, the frequency threshold marking the transition from positive to negative effect of relative humidity depends on the reactivity of the metal with humid air. For example, the fretting wear investigation of an Al-Zn-Mg alloy (Ref 114) showed a similar wear rate in dry air as in dry argon, thus discounting oxygen as an active agent. This was explained by the very high reactivity of this alloy inducing systematic adhesive metal-metal wear processes with or without the presence of oxygen. However, in air of 60% RH, the wear rate was much higher because the metal wear debris becomes less adherent than under dry argon and consequently more easily ejected.

In addition, it was found that softening due to overaging of the surface material in the contact region developed in humid air. As mentioned previously, water vapor has a considerable effect on the fretting wear of certain ceramics, particularly silicon carbide and silicon nitride (Ref 102). With silicon carbide, alumina, and zirconia, the high rate of wear at 5% RH is greatly reduced at humidities > 50%, with a steady decrease in the coefficient of friction. Silicon nitride shows a similar wear rate to silicon carbide at 5% RH, but the rate increases linearly with time at $\geq$50% RH. This is related to the propensity of silicon nitride to be transformed into silica.

Aqueous Electrolytes

Fretting of corrosion-resistant metals in aqueous environments was investigated originally because of problems associated with orthopedic implants in the human body. In some of these devices, metal-to-metal contacts (for example, screws and bone plates) could suffer fretting due to the activity of the patient. In potentiostatic experiments on an austenitic stainless steel, it was found that the corrosion current increased linearly with the amplitude of slip at a fixed frequency and also was linearly related to frequency at a fixed amplitude (Ref 115). When potential control was not applied, there were large drops in potential, with a slow recovery when the fretting action ceased (Fig. 34).

In studies in physiological saline (artificial body fluid) of fretting of type 316L stainless steel and Co-Cr-Mo alloy, the latter was found to have the lower wear rate, although the addition of albumin reduced the wear rate of the stainless steel (Ref 116). In tests with a fretting simulator using screws and a bone plate of type 316L stainless steel, the weight loss of the screws was an order of magnitude greater in 0.9% NaCl compared with the same solution to which 10% bovine serum had been added (Ref 117). Measurements of potential drop on fretting obtained in laboratory experiments were compared with in vivo measurements on bone plates fitted in sheep walking on a treadmill. The potential drop was found to be related to the load at low levels of torque to which the screws had been tightened (Ref 118). It has since been established that the effect of proteins on fretting corrosion depends on the relation of the pH of the solution to the isoelectric point of the protein. At pH values below the isoelectric point, no effect is seen, but at pH values above the isoelectric point, there is a reduction in the wear rate (Ref 119).

The investigation of corrosion-resistant materials under fretting conditions in aqueous electrolytes was obviously of considerable interest, because the materials rely on a protective oxide film for their corrosion properties. Continual disruption of this film is known to produce high corrosion rates, as confirmed by measurements of weight loss or volume of pits, which equates to rapid wear rates. The development of offshore oil rigs provided many more examples of fretting corrosion occurring on less corrosion-resistant materials, such as the weldable steels used in the construction of the rigs and the steel ropes used to moor them in the marine environment. The specific wear rate for a 1.5% Mn steel in air was 1.07×10^{-16} $m^3/N \cdot m$, but in seawater it increased to 10.0×10^{-16} $m^3/N \cdot m$ and 235.5×10^{-16} $m^3/N \cdot m$ at 1 Hz (Ref 120). Fortunately, application of cathodic protection of −950 mV versus standard calomel electrode (SCE) reduced the wear rate almost to that in air.

Steel ropes are used extensively in marine conditions. Development of the offshore oil industry has increased the use of these ropes as moorings for oil rigs. The fretting behavior of these wires in artificial seawater has been extensively investigated (Ref 120). In crossed-cylinder tests with an amplitude of slip of 50 μm (0.002 in.), a normal load of 3 N (0.3 kgf), and a frequency of 30 Hz, it was found that the wear volume after 5×10^6 cycles for 0.64% C steel was 55×10^{-4} mm^3 (34×10^{-8} $in.^3$) in air, 167×10^{-4} mm^3 (102×10^{-8} $in.^3$) in seawater, but decreased to 4×10^{-4} mm^3 (2×10^{-8} $in.^3$) when a potential of −950 mV versus SCE was applied (Ref 120). In 3.5% NaCl solution, the wear was even higher at 214×10^{-4} mm^3 (130×10^{-8} $in.^3$), indicating that the magnesium salts in the seawater were having some inhibiting effect. The effect of coating the wire by hot dip galvanizing was similar to the effect of cathodic protection, reducing the wear to ~10×10^{-4} mm^3 (~6×10^{-8} $in.^3$) in seawater.

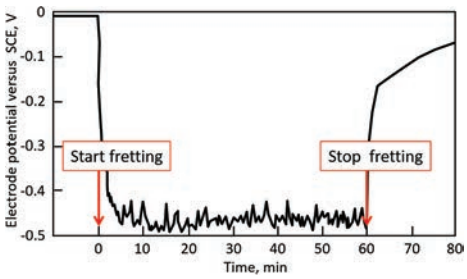

Fig. 34 Potential drop obtained when fretting Ti-6Al-4V (IMI 318) titanium alloy in a saline solution. SCE, saturated calomel electrode

New models in which the total tribocorrosion wear volume was established as the sum of pure mechanical friction wear volume, pure corrosion wear volume, and synergistic mechanical-corrosion wear volume contributions have been established. These approaches tend to describe the fretting wear rate under corrosive situations well (Ref 121).

Low and High Temperature

The increasing development of space engineering has meant that dynamic systems must operate not only in a vacuum but also at very low temperatures. Fretting of a spherical surface on a flat, both composed of austenitic stainless steel, at 4 K (−452 °F) in liquid helium resulted in high friction but little wear, very similar to the situation in high vacuum (see the section "Vacuum" in this article). The explanation was similar; that is, oxide films did not grow at this temperature. At 77 K (−320 °F), the friction and wear were the same as at 293 K (68 °F) in high vacuum (see the section "Vacuum" in this article). The explanation again was similar; that is, oxide films did not grow at this temperature. Much more attention has been given to high-temperature fretting in oxidizing atmospheres, because this is a situation that is very common in practice (for example, in gas turbine aeroengines and in the AGR device). Pioneer work (Ref 122) showed that there was a great reduction in the coefficient of friction and wear when mild steel was fretted in air at temperatures up to 500 °C (930 °F).

In argon, however, surface damage was severe. At approximately this time, the reciprocal sliding of certain alloys at high temperature in an oxidizing atmosphere was investigated, and it was discovered that many alloys containing combinations of iron, nickel, and chromium developed a very smooth oxide, which was termed glaze layer oxide, which had low friction and low wear (Ref 123). Fretting wear tests at amplitudes of 10 and 40 μm (0.0004 and 0.0016 in.) showed low coefficients of friction at 280 and 540 °C (535 and 1005 °F) compared with room temperature, and corresponding reductions in wear damage

(Ref 124). However, if the air pressure is reduced to 1 mPa (1.5×10^{-7} psi), severe surface cracking is produced (Ref 125). The alloys that are capable of forming the glaze oxide are those on which an oxide with a spinel structure can develop (for example, mild steel [$FeO{\cdot}Fe_2O_3$], stainless steels [$FeO{\cdot}Cr_2O_3{\cdot}NiO$, $Cr_2O_3{\cdot}NiO{\cdot}Fe_2O_3$], and nickel-chromium alloys [$NiO{\cdot}Cr_2O_3$]). If the oxide film is damaged, it is self-repairing at the high temperature but does not survive at room temperature (Ref 126, 127).

Many investigations have been performed to better formalize the fretting wear responses of nickel-base superalloys as a function of temperature (Ref 128–130), confirming a decrease of the wear rate under high temperature when a lubricious and protective glaze can be formed. Similar tendencies were also found for high-strength chromium steels (Ref 131, 132).

Cobalt alloys display similar nonmonotonic tendencies (Ref 133–136). The investigation of cobalt superalloy HS25 manifests three-stage evolutions of the wear volume extension as a function of temperature (Fig. 35). Up to T_1 (approximately 150 °C, or 300 °F), the wear volume increases due to an increase of the tribo-oxidation process. The wear extension versus fretting cycles is linear, inducing a continuous damage extension. Then between T_1 and T_2 (approximately 300 °C, or 570 °F), the formation of an accommodating compacted oxide debris layer reduces the wear volume extension. The wear extension is bilinear, with an initial fast rising followed by a smoother increase when the compacted layer is formed.

The third domain, III, when $T > T_2$, corresponds to the glaze layer wear regime. Above this so-called threshold glaze layer temperature ($T_{GL} = T_2$), a sintering-like process leads to the formation of a fully protective glaze layer structure, which drastically reduces the wear rate. The wear evolution is also bilinear; however, when the glaze layer is formed, the wear rate converges to zero, which implies that there is no more additional wear extension. Titanium alloys do not behave in quite the same way, because they do not display the formation of protective glaze structures.

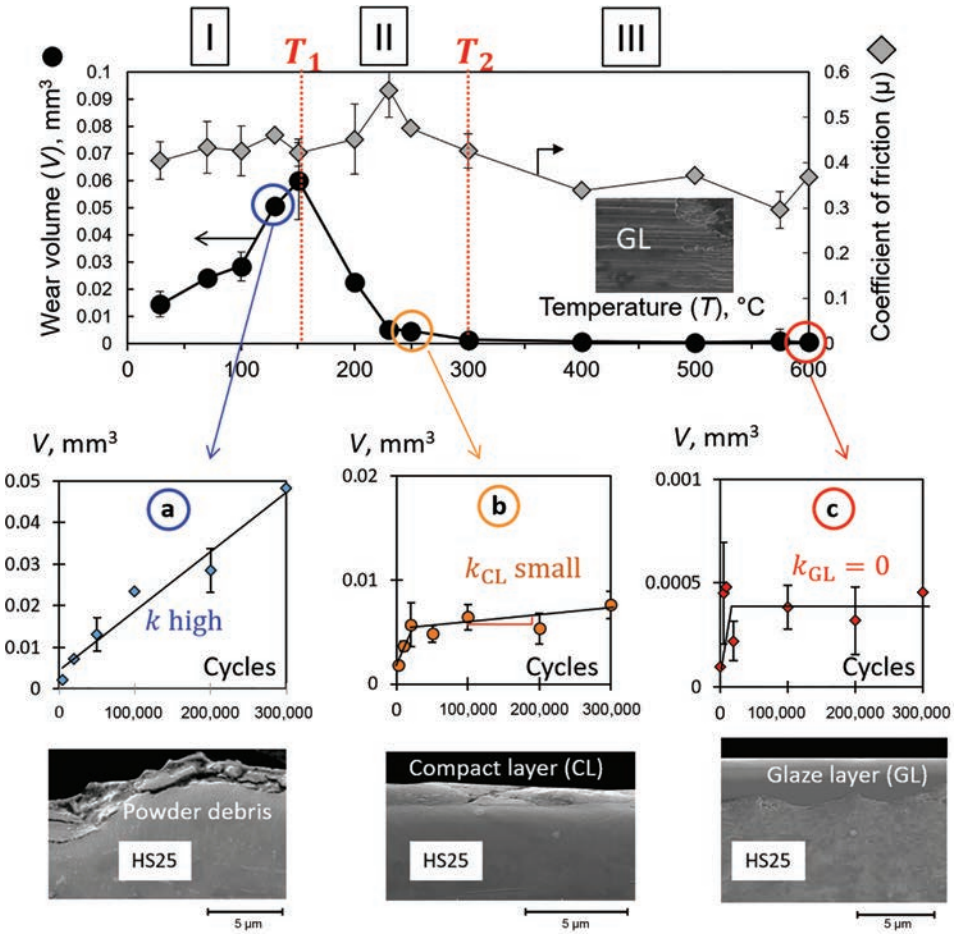

Fig. 35 Evolution of the fretting wear response of an HS25 cobalt-base alloy versus temperature, *k*, wear rate versus fretting cycles. Adapted from Ref 133, 134

Measurement of Fretting Wear

Profilometry

The very small amount of material that is removed in most fretting experiments renders the traditional method of measuring wear by weight loss impractical (Ref 137). The method of surveying the surface by three-dimensional (3D) surface profilometry gives the best quantitative and descriptive assessments of the fretting wear damage. Figure 36 illustrates the 3D worn profile of an HS25/alumina crossed-cylinder arrangement after a 10 min alcohol ultrasonic cleaning to remove the remaining wear debris. Wear was observed only on the HS25 cylinder, and no damage was detected on the alumina counterpart. By extracting the original cylindrical shape of the HS25 specimen, an equivalent sphere-on-flat fretting scar is extracted. Using a 3D profile, the wear volume (V) can be estimated by measuring the volume below the surface plane. This analysis also permits extraction of the maximum wear depth (h_{max}), which is a crucial parameter to quantify surface damages and, more particularly, to predict coating durability (i.e., when the substrate is reached). In addition, the fretting scar morphology is an important parameter. To quantify the fretting scar morphology, one strategy consists of extracting two-dimensional equivalent profiles on both fretted interfaces and then combining the profiles. Depending on the contact condition, either a U-shape (full abrasive wear) or W-shape (metal transfers in the center) can be observed (Ref 68).

Mechanism of Fretting Wear

It is generally agreed that when fretting wear is taking place between two flat surfaces or two conforming cylindrical surfaces (i.e., conditions in which escape of debris is not as easy), the progress with time (or number of cycles) can be recognized as occurring in three stages (Ref 106, 138):

1. Initial stage of a few thousand cycles when metal-to-metal contact is prevalent, resulting in local welding, roughening of the surface, and high friction. Fatigue microcracks are initiated in this stage if the movement is a result of cyclic stressing (Ref 139).
2. Formation of beds of compacted oxide, with a fall in the coefficient of friction and erratic behavior in contact resistance as it oscillates between high and low values
3. Onset of a steady state in which the friction is more or less constant

These changes are illustrated in Fig. 37. The length of the initial stage depends on the amplitude of slip and the normal load (Fig. 38). Observation of the debris on steel shows that it is platelike (Fig. 32). One of the early theories of fretting wear maintained that the debris arose by continual scraping and regrowth of oxide film (Ref 140).

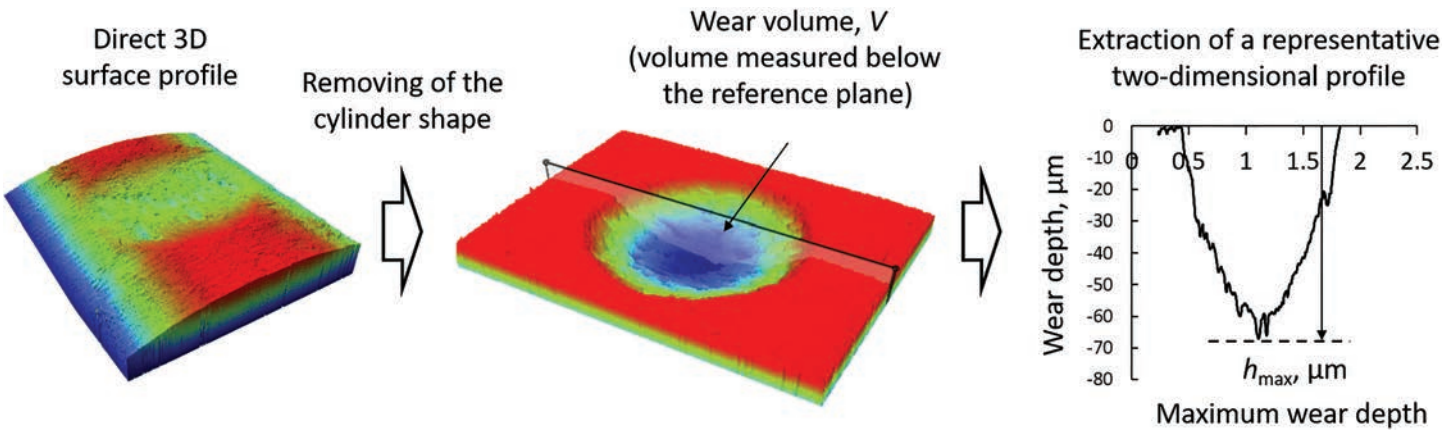

Fig. 36 Three-dimensional (3D) surface profile of a crossed-cylinder fretting wear interface (extraction of wear volume and maximum wear depth). Adapted from Ref 134. Reprinted with permission from Elsevier

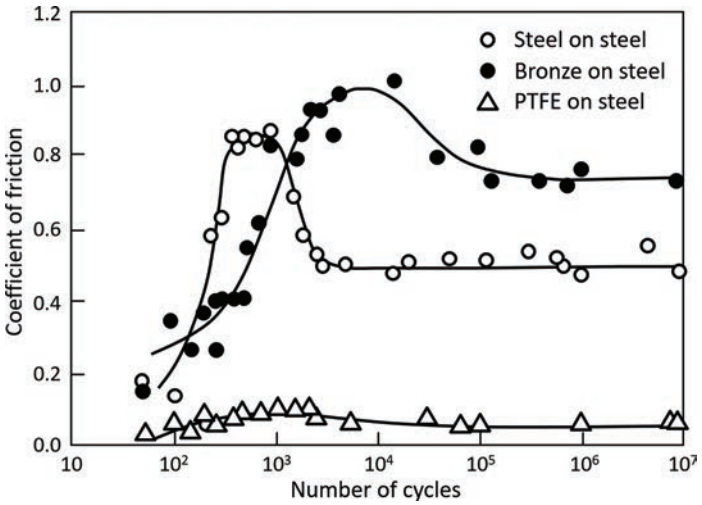

Fig. 37 Plot of coefficient of friction versus number of fretting cycles for three selected materials tested on steel. PTFE, polytetrafluoroethylene. Adapted from Ref 139

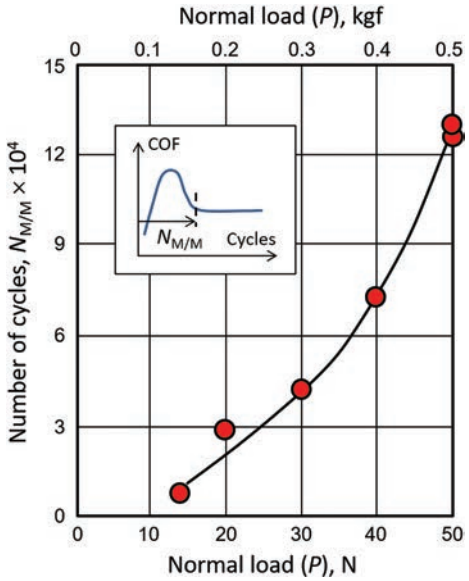

Fig. 38 Relation between initial period of metal-to-metal (M/M) contact and normal load. COF, coefficient of friction. Adapted from Ref 139

A modification of this idea suggests, from evidence of sections through a fretted surface on a carbon steel, that there are three well-defined zones (Ref 141):

- *Zone 1:* Outer layer of compacted oxide
- *Zone 2:* Severe deformation in which grains are comminuted and oriented in the fretting direction
- *Zone 3:* Plastic deformation (from which it is concluded that in the steady-wear state, flakelike debris is formed by stripping oxide layers from the metal surface) (Ref 141)

The opposite point of view is that metal particles, which become progressively ground up and oxidized between the fretting surfaces, are removed. The evidence for this is that with reactive metals, such as aluminum and titanium, the debris is flakelike but contains metal (Ref 142). How the metal particles are generated is still a subject of controversy. However, in certain instances, there is evidence that the particles are generated in the later stages of a delamination process (Fig. 39). It is possible that both processes, the removal of oxide and the removal of metal, could be occurring simultaneously in different regions of the surface. In the initial stage, peaks and valleys are formed due to local welding, and these variations appear to persist. The in-between areas become filled with compacted debris with a layerlike structure, from which oxide flakes can become detached. These areas of compacted debris are maintained by metal particles produced by the continuing metal-to-metal contacts. Although the oxide debris is usually harder than the metal from which it arises, abrasion by the oxide does not contribute to the wear of steels.

In fact, as previously detailed by the third-body theory, the debris, by limiting metal-to-metal contact and possibly taking up some of the movement between the surfaces, has more of a protective effect (Ref 63).

Fretting is not always evident from surface observations, because, like any other tribological processes, adhesive, abrasive, and delamination surface damage can be observed. However, by investigating the kinematics of the assemblies using, for instance, finite-element simulations, microoscillating movements can be estimated and related to fretting. Moreover, there is an irrefutable way to confirm fretting phenomena. Due to the stress-loading path, the initial crack generated in the sliding zone will systematically propagate obliquely toward the inner part of the contact. Hence, using cross-sectional observation, if symmetrical crack patterns are observed at each side of the median axis of the contact, a fretting loading can be confirmed even for the gross slip condition (Fig. 39b). However, this analysis requires a destructive cross-sectional analysis.

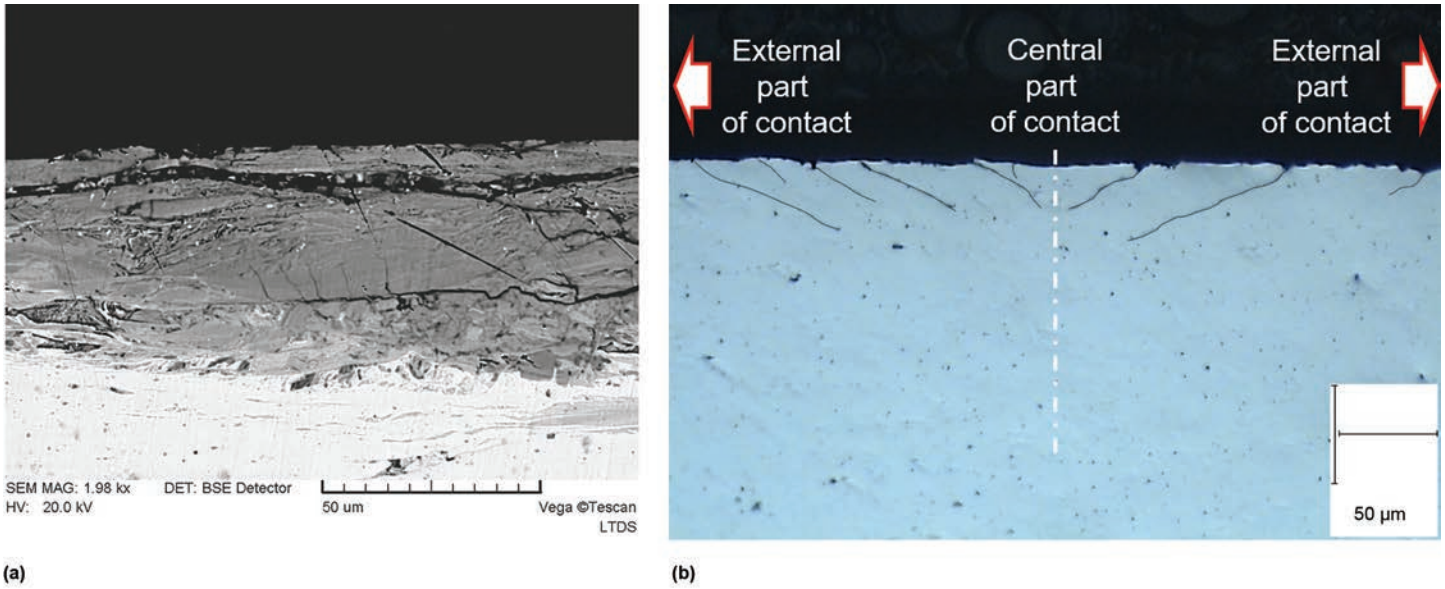

Fig. 39 (a) Typical adhesive wear, plastic deformation, and delamination in the fretting interface. (b) Confirmation of fretting by observing a symmetrical crack pattern propagating toward the inner part of the interface (cylinder-on-flat contact at the gross slip condition)

In addition, when surface wear occurs, the crack incipient pattern can be removed and no explicit conclusion can be drawn.

Prevention of Fretting Damage

The steps that can be taken to reduce or eliminate the damage due to fretting are extremely diverse, and each case or prospective case must be analyzed individually in order to select the most promising method to be applied. In this article, it is possible to give only some general indications of how the problems can be tackled. Reference 143 points out that it is useful to know whether the movement is force controlled, displacement controlled, or, even better, sliding amplitude controlled. Force-controlled fretting is experienced in the case of partial slip; therefore, increasing the coefficient of friction or increasing the normal load will reduce the slip. In sliding-controlled fretting, in which slip occurs over the whole interface, the sliding amplitude is constant, and wear will be reduced by reducing the normal load as well as the coefficient of friction. Note that in testing, to ensure a constant sliding amplitude, the displacement amplitude must be continuously monitored to compensate for the fluctuation of the test system, which itself is induced by the variation of the tangential force (Ref 41). On the other hand, keeping a constant displacement amplitude and varying the normal load will change the effective sliding amplitude, because the system accommodation evolves in proportion to the tangential force amplitude (i.e., normal load).

Improved Design

Because fretting arises only where there is relative movement between two surfaces, the elimination of this movement is a prime objective. Fretting often arises as a result of a stress concentration. In any case, reducing the stress via improved design (for example, raised wheel seats or stress-relieving grooves in hub/axle assemblies) is demanded by fatigue considerations. Increasing the normal pressure by reducing the area of contact (when the normal load is to be kept constant) or increasing the normal load will reduce the area of slip, but such action may introduce fatigue problems. The ultimate goal is to make the component in one piece and to eliminate the junction, but this is not always possible.

Surface Finish

Rough surfaces are less prone to fretting damage than highly polished surfaces. Rough surfaces can be obtained by peening with glass beads or steel shot. Shot peening has the advantage of work hardening the surface, although the residual compressive stress appears to have little effect on the wear process; it has considerable effect, however, if fatigue crack initiation and propagation are involved. Shot peening often is applied as a surface preparation for the application of coatings.

Coatings

Surface treatments that radically change the chemical composition of the surface can be divided into three categories:

- Foreign atoms or ions are introduced into the existing surface by diffusion (for example, carburizing, nitriding [Ref 144], chromizing, sherardizing, and aluminizing) or by bombardment (for example, ion implantation).
- The surface reacts with a chosen environment to form a compound (for example, oxidation, anodizing, and phosphating) (Ref 145).
- An entirely foreign material is applied to the surface (for example, electrodeposition, plasma spray, ion plating, physical vapor deposition, and chemical vapor deposition) (Ref 146–148).

Most of these coatings, that is, titanium nitride and diamond-like carbon, are harder than the substrate and consequently significantly improve the fretting wear resistance. However, they are also more brittle than the substrate, which, if it is not strong enough, will plastically deform in the fretting contact, in which local stresses can be high. This plastic deformation will crack and break up the coating. If the coating is particularly hard (for example, titanium nitride, with a hardness of 300 HV), further damage can occur by abrasion (Ref 149). Carburizing and nitriding of steels is a well-established thermochemical treatment for reducing wear in gears and is also effective against fretting (Ref 150). Surface coatings are undoubtedly the optimum strategy to protect bulk material against fretting wear damage (Ref 151).

Many developments have been pursued to improve solid lubricant coatings, which reduce the coefficient of friction and limit seizure phenomena (Ref 152, 153). However, to predict the durability of a coating, an alternative strategy to wear volume analysis must be adopted. Indeed, the coating durability is usually related to the critical loading cycles (N_c) when the sliding interface reaches the substrate interface. For solid lubricant coatings, N_c can be easily detected by measuring the discontinuous increase of the coefficient of friction. When the coating does not lead to significant

fluctuation of the coefficient of friction, N_c can be estimated by performing interrupted tests and measuring the maximum wear depth. When the depth exceeds the coating thickness, this implies failure of the coating. The durability of a coating N_c can then be expressed as a function of the applied displacement amplitude (Ref 154) (Fig. 40). It can also be formalized as a function of the maximum friction energy density or Archard density parameter inputted in the interface during a fretting cycle (Ref 59, 155). Using this approach, pressure and sliding amplitude can be combined through a single energy-loading variable. Power-law formulation can be defined so that the coating endurance can be related to a given friction energy capacity (χ), characterizing the fretting performance of a given surface treatment (i.e., coating):

$$N_c = \frac{\chi}{\omega_{max}} \quad \text{(Eq 27)}$$

with ω_{max} being the maximum Archard work density inputted in the contact during a fretting cycle, given by:

$$\omega_{max} = 4 \times \delta_S \times p_{max} \quad \text{(Eq 28)}$$

where p_{max} is the maximum pressure value in the contact.

The growth of oxide glaze layer films at high temperatures has been employed to provide wear-resistant, self-repairing coatings. These have been improved by ion implantation, particularly in titanium alloys, to provide coatings that have low friction and low wear. Anodizing is applied to aluminum alloys, and the hard coating provides protection against fretting, but it may cause wear of the opposing surface (Ref 156).

Inserts

Separation of the two surfaces by an insert, either a shim of a soft metal or a shim of a polymer with a low elastic modulus, can sometimes be effective. The intention is to take up the movement by either plastic deformation or elastic deformation of the material. A combination of metal and polymer can be more effective because it combines the advantages of both materials—the low elasticity of the polymer and the good conductivity of the metal. Bronze-filled polytetrafluorethylene, when fretted against steel, has a very low friction coefficient and undetectable wear (Ref 157).

Lubricants

Grease and oil are usually difficult to apply in fretting contacts because of the difficulty of maintaining the lubricant in the contact, but lubricants are included in the construction of steel ropes (for example, locked coil ropes) (Ref 158).

In a survey of the effect of additives to a base mineral on the fretting wear of steel surfaces, zinc di-*n*-octyldithiophosphate was found to be most effective (Ref 159).

Figure 41 illustrates the evolution of a stabilized coefficient of friction of a greased cylinder-on-flat steel interface. As long as the contact is running under partial slip condition, the friction response is similar to dry contact (Ref 161–163). It can be even higher at the gross slip transition, particularly for smooth surfaces, because the grease can limit the

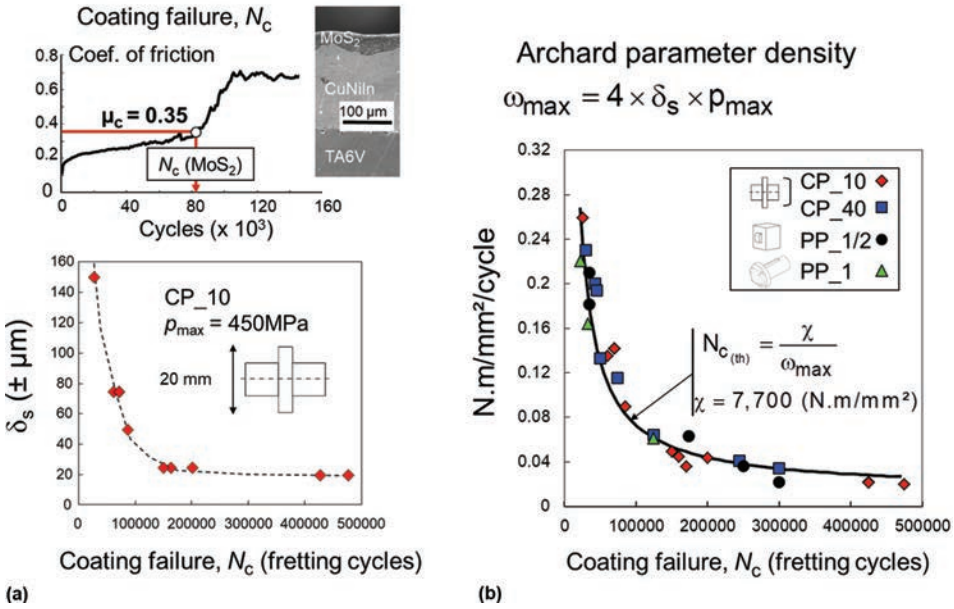

Fig. 40 Quantification of coating durability under fretting wear (analysis of a MoS_2 solid lubricant). (a) Coating failure (N_c) when the substrate is reached (friction discontinuity), with evolution as a function of sliding amplitude (δ_S). (b) Quantification of N_c as a function of the maximum local Archard work density for various contact geometries. CP, cylinder/plane; PP, punch/plane; p_{max}, maximum contact pressure. Adapted from Ref 155. Reprinted with permission from Elsevier

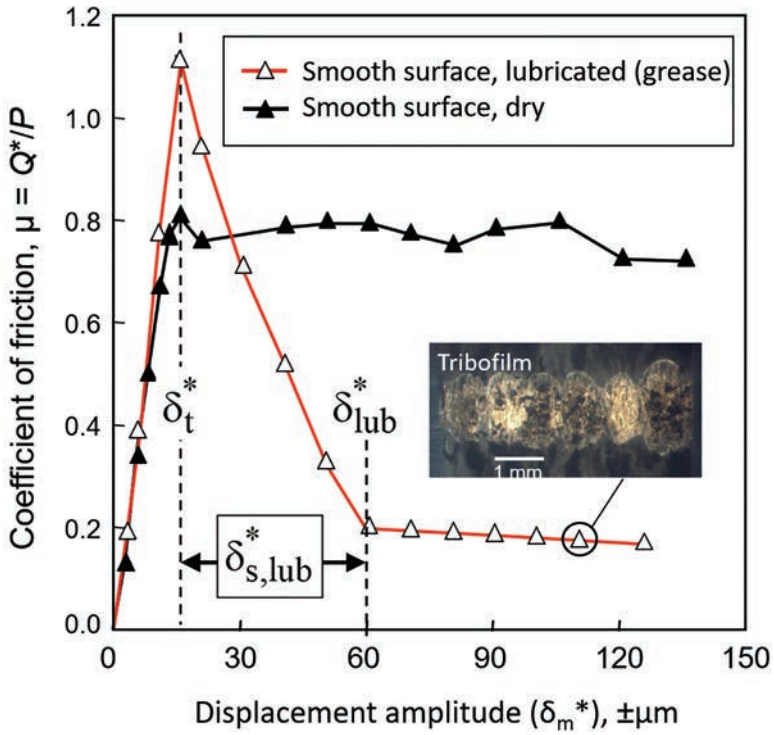

Fig. 41 Comparison of the stabilized friction coefficient (5000 cycles test duration) of a cylinder-on-flat smooth surface as a function of the applied measured displacement amplitude between a dry and a grease-lubricated contact. Adapted from Ref 160

access of oxygen within the interface, which, by favoring local seizure, may induce very high friction values. Then, above the gross slip transition, the activation of small sliding over the whole interface allows the introduction of lubricant inside the contact. This triggers a fast drop of the friction value. The larger the sliding amplitude, δ_S, the smaller the coefficient of friction (Ref 160). Following this, above a threshold lubricating sliding amplitude, $\delta_{S,lub}$, a tribofilm is formed, and the friction value is stabilized at approximately 0.2. This threshold amplitude, $\delta_{S,lub}$, depends on many factors, such as the surface roughness, the composition of the oil, as well as the viscosity of the oil or grease. It was found that the lower the viscosity, the faster the transition toward a low-friction regime (Ref 163). As a result, grease can be an interesting palliative but only for very large fretting sliding amplitudes equivalent to a reciprocating sliding condition. For small- and medium-displacement amplitude, solid lubricant coatings are preferred, although, like any other surface coating, they tend to wear away.

Examples of Fretting Failures

When steel parts are lubricated properly, the presence of oxide debris often is indicative of fretting. If a part is unlubricated or experiences a lack of lubrication, oxide debris may not necessarily signify fretting but rather other types of wear that can be prevented by proper lubrication. Fretting may not be completely remedied by lubrication (Ref 164); however, this does not mean that fretting damage cannot be mitigated by lubrication. In wire ropes, for example, fretting between strands can be prevented by proper lubrication (Ref 164).

Fretting differs from ordinary wear further in that the bulk of the debris produced is retained at the site of fretting. In ferrous materials, the fretting process creates a mass of reddish oxide particles. Fretting also occurs in nonoxidizing materials, such as gold, platinum, and cupric oxide. Fretting debris formed by many nonferrous alloys is largely unoxidized and larger in particle size than that of ferrous materials. On the other hand, in hard materials such as a tool steel and chromium, the initial wear particles are very small, with much oxide present (Ref 164). Little debris is present in an inert or protective atmosphere, although surface damage can be extensive.

If fretting is present, macroscopic examination of the affected surface area can be done after the corrosion has been scrubbed off with a paste of alumina and hexane, for example. The examination will reveal very reflective areas, as well as depressions and pits containing black patches of Fe_3O_4, which are produced when the oxygen supply is limited. If only ordinary corrosion is present, microscopic examination will reveal small but well-defined corrosion pits that have produced rust rosettes consisting of abundant hydrated iron oxide (Ref 164). Figure 42 shows a screw hole with fretting and fretting corrosion of a type 316LR stainless steel bone plate for an orthopedic implant.

Fretting in Rolling-Element Bearings

False Brinelling

The term *false Brinelling* refers to a fretting-type damage that occurs in machine components such as ball bearings, in which craters caused by the vibration of the ball against the race are circular and resemble Brinell impressions. False Brinelling is caused by vibrations or oscillations over a few degrees of arc between rolling elements and raceways in a nonrotating bearing (Fig. 43). At the contact areas between the rolling elements and raceways, lubricant is squeezed out, resulting in metal-to-metal contact and localized wear. False Brinelling does not occur during normal

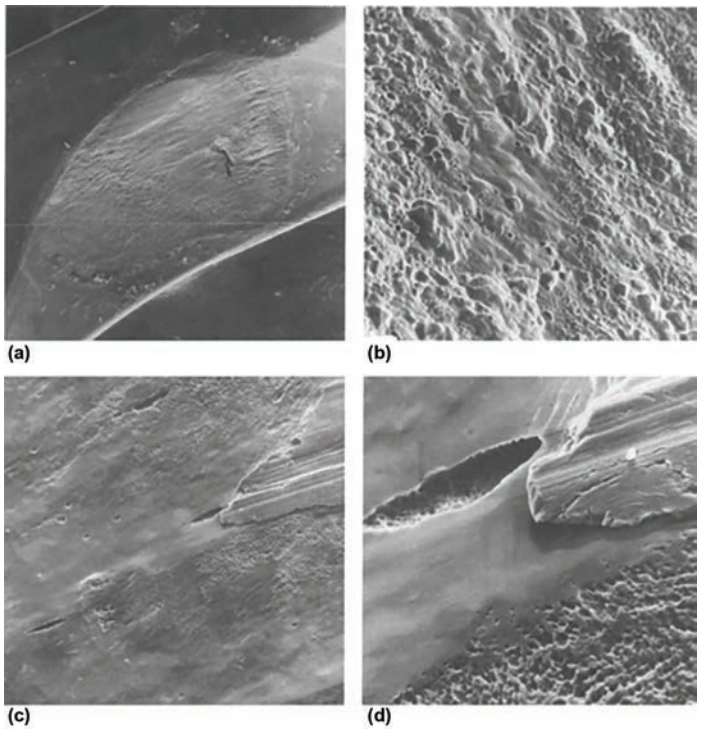

Fig. 42 Fretting and fretting corrosion at the contact area between the screw hole of a type 316LR stainless steel bone plate and the corresponding screw head. (a) Overview of wear on plate hole showing mechanical and pitting corrosion attack. Original magnification: 15×. (b) Higher-magnification view of shallow pitting corrosion attack from periphery of contact area. Original magnification: 355×. (c) Contact area showing the effects of mechanical material transport (material tongue in right upper corner), fretting and wear (burnished areas), and corrosion (shallow pitting). Original magnification: 355×. (d) Higher-magnification view of Fig. 42(c). Original magnification: 650×

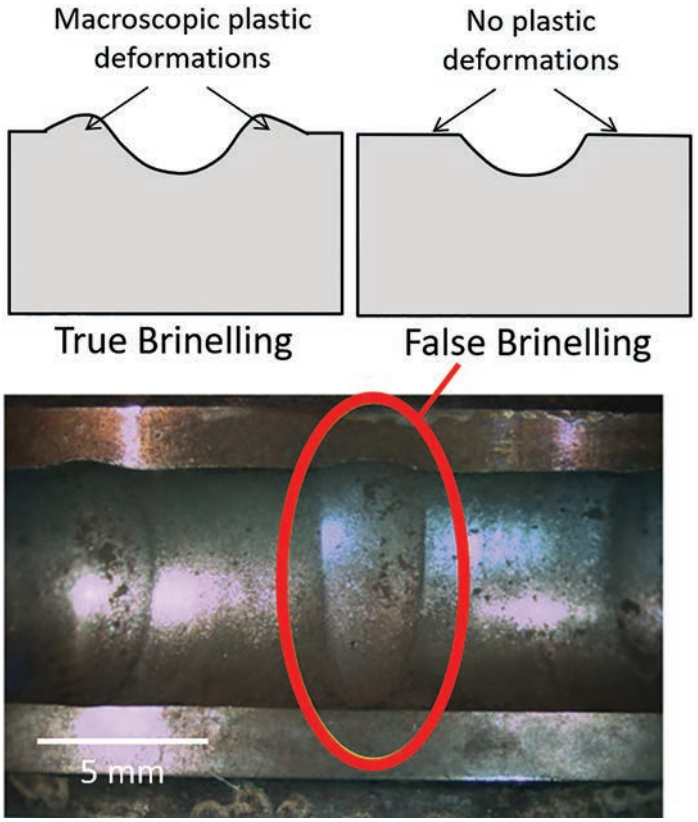

Fig. 43 Comparison between true Brinelling and false Brinelling. True indentation Brinelling displays plastic deformation at the contact border (positive displacement volume = negative displacement volume), which is not observed in fretting-rolling wear processes involving false Brinelling, because material was removed by a debris ejection process (observation of false Brinelling damage in a ball bearing assembly). Adapted from Ref 34. Reprinted with permission from Elsevier

running but is found in the bearings of machines subjected to vibration while at rest. False Brinelling usually occurs during transit. Transport by rail or truck is conducive to this form of damage. Even transport by sea does not guarantee immunity, particularly where pronounced vibrations from diesel engines may be present.

For example, false Brinelling also has been found in the roller-bearing axle boxes of railway cars that have been standing for some time in sidings and that are subjected to vibrations from passing trains. When equipment is to be transported, the machine should be dismantled, and one of the following preventive measures should be adopted: Remove the rolling-element bearings and fit temporary wooden packings in their place, or use clamps to lock rotors of electric motors rigidly to the frames and, at the same time, relieve the bearing of the dead-weight load. In other instances, the machinery could be packed so that the axis of the rotating portion is in the vertical plane, thereby preventing damage by stationary microsliding/rotating. In many instances, false Brinelling remains undetected until the machine is started, at which time noisy operation is immediately evident. Figure 44 shows a portion of a shaft that served as the inner raceway for a drawn-cup needle-roller bearing on which severe false Brinelling damage was observed.

There are several features that permit false Brinelling to be distinguished from true Brinelling. True Brinelling, or denting, is a permanent deformation produced by excessive pressure or impact loading of a stationary bearing. Improper mounting procedures, such as the forcing of a tight fitting or cocked outer ring into a housing, are common causes of true Brinelling. True Brinelling also can be caused by vibrations in ultrasonic cleaning. True Brinelling is characterized by hollows or dents produced by plastic flow of metal.

Another type of fretting damage observed in machinery is known as fitting rust, where gages, shims, or other parts are clamped together and experience vibration. Fitting rust is the contact corrosion that takes place between the bore of the bearing and the shaft, or between the outside surface of the bearing and the bore of the housing.

Recommendations for reducing fretting in rolling-element bearings include:

- Keep radial play in the bearings at the lowest practical value.
- Increase the angle of oscillation (if possible) to secure roller or ball overlap in order to drag fresh lubricant into the area. If the surfaces can be separated by lubricant, fretting of the metal cannot occur.
- Relubricate frequently to purge the red iron oxide debris and reinstate the lubricating film.
- Use a larger bearing of higher capacity to reduce contact loads.
- Increase the hardness of the elements as much as possible. The commercial antifriction bearing already has fully hardened components. For best results, the shaft, if used as an inner raceway, should be hardened to 58 HRC minimum.
- Use a grease that has been specially formulated to provide maximum feeding of lubricant to areas susceptible to fretting damage. If the bearing is oil lubricated, flood it if possible.

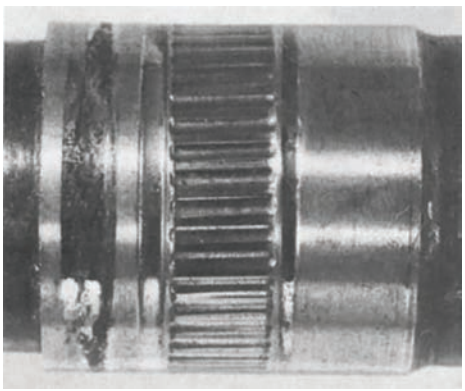

Fig. 44 Severe damage from fretting (false Brinelling) on the surface of a shaft that served as the inner raceway for a needle-roller bearing

Example 1: Fretting Failure of Raceways on 52100 Steel Rings of an Automotive Front-Wheel Bearing

The front-wheel outer angular contact ball bearing shown in Fig. 45 generated considerable noise shortly after delivery of the vehicle. The entire bearing assembly was removed and submitted to the laboratory for failure analysis. The inner and outer rings were made of seamless cold-drawn 52100 steel tubing, the balls were forged from 52100 steel, and the retainer was stamped from 1008 steel strip. The inner ring, outer ring, and balls were austenitized at 845 °C (~1550 °F), oil quenched, and tempered to a hardness of 60 to 64 HRC.

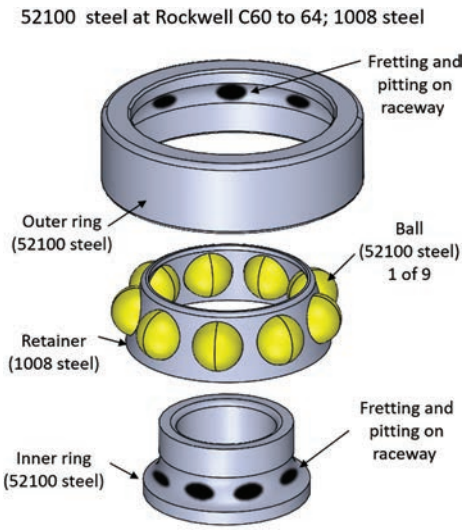

Fig. 45 Automotive front-wheel bearing that failed by fretting of raceways on inner and outer 52100 steel rings

Investigation

Visual examination of the outer raceway revealed severe fretting and pitting in the ball-contact areas at spacings equivalent to those of the balls in the retainer. The areas were elongated, indicating that only a slight oscillation of the ring or wheel had occurred. Similarly spaced but less severely damaged areas were observed on the inner raceway.

Conclusions

Failure was caused by fretting due to vibration of the stationary vehicle position without bearing rotation. These vibrations were incurred during transportation of the vehicle. This bearing had experienced little, if any, service but showed conclusive evidence of fretting between the balls and raceway.

Recommendations

Methods of securing the vehicle during transportation should be improved to eliminate vibrations.

Example 2: Fretting of Freon Compressor Shaft because of a Loose Bearing (Ref 164)

The shaft-and-bearing assembly (Fig. 46a) in a freon compressor was subjected to severe pounding and vibration after six years of service. After approximately one year of service, the compressor had been shut down to replace a bearing seal. One month before the shaft failed, a second seal failure occurred, requiring the collar, spacer sleeve, seal, roller bearing, and lock washer to be replaced The shaft was made of 4140 steel and heat treated to a hardness of 20 to 26 HRC. The seal, bearing, and lock washer were commercial components.

Investigation

Although the specifications did not call for hard facing of the bearing surface on the shaft, maintenance department personnel thought the shaft had been hard faced. The shaft, spacer sleeve, roller bearing, and lock washer were sent to the laboratory for examination. Visual examination of the compressor shaft disclosed quantities of disturbed metal and partial closing of the keyway at the surface where it was contacted by a roller bearing, as shown in Fig. 46(b). The failed surface contained a groove approximately 1 mm (0.040 in.) deep and was coated with a black corrosion deposit. The spacer sleeve, roller bearing, and lock washer also were coated with the black deposit. Deposits collected from the failed area and from the spacer sleeve, roller bearing, and lock washer were identified by x-ray diffraction as ferric

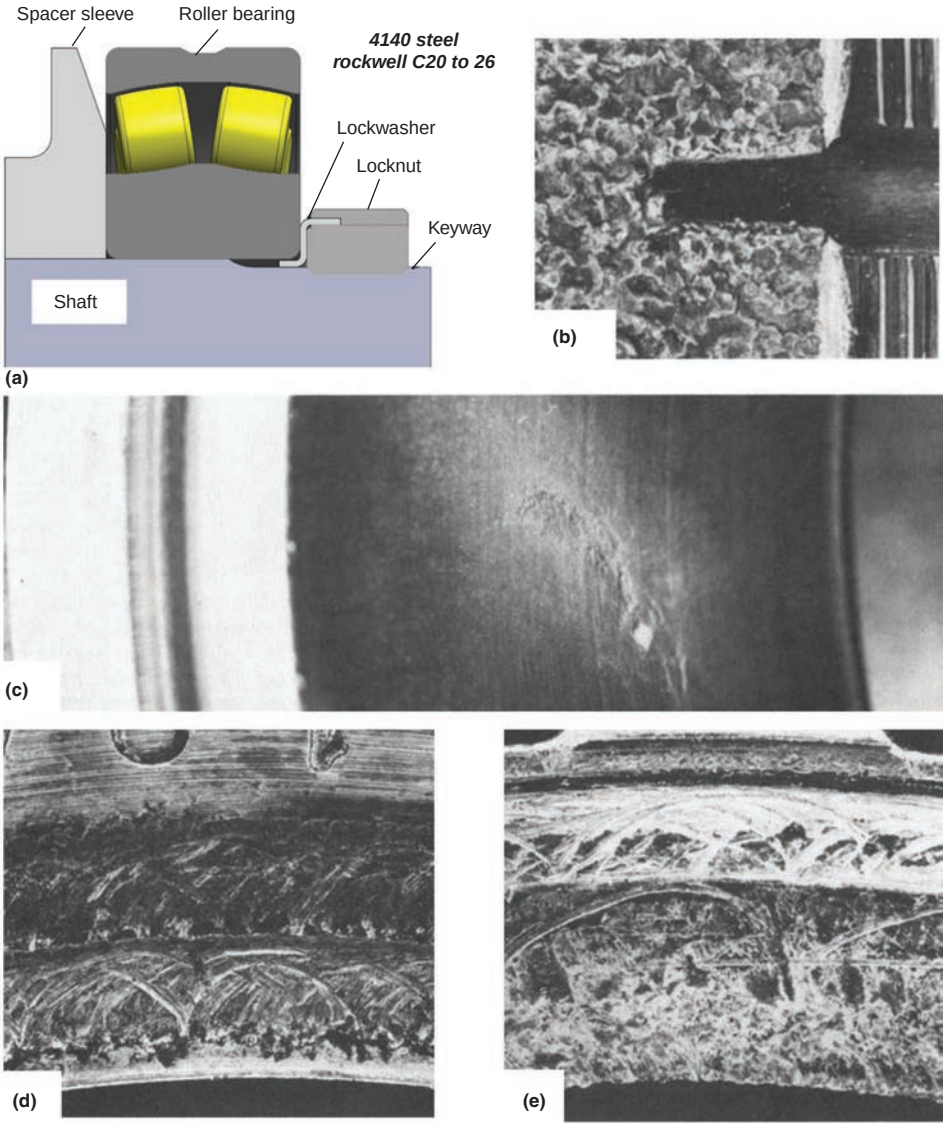

Fig. 46 Freon compressor shaft of 4140 steel that failed by fretting corrosion in the bearing area. (a) Shaft and bearing assembly. (b) Failed region of shaft showing disturbed metal and partly closed keyway. (c) Shaft side of bearing inner ring showing pitting similar to fretting damage. (d) Bearing side of spacer sleeve showing disturbed metal. (e) Bearing side of lock washer showing disturbed metal. Source: Ref 164

oxide (α-Fe_2O_3) with minor constituents of metallic iron and copper. Discoloration of the deposit was caused by the grease lubricant and mishandling during disassembly. Spectrochemical analysis of scrapings taken from an affected area and an unaffected area of the bearing surface on the shaft and from areas adjacent to and away from the bearing surface of the shaft indicated that all surfaces were fabricated from 4140 steel. These findings discounted the theory that the bearing surface had been hard faced. Readings taken along the shaft showed that the hardness of the area beneath the bearing was 24 HRC, while the area beneath the sleeve had a hardness of 90 HRB (approximately 10 HRC). This suggests that the area of the shaft beneath the bearing had been heat treated. The hardness of the inner bearing race was 54 HRC.

Microscopic examination of the shaft side of the inner bearing race showed pitting similar to that associated with fretting corrosion (Fig. 40c). Examination of the surfaces of the spacer sleeve and of the lock washer that contacted the roller bearing disclosed disturbed metal, indicating there had been movement between the sleeve and the bearing, and between the bearing and the lock washer (Fig. 46d, e). The direction of the disturbed metal on the sleeve and the lock washer showed that movement was both radial and circumferential. The peened appearance of the metal that partly covered the keyway indicated movement between the shaft and the inner bearing race. The inner bearing race could not move radially, because it was backed by the rollers, outer race, and compressor shell, which were in good condition after the failure. Therefore, the shaft must have moved radially during failure. Because the lock washer and spacer sleeve were attached to the shaft and moved with it, the circular scratches on the contacting surfaces of the bearing and the sleeve, and those of the bearing and the lock washer, indicate radial motion of the shaft. The scratches on the sleeve and lock washer were approximately 2 mm (0.080 in.) long, which was equal to the loss in diameter of the shaft at the failed area.

Conclusions

Shaft failure was initiated by fretting between the bearing race and the bearing surface on the shaft because of improper bearing installation. Once clearance was established between the bearing and the shaft, the shaft began pounding on the inner bearing race, causing final failure of the shaft surface.

Recommendations

Proper fitting of the shaft and bearing race is essential in preventing movement of the bearing on the shaft. Also, the lock washer and locknut must be installed properly.

ACKNOWLEDGMENTS

This article was adapted in part from "Fretting Wear Failures," *Failure Analysis and Prevention*, Volume 11, *ASM Handbook*, ASM International, 2002, p 922–940.

The author would like to specifically thank Miss S. Baydoun for the reading of this article.

REFERENCES

1. D. Hoeppner, *Mechanisms of Fretting Fatigue and Their Impact on Test Methods Development*, STP 1159, American Society for Testing and Materials, 1992, p 23–32
2. R.B. Waterhouse, Wear , *Wear*, Vol 100 (No. 1–3), 1984, p 107–118
3. E.M. Eden, W.N. Rose, and F.L. Cunningham, Endurance of Metals, *Proc. Inst. Mech. Eng.*, Vol 4, 1911, p 839–974
4. G.A. Tomlinson, The Rusting of Steel Surfaces in Contact, *Proc. R. Soc. (London) A*, Vol 115, 1927, p 472–483
5. E.J. Warlow-Davies, Fretting Corrosion and Fatigue Strength, *Proc. Inst. Mech. Eng.*, Vol 146, 1941, p 32–38
6. J.R. McDowell, *Fretting Corrosion Tendencies of Several Combinations of Materials, Symposium on Fretting Corrosion*, STP 144, American Society for Testing and Materials, 1953, p 2439
7. M.J. Neale and M. Gee, Chap. 2, Industrial Wear Problems, *A Guide to Wear Problems and Testing for Industry*,

William Andrew Publishing, Suffolk, U. K., 2001, p 3-III
8. J.F. Warriner, "Thin Shell Bearings for Medium Speed Diesel Engines," No. 364, Diesel Engineers and Users Association, Feb 1975
9. J. Chao, Fretting-Fatigue Induced Failure of a Connecting Rod, *Eng. Fail. Anal.*, Vol 96, 2019, p 186–201
10. "Fretting/Corrosion in Main Bearing Bore," Service Letter SL2017-645/JNN, MAN Diesel & Turbo, April 2017
11. M. Pujatti, M. Suhadolc, and D. Piculin, Fretting-Initiated Fatigue in Large Bore Engines Connecting Rods, *Proc. Eng.*, Vol 74, 2014, p 356–359
12. R.G. Mitchell, An Airline View of the Corrosion Problem, *Ind. Corros.*, July 1983, p 11–17
13. C. Jiménez-Peña, R. H. Talemi, B. Rossi, and D. Debruyne, Investigations on the Fretting Fatigue Failure Mechanism of Bolted Joints in High Strength Steel Subjected to Different Levels of Pre-Tension, *Tribol. Int.*, Vol 108, 2017, p 128–140
14. T. Benhaddou, P. Stephan, A. Daidie, F. Alkatan, C. Chirol, and J.B. Tuery, Effect of Axial Preload on Durability of Aerospace Fastened Joints, *Int. J. Mech. Sci.*, Vol 137, 2018, p 214–223
15. P. Greenfield and R.W. Suhr, The Factors Affecting the High-Cycle Fatigue Strength of Low-Pressure Turbine and Generator Rotors, *Proc. of International Conference on Fatigue of Engineering Materials and Structures*, Sept 15–19, 1986 (Sheffield), *Inst. Mech. Eng.*, Vol 1, 1986, p 165–186
16. K. Anandavel and R.V. Prakash, Effect of Three-Dimensional Loading on Macroscopic Fretting Aspects of an Aero-Engine Blade-Disc Dovetail Interface, *Tribol. Int.*, Vol 44 (No. 11), 2011, p 1544–1555
17. C. Mary, S. Fouvry, J.M. Martin, and B. Bonnet, Pressure and Temperature Effects on Fretting Wear Damage of a Cu-Ni-In Plasma Coating versus Ti17 Titanium Alloy Contact, *Wear*, Vol 272 (No. 1), 2011, p 18–37
18. A. Cruzado, M.A. Urchegui, and X. Gómez, Finite Element Modeling and Experimental Validation of Fretting Wear Scars in Thin Steel Wires, *Wear*, Vol 289, 2012, p 26–38
19. S. Lalonde, R. Guilbault, and S. Langlois, Numerical Analysis of ACSR Conductor-Clamp Systems Undergoing Wind-Induced Cyclic Loads, *IEEE Trans. Power Deliv.*, Vol 33 (No. 4), 2018, p 1518–1526
20. G. Chen, X. Wang, J. Wang, J. Liu, T. Zhang, and W. Tang, Damage Investigation of the Aged Aluminium Cable Steel Reinforced (ACSR) Conductors in a High-Voltage Transmission Line, *Eng. Fail. Anal.*, Vol 19, 2012, p 13–21
21. V.F. Steier, T. Doca, and J.A. Araújo, Fretting Wear Investigation of 1350-H19 Aluminum Wires Tested against Treated Surfaces, *Wear*, Vol 414–415, 2018, p 1–8
22. J. Said, S. Garcin, S. Fouvry, G. Cailletaud, C. Yang, and F. Hafid, A Multi-Scale Strategy to Predict Fretting-Fatigue Endurance of Overhead Conductors, *Tribol. Int.*, Vol 143, 2020, p 106053
23. D.K. Zhang, S.R. Ge, and Y.H. Qiang, Research on the Fatigue and Fracture Behavior due to the Fretting Wear of Steel Wire in Hoisting Rope, *Wear*, Vol 255 (No. 7–12), 2003, p 1233–1237
24. H.W. Fricker, Fretting in Tube Supports of Heat Exchangers, *Proc. of Conference on Component Design in High Temperature Reactors Using Helium as a Coolant*, Nuclear Engineering Group of Institution of Mechanical Engineers, *May* 3–4, 1972, p 213–231
25. Z.B. Cai, Z. Yang Li, M.G. Yin, M.H. Zhu, and Z.R. Zhou, A Review of Fretting Study on Nuclear Power Equipment, *Tribol. Int.*, Vol 144, 2020, p 106095
26. P.J. Blau, A Microstructure-Based Wear Model for Grid-to-Rod Fretting of Clad Nuclear Fuel Rods, *Wear*, Vol 426–427, 2019, p 750–759
27. M. Antler, Electrical Effects of Fretting Connector Contact Materials: A Review, *Wear*, Vol 106, 1985, p 5–33
28. M. Braunovic, Fretting in Electrical/Electronic Connections: A Review, *IEICE Trans. Electron.*, Vol 92 (No. 8), 2009, p 982–991
29. E. Larsson, A.M. Andersson, and A. Kassman Rudolphi, Grease Lubricated Fretting of Silver Coated Copper Electrical Contacts, *Wear*, Vol 376–377, 2017, p 634–642
30. S. Noel, D. Alamarguy, A. Brezard-Oudot, and P. Gendre An Investigation of Fretting Wear Behavior of Nickel Coatings for Electrical Contacts Application in Dry and Lubricated Conditions, *Wear*, Vol 301, 2013, p 551–561
31. C. Chen, G.T. Flowers, M. Bozack, and J. Suhling Modeling and Analysis of a Connector System for the Prediction of Vibration-Induced Fretting Degradation, *Proc. 55th IEEE Holm Conference on Electrical Contacts* (Vancouver, British Columbia, Canada), 2009, p 129–135
32. P. Stoyanov, R.R. Chromik, S. Gupta, and J.R. Lince, Micro-Scale Sliding Contacts on Au and Au-MoS_2 Coatings, *Surf. Coat. Technol.*, Vol 205, 2010, p 1449–1454
33. S. Fouvry, P. Jedrzejczyk, and P. Chalandon, Introduction of an Exponential Formulation to Quantify the Electrical Endurance of Micro-Contacts Enduring Fretting Wear: Application to Sn, Ag and Au Coatings, *Wear*, Vol 271 (No. 9–10), 2011, p 1524–1534
34. F. Massi, J. Rocchi, A. Culla, and Y. Berthier, Coupling System Dynamics and Contact Behaviour: Modelling Bearings Subjected to Environmental Induced Vibrations and "False Brinelling" Degradation, *Mech. Syst. Signal Process.*, Vol 24, 2010, p 1068–1080
35. L. Mattei, F. Di Puccio, B. Piccigallo, and E. Ciulli, Lubrication and Wear Modelling of Artificial Hip Joints: A Review, *Tribol. Int.*, Vol 44 (No. 5), 2011, p 532–549
36. J. Geringer, B. Forest, and P. Combrade, Fretting-Corrosion of Materials Used as Orthopaedic Implants, *Wear*, Vol 259, 2005, p 943–951
37. B. Bacroix, M. Lahmari, G. Inglebert, and I. Lemaire Caron, A Modified Oxygen Boost Diffusion Treatment for Ti Alloys and Associated Tribological Properties with Respect to Biological Environment, *Wear*, Vol 271, 2011, p 2720– 2727
38. J. Esguerra-Arce, A. Bermúdez Castañed, A. Esguerra-Arce, Y. Aguilar, and S. Mischler, Fretting Corrosion between Bone and Calcium Phosphate-Calcium Titanate Coatings, *Wear*, Vol 414–415, 2018, p 366–375
39. D. Royhman, M. Patel, J.J. Jacobs, M.A. Wimmer, N.J. Hallab, and M.T. Mathew, In Vitro Simulation of Fretting-Corrosion in Hip Implant Modular Junctions: The Influence of pH, *Med. Eng. Phys.*, Vol 52, 2018, p 1–9
40. R. English, A. Ashkanfar, and G. Rothwell, The Effect of Different Assembly Loads on Taper Junction Fretting Wear in Total Hip Replacements, *Tribol. Int.*, Vol 95, 2016, p 199–210
41. S. Fouvry, P. Kapsa, and V. Vincent, Quantification of Fretting Damage, *Wear*, Vol 200 (No. 1–2), 1996, p 186–205
42. S. Fouvry and P. Kapsa, An Energy Description of Hard Coating Wear Mechanisms, *Surf. Coat. Technol.*, Vol 138 (No. 2), 2001, p 141–148
43. P.J. Kennedy, M.B. Peterson, and L. Stallings, An Evaluation of Fretting at Small Slip Amplitudes, *Materials Evaluation under Fretting Conditions*, STP 780, *American Society for Testing and Materials*, 1982, p 30–48
44. O. Vingsbo and S. Söderberg, On Fretting Maps, *Wear*, Vol 126, 1988, p 131–147
45. R.D. Mindlin and H. Deresiewicz, Elastic Spheres in Contact under Varying Oblique Forces, *Trans. ASME Ser. E, J. Appl. Mech.*, Vol 20, 1953, p 327–344
46. K.L. Johnson, *Contact Mechanics*, Cambridge University Press, Cambridge, 1985
47. S. Fouvry, P. Kapsa, and L. Vincent, Analysis of Sliding Behaviour for Fretting Loadings: Determination of Transition Criteria, *Wear*, Vol 185, 1995, p 35–46
48. M. Varenberg, I. Etsion, and G. Halperin, Slip Index: A New Unified Approach to Fretting, *Tribol. Lett.*, Vol 17 (No. 3), 2004, p 569–573
49. S. Heredia and S. Fouvry, Introduction of a New Sliding Regime Criterion to

Quantify Partial, Mixed and Gross Slip Fretting Regimes: Correlation with Wear and Cracking Processes, *Wear*, Vol 269 (No. 7–8), 2010, p 515–524
50. Z.R. Zhou, S. Fayeulle, and L. Vincent, Cracking Behaviour of Various Aluminium Alloys during Fretting Wear, *Wear*, Vol 155, 1992, p 317–330
51. Z. Zhou, Mixed Fretting Regime, *Wear*, Vol 181–183, 1995, p 531–536
52. M. Lavella, Partial-Gross Slip Fretting Transition of Martensitic Stainless Steels, *Tribol. Int.*, Vol 146, 2020, p 106163
53. A. Benítez, J. Denape, and J.-Y. Paris, Interaction between Systems and Materials in Fretting, *Wear*, Vol 368–369, 2016, p 183–195
54. H.C. Meng and K.C. Ludema, Wear Models and Predictive Equations: Their Form and Content, *Wear*, Vol 181–183, 1995, p 443–457
55. J.F. Archard, Contact and Rubbing of Flat Surfaces, *J. Appl. Phys.*, Vol 24 (No. 8), 1953, p 981
56. H. Mohrbacker, B. Blanpain, J.P. Celis, J.R. Roos, L. Stals, and M. Van Stappen, Oxidational Wear of TiN Coatings on Tool Steel and Nitride Tool Steel in Unlubricated Fretting, *Wear*, Vol 188, 1995, p 130–137
57. S. Fouvry, T. Liskiewicz, and C. Paulin, A Global-Local Wear Approach to Quantify the Contact Endurance under Reciprocating-Fretting Sliding Conditions, *Wear*, Vol 263 (No. 1–6), Sept 10, 2007, p 518–531
58. A. Ramalho, A. Merstallinger, and A. Cavaleiro, Fretting Behaviour of W-Si Coated Steels in Vacuum Environments, *Wear*, Vol 261, 2006, p 79–85
59. T. Liskiewicz and S. Fouvry, Development of a Friction Energy Capacity Approach to Predict the Surface Coating Endurance under Complex Oscillating Sliding Conditions, *Tribol. Int.*, Vol 38 (No. 1), 2005, p 69–79
60. E. Sauger, S. Fouvry, L. Ponsonnet, P. Kapsa, J. Martin, et al., Tribologically Transformed Structure in Fretting, *Wear*, Vol 245 (No. 1), 2000, p 39–52
61. V. Nurmi, J. Hintikka, J. Juoksukangas, M. Honkanen, M. Vippola, A. Lehtovaara, et al., The Formation and Characterization of Fretting-Induced Degradation Layers Using Quenched and Tempered Steel, *Tribol. Int.*, Vol 131, 2019, p 258–267
62. N. Fillot, I. Iordanoff, and Y. Berthier, Modelling Third Body Flows with a Discrete Element Method—A Tool for Understanding Wear with Adhesive Particles, *Tribol. Int.*, Vol 40, 2007, p 973–981
63. M. Godet, Third-Bodies in Tribology, *Wear*, Vol 136, 1990, p 29–45
64. J.D. Lemm, A.R. Warmuth, S.R. Pearson, and P.H. Shipway, The Influence of Surface Hardness on the Fretting Wear of Steel Pairs—Its Role in Debris Retention in the Contact, *Tribol. Int.*, Vol 81, 2015, p 258–266
65. M. Varenberg, G. Halperin, and I. Etsion, Different Aspects of the Role of Wear Debris in Fretting Wear, *Wear*, Vol 252 (No.11), 2002, p 902–910
66. R. Waterhouse and D. Taylor, Fretting Debris and the Delamination Theory of Wear, *Wear*, Vol 29 (No. 3), 1974, p 337–344
67. S. Descartes and Y. Berthier, Rheology and Flows of Solid Third Bodies: Background and Application to an $MoSO_2$ Coating, *Wear*, Vol 252 (No. 7–8), 2002, p 546–556
68. S. Fouvry, P. Arnaud, A. Mignot, and P. Neubauer, Contact Size, Frequency and Cyclic Normal Force Effects on Ti-6Al-4V Fretting Wear Processes: An Approach Combining Friction Power and Contact Oxygenation, *Tribol. Int.*, Vol 113, 2017, p 460–473
69. S. Baydoun and S. Fouvry, An Experimental Investigation of Adhesive Wear Extension in Fretting Interface: Application of the Contact Oxygenation Concept, *Tribol. Int.*, Vol 147, 2020, p 106266
70. A.R. Warmuth, S.R. Pearson, P.H. Shipway, and W. Sun, The Effect of Contact Geometry on Fretting Wear Rates and Mechanisms for a High Strength Steel, *Wear*, Vol 301 (No. 1–2), 2013, p 491–500
71. S. Baydoun, P. Arnaud, and S. Fouvry, Modelling Adhesive Wear Extension in Fretting Interfaces: An Advection-Dispersion-Reaction Contact Oxygenation Approach, *Tribol. Int.*, Vol 151, 2020, p 106490
72. S. Fouvry, P. Duo, and P. Perruchaut, A Quantitative Approach of Ti-6Al-4V Fretting Damage: Friction, Wear and Crack Nucleation, *Wear*, Vol 257 (No. 9–10), 2004, p 916–929
73. S. Fouvry, C. Paulin, and S. Deyber, Impact of Contact Size and Complex Gross-Partial Slip Conditions on Ti-6Al-4V/Ti-6Al-4V Fretting Wear, *Tribol. Int.*, Vol 42 (No. 3), 2009, p 461–474
74. I.M. Feng and H.H. Uhlig, Fretting Corrosion of Mild Steel in Air and Nitrogen, *J. Appl. Mech.*, Vol 21, 1954, p 395–400
75. S. Goto and R.B. Waterhouse, Fretting and Fretting-Fatigue of Titanium Alloys under Conditions of High Normal Load, *Proc. Fourth International Conference on Titanium*, Vol 3, TMS/AIME, 1980, p 1337–1384
76. F.P. Bowden and D. Tabor, *The Friction and Lubrication of Solids*, Oxford University Press, 1950, p 19
77. S. Baydoun, S. Fouvry, S. Descartes, and P. Arnaud, Fretting Wear Rate Evolution of a Flat-on-Flat Low Alloyed Steel Contact: A Weighted Friction Energy Formulation, *Wear*, Vol 426–427, 2019, p 676–693
78. R.B. Waterhouse, Fretting, *Treatise on Materials Science and Technology*, D. Scott, Ed., Academic Press, 1978, p 259–286
79. S. Söderberg, U. Bryggman, and T. McCullough, Frequency Effects in Fretting Wear, *Wear*, Vol 110, 1986, p 19–34
80. M. Kuno and R.B. Waterhouse, The Effect of Oscillatory Direction on Fretting Wear under Crossed Cylinder Contact Conditions, *Eurotrib 89, Proc. Fifth International Congress on Tribology*, Vol 3, June 12–15, 1989 (Helsinki), p 30–35
81. N.L. Golego, M.N. Rozhkov, V.P. Onoprienko, A.S. Nakrakui, and N.V. Kozii, Wear of Materials in Fretting Corrosion in Connection with Conditions of Vibrocontact Interaction, *Fiz. Khim. Mekh. Mater.*, Vol 21, 1985, p 71–75
82. A. Pannemaeckerde, H. Attia, and G. Williams, A Novel Acceleration-Controlled Random Vibration Fretting Test Methodology: From Classical Sinusoidal to Gaussian Random Excitation, *Wear*, Vol 438–439, 2019, p 203050
83. J.H. Cha, M.W. Wambsganss, and J.A. Jendrzejcyk, Experimental Study on Impact/Fretting Wear in Heat Exchanger Tubes, *J. Pressure Vessel Technol. (Trans. ASME)*, Vol 109, 1987, p 265–274
84. A.W.J. Geede, C.P.L. Commissaris, and J.H. Zaat, The Wear of Sintered Aluminium Powder (SAP) under Directions of Vibrational Contact, *Wear*, Vol 7, 1964, p 535–550
85. P.L. Ko, Experimental Studies of Tube Fretting in Steam Generators and Heat Exchangers, *J. Pressure Vessel Technol. (Trans. ASME)*, Vol 101, 1979, p 125–133
86. H. Attia, Y.B. Gessesse, and M.O.M. Osman, New Parameter for Characterizing and Correlating Impact-Sliding Fretting Wear to Energy Dissipation—Experimental Investigation, *Wear*, Vol 263 (No. 1–6), 2007, p 419–429
87. T. Souilliart, E. Rigaud, A. LeBot, and C. Phalippou, An Energy Approach for Impact Wear in Water Environment, *Wear*, Vol 376–377, 2017, p 738–746
88. S.F. Calhoun, "*Effects of Metal Hardness and Surface Finish upon Fretting Corrosion*," Technical Report 63-1835, Rock Island Arsenal, May 28, 1963
89. K.J. Kubiak, T.W. Liskiewicz, and T.G. Mathia, Surface Morphology in Engineering Applications: Influence of Roughness on Sliding and Wear in Dry Fretting, *Tribol. Int.*, Vol 44, 2011, p 1427–1432
90. R.B. Waterhouse, Residual Stresses and Fretting, *International Guidebook on Residual Stresses*, A. Niku-Lari, Ed., Pergamon, Oxford, 1987, p 511–525

91. C.A. Bergman, R.C. Cobb, and R.B. Waterhouse, The Effect of Shot-Peening on the Friction and Wear of a Carbon Steel in Fretting Conditions, *Wear of Materials*, American Society of Mechanical Engineers, 1987, p 33–37
92. K. Kubiak, S. Fouvry, and A.M. Marechal, A Practical Methodology to Select Fretting Palliatives: Application to Shot Peening Hard Chromium and WC-Co Coatings, *Wear*, Vol 259 (No. 1–6), 2005, p 367–376
93. G. Fair, B. Noble, and R.B. Waterhouse, The Stability of Compressive Stresses Induced by Shot-Peening under Conditions of Fatigue and Fretting-Fatigue, *Advances in Surface Treatments*, Vol I, A. Niku-Lari, Ed., Pergamon, Oxford, 1984, p 3–8
94. M. Kuno, R.B. Waterhouse, D. Nowell, and D.A. Hills, Initiation and Growth of Fretting Fatigue Cracks in the Partial Slip Regime, *Fatigue Fract. Eng. Mater. Struct.*, Vol 12, 1989, p 387–398
95. K. Kubiak, S. Fouvry, A.M. Marechal, and J.M. Vernet, Behaviour of Shot Peening Combined with WC-Co HVOF Coating under Complex Fretting Wear and Fretting Fatigue Loading Conditions, *Surf. Coat. Technol.*, Vol 201, 2006, p 4323–4328
96. T. Kayaba and A. Iwabuchi, Effect of the Hardness of Hardened Steels and the Action of Oxides on Fretting Wear, *Wear*, Vol 66, 1981, p 27–41
97. K.G. Budinski, Effect of Hardness Differential on Metal-to-Metal Fretting Damage, *Wear*, Vol 301, 2013, p 501–507
98. J. Sato, M. Sato, and S. Yamamoto, Fretting Wear of Stainless Steel, *Wear*, Vol 69, 1981, p 167–177
99. P.A. Higham, F.H. Stott, and B. Bethune, The Influence of Polymer Composition on the Wear of the Metal Surface during the Fretting of Steel on Polymer, *Wear*, Vol 47, 1978, p 71–80
100. O. Jacobs, K. Friedrich, G. Marom, K. Schulte, and H.D. Wagner, Fretting Wear Performance of Glass-Carbon and Aramid Fibre/Epoxy- and PEEK-Composites, *Wear*, Vol 135, 1990, p 207–216
101. M. Kuno, R.B. Waterhouse, and B.R. Pearson, Fretting Wear in Sintered Alumina and Tungsten Carbide Cermet-Metal Couples, *Wear of Materials 1987*, American Society of Mechanical Engineers, 1987, p 371–380
102. D. Klaffke, Fretting Wear of Ceramics, *Tribol. Int.*, Vol 22, 1989, p 89–101
103. D.R. Horn, R.B. Waterhouse, and B.R. Pearson, Fretting Wear of Sintered Alumina, *Wear*, Vol 113, 1986, p 225–232
104. J.F. Andrews, P.D. Donovan, and J. Stringer, Fretting Corrosion Products of Aluminium Alloys, *Br. Corros. J.*, Vol 3, 1968, p 85–87
105. C. Colombier, Y. Berthier, A. Floquet, L. Vincent, and M. Godet, Fretting: Load Carrying Capacity of Wear Debris, *J. Tribol. (Trans. ASME)*, Vol 106, 1984, p 194–201
106. D. Aldham, J. Warburton, and R.E. Pendlebury, The Unlubricated Fretting Wear of Mild Steel in Air, *Wear*, Vol 106, 1985, p 177–201
107. A. Iwabuchi, T. Kayaba, and K. Kata, Effect of Atmospheric Pressure on Friction and Wear of 0.45% C Steel in Fretting, *Wear*, Vol 91, 1983, p 289–305
108. A. Iwabuchi, K. Kato, and T. Kayaba, Fretting Properties of SUS304 Stainless Steel in Vacuum Environment, *Wear*, Vol 110, 1986, p 205–216
109. A. Iwabuchi, H. Matsuzaki, and K. Hori, The Effect of Ambient Pressure on the Tribological Properties of an Amorphous Alloy in Fretting, *Wear of Materials 1989*, American Society of Mechanical Engineers, 1989, p 595–600
110. H. Goto and D.H. Buckley, The Influence of Water Vapour in Air on the Friction Behaviour of Pure Metals during Fretting, *Tribol. Int.*, Vol 18, 1985, p 237–245
111. H. Chen, P.Q. Wu, C. Quaeyhaegens, K. W. Xu, L.M. Stals, J.W. He, and J.-P. Celis, Comparison of Fretting Wear of Cr-Rich CrN and TiN Coatings in Air of Different Relative Humidities, *Wear*, Vol 253, 2002, p 527–532
112. R. Rybiak, S. Fouvry, T. Liskiewicz, and B. Wendler, Fretting Wear of a TiN PVD Coating under Variable Relative Humidity Conditions—Development of a "Composite" Wear Law, *Surf. Coat. Technol.*, Vol 202 (No. 9), 2008, p 1753–1763
113. Z. Cai, M. Zhu, H. Shen, Z. Zhou, and X. Jin, Torsional Fretting Wear Behaviour of 7075 Aluminium Alloy in Various Relative Humidity Environments, *Wear*, Vol 267, 2009, p 330–339
114. H. Goto, M. Ashida, and K. Endo, The Influence of Oxygen and Water Vapour on the Friction and Wear of an Aluminum Alloy under Fretting Conditions, *Wear*, Vol 116, 1987, p 141–155
115. M.P. Sherwin, D.E. Taylor, and R.B. Waterhouse, An Electrochemical Investigation of Fretting Corrosion in Stainless Steel, *Corros. Sci.*, Vol 11, 1971, p 419–429
116. S.D. Cook, G.J. Gianoli, A.J.T. Clemow, and R.J. Haddad, Fretting Corrosion in Orthopaedic Alloys, *Biomater. Med. Dev. Art. Org.*, Vol 11, 1983–1984, p 281–292
117. S.A. Brown and K. Merritt, Fretting Corrosion in Saline and Serum, *J. Biomed. Mater. Res.*, Vol 15, 1981, p 479–488
118. S.A. Brown and J.P. Simpson, Crevice and Fretting Corrosion of Stainless Steel Plates and Screws, *J. Biomed. Mater. Res.*, Vol 15, 1981, p 867–878
119. K. Merritt and S.A. Brown, Effect of Proteins and pH on Fretting Corrosion and Metal Ion Release, *J. Biomed. Mater. Res.*, Vol 22, 1988, p 111–120
120. B.R. Pearson and R.B. Waterhouse, The Fretting Corrosion in Seawater of Materials Used in Offshore Structures, *Proc. Ninth International Congress on Metallic Corrosion*, Vol 2, June 5–9, 1984 (Toronto), NRC Canada, 1984, p 334–341
121. S. Barril, S. Mischler, and D. Landolt, Influence of Fretting Regimes on the Tribocorrosion Behaviour of Ti6Al4V in 0.9 wt.% Sodium Chloride Solution, *Wear*, Vol 256, 2004, p 963–972
122. P.L. Hurricks, The Fretting Wear of Mild Steel from 200 to 500 °C, *Wear*, Vol 30, 1974, p 189–212
123. F.H. Stott, D.S. Lui, and G.C. Wood, The Structure and Mechanism of the "Glaze" Oxide Layers Produced on Nickel-Based Alloys during Wear at High Temperatures, *Corros. Sci.*, Vol 13, 1973, p 449–469
124. M.M. Hamdy and R.B. Waterhouse, The Fretting Wear of Ti-6Al-4V and Aged Inconel 718 at Elevated Temperatures, *Wear*, Vol 71, 1981, p 237–248
125. A. Iwabuchi, Fretting Wear of Inconel 625 at High Temperature and in High Vacuum, *Wear*, Vol 106, 1985, p 163–175
126. M.M. Hamdy and R.B. Waterhouse, The Stability of the Protective Glaze Oxide Formed during High Temperature Fretting of an Aged Nickel-Based Alloy, Inconel 718, *Wear of Materials 1983*, American Society of Mechanical Engineers, 1983, p 546–549
127. R. Rybiak, S. Fouvry, and B. Bonnet, Fretting Wear of Stainless Steels under Variable Temperature Conditions: Introduction of a "Composite" Wear Law, *Wear*, Vol 268, 2010, p 413–423
128. H. Ming, X. Liu, H. Yan, Z. Zhang, J. Wang, L. Gao, J. Lai, and E.H. Han, Understanding the Microstructure Evolution of Ni-Based Superalloy within Two Different Fretting Wear Regimes in High Temperature High Pressure Water, *Scr. Mater.*, Vol 170, 2019, p 111–115
129. A. Ahmadia, F. Sadeghia, and S. Shaffer, In-Situ Friction and Fretting Wear Measurements of Inconel 617 at Elevated Temperatures, *Wear*, Vol 410–411, 2018, p 110–118
130. M. Lavella and D. Botto, Fretting Wear Characterization by Point Contact of Nickel Superalloy Interfaces, *Wear*, Vol 271, 2011, p 1543–1551
131. S.R. Pearson, P.H. Shipway, J.O. Abere, and R.A.A. Hewitt, The Effect of Temperature on Wear and Friction of a High Strength Steel in Fretting, *Wear*, Vol 303 (No. 1–2), 2013, p 622–631
132. M.R. Hirsch and R.W. Neu, Influence of Temperature on the Fretting Response between AISI 301 Stainless Steel and AISI 52100 Steel, *Tribol. Int.*, Vol 68, 2013, p 77–84

133. A. Dreano, S. Fouvry, and G. Guillonneau, A Combined Friction Energy and Tribo-Oxidation Formulation to Describe the High Temperature Fretting Wear Response of a Cobalt-Based Alloy, *Wear*, Vol 426–427, 2019, p 712–724
134. A. Dreano, S. Fouvry, and G. Guillonneau, Understanding and Formalization of the Fretting-Wear Behavior of a Cobalt-Based Alloy at High Temperature, *Wear*, Vol 452–453, 2020, p 203297, https://doi.org/10.1016/j.wear.2020.203297
135. A. Viat, G. Guillonneau, S. Fouvry, G. Kermouche, S. Sao Joao, J. Wehrs, J. Michler, and J.F. Henne, Brittle to Ductile Transition of Tribomaterial in Relation to Wear Response at High Temperatures, *Wear*, Vol 392–393, 2017, p 60–68
136. A. Korashy, H. Attia, V. Thomson, and S. Oskooei, Fretting Wear Behavior of Cobalt-Based Superalloys at High Temperature—A Comparative Study, *Tribol. Int.*, Vol 145, 2020, p 106155
137. D.G. Chetwynd, F.A. McKee, and C.H. Wride, The Measurement of Wear Damage, *Proc. Inst. Mech. Eng.*, Vol 201 (No. 4C), 1987, p 251–258
138. P.L. Hurricks, The Mechanism of Fretting—A Review, *Wear*, Vol 15, 1970, p 389–409
139. R.B. Waterhouse, The Role of Adhesion and Delamination in the Fretting Wear of Metallic Materials, *Wear*, Vol 45, 1977, p 355–364
140. H.H. Uhlig, Mechanism of Fretting Corrosion, *J. Appl. Mech.*, Vol 21, 1954, p 401–407
141. X. Zhang, C. Zhang, and C. Zhu, Slip Amplitude Effects and Microstructural Characteristics of Surface Layers in Fretting Wear of Carbon Steel, *Wear*, Vol 134, 1989, p 297–309
142. R.B. Waterhouse, Fretting Corrosion and Fretting Fatigue in the Transport Industry, *Proc. Sixth European Congress on Metallic Corrosion*, Sept 19–23, 1977 (London)
143. J. Beard, The Rational Selection of Palliatives for Avoidance of Fretting, *Tribology—Friction, Lubrication and Wear, Fifty Years On, Conference Proceedings*, Vol 1, July 1–3, 1987 (London), Institute of Mechanical Engineers, 1987, p 311–319
144. K. Kubiak, S. Fouvry, and B.G. Wendler, Comparison of Shot Peening and Nitriding Surface Treatments under Complex Fretting Loadings, *Mater. Sci. Forum*, Vol 513, 2006, p 105–118
145. Y.H. Lee, I.H. Kim, H.K. Kim, and H.G. Kim, Role of ZrO_2 Oxide Layer on the Fretting Wear Resistance of a Nuclear Fuel Rod, *Tribol. Int.*, Vol 145, 2020, p 106146
146. C.H. Hager, J. Sanders, S. Sharma, and A.A. Voevodin, The Use of Nickel Graphite Composite Coatings for the Mitigation of Gross Slip Fretting Wear on Ti6Al4V Interfaces, *Wear*, Vol 267, 2009, p 1470–1481
147. M. Kalin and J. Vizintin, The Tribological Performance of DLC Coatings under Oil-Lubricated Fretting Conditions, *Tribol. Int.*, Vol 39, 2006, p 1060–1067
148. Y. Zhang, S. Descartes, and R.R. Chromik, Influence of WC on Third Body Behavior during Fretting of Cold-Sprayed $CuMoS_2WC$ Composites, *Tribol. Int.*, Vol 134, 2019, p 15–25
149. R.C. Cobb and R.B. Waterhouse, *The Fretting Wear of Certain Hard Coatings Including TiN Applied to a 0.4C Steel*, *Tribology—Friction, Lubrication and Wear, Fifty Years On, Conference Proceedings*, Vol 1, July 1–3, 1987 (London), Institute of Mechanical Engineers, 1987, p 303–310
150. J.C. Gregory, A Salt Bath Treatment to Improve the Resistance of Ferrous Metals to Scuffing, Wear, Fretting, and Fatigue, *Wear*, Vol 9, 1966, p 249–281
151. S. Fouvry, V. Fridrici, C. Langlade, P. Kapsa, and L. Vincent, Palliatives in Fretting: A Dynamical Approach, *Tribol. Int.*, Vol 39, 2006, p 1005–1015
152. D. Godfrey and E.E. Bisson, "*Bonding of Molybdenum Disulphide to Various Materials to Form a Solid Lubricating Film, Part II: Friction and Endurance Characteristics of Films Bonded by Practical Methods*," Technical Note 2802, NACA, 1952
153. A.M. Korsunsky, A.R. Torosyan, and K. Kim, Development and Characterization of Low Friction Coatings for Protection against Fretting Wear in Aerospace Components, *Thin Solid Films*, Vol 516, 2008, p 5690–5699
154. C. Langlade, B. Vannes, M. Taillandier, and M. Pierantoni, Fretting Behavior of Low-Friction Coatings: Contribution to Industrial Selection, *Tribol. Int.*, Vol 34, 2001, p 49–56
155. S. Fouvry and C. Paulin, An Effective Friction Energy Density Approach to Predict Solid Lubricant Friction Endurance: Application to Fretting Wear, *Wear*, Vol 319, 2014, p 211–226
156. R.B. Waterhouse, The Effect of Surface Treatments on the Fretting Wear of an Aluminum Alloy (RR58)/Steel (BS970 080 M40) Couple, *Proc. Conference on Surface Engineering, Current Trends and Future Prospects*, S.A. Meguid, Ed., June 25–27, 1990 (Toronto), Elsevier Applied Science, 1990, p 325–334
157. D.J. Varley and R.B. Waterhouse, Fretting of Bronze-Filled PTFE against Mild Steel, *Proc. Japanese International Tribology Conference*, Vol 2, Oct 29–Nov 1, 1990 (Nagoya), Japanese Society of Tribologists, 1990, p 821–825
158. D.E. Taylor and R.B. Waterhouse, Fretting Fatigue in Steel Ropes, *Lubr. Eng.*, Vol 27, 1971, p 123–127
159. J. Sato, M. Shima, T. Sugiwara, and A. Tahara, Effect of Lubricants on Fretting Wear of Steel, *Wear*, Vol 125, 1988, p 83–95
160. L. Haviez, S. Fouvry, R. Toscano, and G. Yantio, An Energy-Based Approach to Understand the Effect of Fretting Displacement Amplitude on Grease-Lubricated Interface, *Wear*, Vol 338, 2015, p 422–429
161. M. Shima, H. Suetake, I.R. McColl, R.B. Waterhouse, and M. Takeuchi, *Wear*, Vol 210, 1997, p 304–310
162. Z.R. Zhou and L. Vincent, Lubrication in Fretting—A Review, *Wear*, Vol 225–229, 1999, p 962–996
163. Z. Zhou, Q. Liu, M. Zhu, L. Tanjala, P. Kapsa, and L. Vincent, An Investigation of Fretting Behavior of Several Metallic Materials under Grease Lubrication, *Tribol. Int.*, Vol 33, 2000, p 69–74
164. F.E. Krueger, Fretting Failures, *Failure Analysis and Prevention*, Vol 10, *Metals Handbook*, 8th ed., American Society for Metals, 1975, p 155